Characterization of the Zebrafish Panx1a Phosphorylation Profile and Interactome in the Regulation of the Channel Function and Trafficking

KSENIA TIMONINA

A DISSERTATION SUBMITTED TO

THE FACULTY OF GRADUATE STUDIES

IN PARTIAL FULFILLMENT OF THE REQUIREMENTS FOR THE DEGREE OF

DOCTOR OF PHILOSOPHY

GRADUATE PROGRAM IN BIOLOGY

YORK UNIVERSITY

TORONTO, ONTARIO

October 2022

ABSTRACT

Pannexin-1 (Panx1) is an integral membrane protein that forms heptameric channels, involved in the communication between the intracellular and the extracellular environment. Its primary function is to passage small molecules, such as ATP, in and out of the cell, which can trigger vital cellular responses like cell death. Panx1s have been implicated in various diseases, including epilepsy, ischemia, and inflammation. They also play roles in the sensory processing systems, such as vision, hearing, olfaction, and taste. Although it is clear that Panx1s are vital to the function of biological processes, the exact mechanism of how these channels operate and what activates/inactivates them is still under investigation. Using the zebrafish orthologues of Panx1, we explore the structural properties responsible for the trafficking of the channel while maintaining a focus on the phospho-proteomics and the kinase-dependent signaling involving Panx1. We identified a critical residue highly conserved in the third transmembrane domain, Y205 of the zebrafish Panx1a protein, which plays a role in the stabilization of the protein, likely through aromatic-aromatic interactions. Our results show that this residue is not subject to phosphorylation but is vital for the localization of the channel at the cell surface. Using protein purification techniques combined with mass spectrometry analysis, we identified several phosphorylated residues in the cytoplasmic loop of Panx1a and explored the potential interacting kinases of the protein. We studied the interactions between Panx1a with two kinases: ERK2 and CaMKIIa. Our results indicated that a strong interaction exists with CaMKIIa, which plays a role in the trafficking dynamics of Panx1a to the cell membrane. The overexpression of CaMKIIa led to an accumulation of Panx1a in the intracellular compartments. We investigated the effects of various CaMKIIa functional and structural mutants on expression and interaction with Panx1a. We found that the constitutively active T286D CaMKIIa mutant leads to a partial rescue in Panx1a expression, suggesting that Panx1a requires phosphorylation by CaMKIIa for proper cell membrane localization. Together, the research in this thesis provides novel findings that contribute to the phospho-proteomic exploration of Panx1 channel activity and regulation.

DEDICATION

I would like to dedicate this dissertation to my amazing and supportive family, my loving husband, and my son.

ACKNOWLEDGEMENTS

First, I would like to thank my supervising professor, Dr. Georg Zoidl. Working alongside such a kind, encouraging, and patient person has been an honor. I have learned a great deal from him, both intellectually and personally. He was instrumental in my decision to pursue graduate studies due to his passion and love of science and his approachable and warm personality.

I would also like to extend my gratitude to Christian Zoidl. Early in my graduate school journey, Christine was significantly influential in shaping me as a scientist by training me in proper lab practices. I have to admit, as an individual that has never been very organized or detail oriented, I have learned invaluable skills from Christiane that have helped me overcome these drawbacks.

Next, a big thank you to my committee members, Dr. Michael Scheid and Dr. Mark Bayfield. I greatly appreciate the academic support and advice provided throughout my graduate studies.

Of course, who can forget my partner in crime, Anna Kotova! Friendships mean everything to me, and finding an individual with whom I can confide in, trust, and enjoy every moment is probably the most important thing that came out of all of this. This experience has been so much more fun and enjoyable with you by my side the entire time.

Finally, thank you to my lab mates in the Zoidl group. It was a pleasure working with you all, and I wish you the best in your future.

STATEMENT OF CONTRIBUTIONS

Ksenia Timonina authors this thesis. Unless specified otherwise, all experiments and writing of the first author manuscripts were performed by Ksenia. Portions of the material included in the thesis have either been published in peer-reviewed journals or are manuscripts in preparation.

Chapter 3: **Timonina, K**., Kotova, A., & Zoidl, G. (2020). Role of an aromatic–aromatic interaction in the assembly and trafficking of the zebrafish panx1a membrane channel. Biomolecules, 10(2), 272. https://doi.org/10.3390/biom10020272

Chapter 5: **Timonina, K**., Kotova, A., Zoidl, G. The trafficking and localization of the zebrafish Panx1a are regulated via interaction with CaMKIIa. Manuscript in preparation.

Co-authors of the manuscripts above have contributed in either performing the experiments, writing/editing of manuscripts, or data interpretation:

Dr. Georg Zoidl oversaw the projects, provided mentorship, assisted with data interpretation/analysis, and helped with manuscript preparation.

Anna Kotova collected data for experiments involving Caveolin-1 co-localization (Chapter 3) and TIRF microscopy (Chapter 5).

I have also made other contributions to publications and manuscripts in preparation (which are not included in this thesis) by performing experiments and writing portions of the manuscripts:

Performed co-localization experiments: Kotova, A., **Timonina, K**., & Zoidl, G. R. (2020). Endocytosis of connexin 36 is mediated by interaction with caveolin-1. International Journal of Molecular Sciences, 21(15), 5401. https://doi.org/10.3390/ijms21155401

Performed dye uptake assays: Tetenborg, S., Liss, V., Breitsprecher, L., **Timonina, K.,** Kotova, A., Hecker, A. J. A., ... & John, O. (2022). Intralumenal docking of Cx36 channels in the ER isolates mis-trafficked protein. bioRxiv. https://doi.org/10.1101/2022.07.15.500247

Performed calcium imaging experiments: Yousefi, T., **Timonina, K**., Zoidl, G., & Kassiri, H. (2021, October). A Temperature-Aware Fully-Wireless mm-Scale Optically-Enhanced Optogenetic Neuro-Stimulator. In 2021 IEEE Biomedical Circuits and Systems Conference (BioCAS) (pp. 01-05). IEEE. https://doi.org/ 10.1109/BioCAS49922.2021.9644947

Performed calcium imaging experiments: Yousefi, T., **Timonina, K**., Zoidl, G., & Kassiri, H. An Implantable Optogenetic Neuro-Stimulator SoC with Extended Optical Pulse-Width Enabled by Supply-Variation-Immune Cycled Light-Toggling Stimulation. IEEE transactions on biomedical circuits and systems. https://doi.org/ 10.1109/TBCAS.2022.3198911.

Performed dye uptake assays: Siu, R. C., Kotova, A., **Timonina, K.**, Zoidl, C., & Zoidl, G. R. (2021). Convergent NMDA receptor—Pannexin1 signaling pathways regulate the interaction of CaMKII with Connexin-36. Communications biology, 4(1), 1-14. https://doi.org/10.1038/s42003-021-02230-x

Collected data for anatomical fish larvae features: Kotova, A., **Timonina, K.**, Zoidl, C., & Zoidl, G. R. Connexin 27.5 is critical for visual perception and processing in zebrafish. Manuscript in preparation.

TABLE OF CONTENTS

LIST OF FIGURES

LIST OF TABLES

LIST OF SUPPLEMENTARY FIGURES

LIST OF ABBREVIATIONS

Symbol	Definition
AMPA	α-amino-3-hydroxy-5-methyl-4-isoxazole propionic acid
AMPK	Amp-activated protein kinase
Å	Angstrom
ATP	adenosine-5'-triphosphate
BFA	Brefeldin A
BSA	Bovine serum albumin
$Ca2^{+}$	Calcium ion
cAMP	3'-5'-cyclic adenosine monophosphate
CaMKII	Calcium/calmodulin-dependent protein kinase type II
Cav	Caveolin
CL	Cytoplasmic loop
CT	Carboxy terminus
CNS	Central nervous system
CoIP	Co-immunoprecipitation
Cryo-EM	Cryo-electron microscopy
Cx	Connexin
DEF	Docking site for ERK, FXFP
DMEM	Dulbecco's Modified Eagle Medium
DNA	Deoxyribonucleic acid
ECFP	Enhanced cyan fluorescent protein
EGFP	Enhanced green fluorescent protein
EYFP	Enhanced yellow fluorescent protein
ECD	Extracellular Domain
ECL	Extracellular loop
Endo H	Endoglycosidase H
ER	Endoplasmic reticulum
EtBr	Ethidium bromide
FRAP	Fluorescent recovery after photobleaching
FRET	Förster Resonance Energy Transfer Analysis
Gly0	Core glycosylation / unglycosylated
Gly1	High Mannose glycosylation
Gly2	Complex glycosylation
GSK3	Glycogen synthase kinase 3
HEK293	Human Embryonic Kidney 293 cells
INX	Innexin
ICL	Intracellular domain

KCl	Potassium chloride
kDa	Kilodaltons
KO	Knockout
MAPK/ERK	Mitogen activated protein kinase
MEK	Mitogen activated protein kinase kinase
mL	Milliliter
mM	Millimolar
Neuro 2a	Neuroblastoma 2a
nl	Nanolitre
NMDAR	N-methyl-D-aspartate receptor
Panx	Pannexin
PBS	Phosphate buffered saline
PCR	Polymerase chain reaction
PKA	Protein kinase A or cAMP-dependent protein kinase
PKG	Protein kinase G
PTM	Post-translational modification
REST	Relative Expression Software Tool
RNA	Ribonucleic acid
ROI	Region of interest
RT	Room temperature
SCAM	Scanning cysteine-alanine mutagenesis
SDS-PAGE	Sodium dodecyl sulfate-polyacrylamide gel electrophoresis
SFK	Src family kinase
SEM	Standard error of the mean
TALEN	Transcription activator-like effector technology
TIRF	Total Internal Reflection Fluorescence
TL	Topfel longfin
TMD	Transmembrane domain
WT	Wild-type
uL	Microlitre
uM	Micromolar
um	Micrometer

Chapter 1. Introduction

1.1. Pannexins overview

Pannexins were first discovered as the vertebrate homologs to the invertebrate gap junction proteins known as Innexins (Panchin et al., 2000). Gap junction proteins form channels that allow for the passage of ions and small molecules from one cell to another. In vertebrates, gap junction proteins are composed of a family of proteins called Connexins (Panchin et al., 2000). Although Pannexins and Connexins share no sequence homology, their subunits have similar topologies. Each subunit comprises four transmembrane domains, two extracellular loops, one intracellular loop, and intracellular N and C terminal tails (Panchin et al., 2000; Yen and Saier Jr, 2007; Baranova et al., 2004).

Although initially believed to form gap junctions, Pannexins function as single membrane channels and do not connect the cytoplasms of adjacent cells (Sosinsky et al., 2011). Instead, Pannexins provide a passage for small molecules between the cytoplasm and the extracellular environment of the cell (Ambrosi et al., 2010). Whereas Connexins localize in “punctate spots” at cell-to-cell contact points, Pannexin channels localize throughout the plasma membrane (Sosinsky et al., 2011). Another critical difference between the two families of proteins is the extracellular cysteine residues. Six conserved cysteine residues reside in the extracellular loops of the Connexin proteins, forming three disulfide intra-connexin bridges, while Pannexins have only four conserved cysteine residues (Sosinsy et al., 2011). The presence of these cysteines was shown to influence the formation of gap junction channels (Dahl et al., 1992). Furthermore, Pannexins undergo a critical post-translation modification, glycosylation, which is not

observed in Connexins (Penuela et al., 2007). This modification is located on the extracellular side of Pannexins and potentially prevents the docking of two channels (Boassa et al., 2007).

1.1.1. Pannexin Family

The Pannexin family is composed of three members: Pannexin-1 (Panx1), Pannexin-2 (Panx2), and Pannexin-3 (Panx3). Each Pannexin member has a similar topology, with some differences in their sequences. The sequence of the C terminal is the most variable among the three members, whereas the N terminal is the highest conserved region (Penuela et al., 2013). Panx1 is closely related to Panx3, whereas Panx2 displays the highest similarity to the invertebrate sequence (Baranova et al., 2004; Bond and Naus, 2014; Ambrosi et al., 2010). It has been suggested that Panx1 can form heteromeric channels with either Panx2 or Panx3, but Panx2 and Panx3 cannot intermix. However, the resulting heteromeric channels are not conductive and are unstable (Bruzzone et al., 2005; Penuela et al., 2009).

Several factors contribute to the differences between the three Pannexins in the Pannexin family. The expression patterns vary between each member. Panx3 is expressed in the skin, osteoblasts, cartilage, heart ventricles, cochlea, and potentially in the brain (Bruzzone et al., 2003; Penuela et al., 2007; Celetti et al., 2010; Wang et al., 2009). Panx2 is expressed in the eye, thyroid, liver, enteric nervous system, brain, and spinal cord (Baranova et al., 2004; Bruzzone et al., 2003; Dvoriantchikova et al., 2006; Vogt et al., 2005; Ray et al., 2006; Le Vasseur et al., 2014). Panx1 is ubiquitously expressed in most tissues (Whyte-Fagundes and Zoidl, 2018). To date, Panx1 has been the most studied of the three. Its expression has been characterized in blood and immune

cells, in sensory systems such as the eye, ear, taste buds, olfactory epithelium, and many organs (Dvoriantchikova et al., 2006; Kienitz et al., 2011; Locovei et al., 2006); Schenk et al., 2008; Seminario-Vidal et al., 2009; Woehrle et al., 2010; Bruzzone et al., 2003; Huang et al., 2007; Dando and Roper, 2009; Wang et al., 2009; Kurtenbach et al., 2014). Their expression at a cellular level also seems to differ. Panx1 shows expression in the plasma membrane, endosomal membranes, and endoplasmic reticulum (ER) membranes (Penuela et al., 2009; Abeele et al., 2006, Boyce et al., 2015). Although Panx3 exhibits a similar localization pattern to Panx1, Panx2 is mainly localized in the intracellular compartments (Penuela et al., 2009; Boassa et al., 2015; Wicki-Stordeur et al., 2013).

Another key factor differentiating the three Pannexins is the post-translational modification of glycosylation. Panx1 has been shown to undergo N-linked glycosylation on asparagine 254 in the second extracellular loop, Panx3 is glycosylated on asparagine 71 in the first extracellular loop, and Panx2 is glycosylated on asparagine 86 in its first extracellular loop (Penuela et al., 2007; Penuela et al., 2009) (**Figure 1.1**). Furthermore, Panx1 and Panx3 can be modified to the complex glycosylated form, whereas Panx2 is only modified to the high mannose glycosylated state (Penuela et al., 2009).

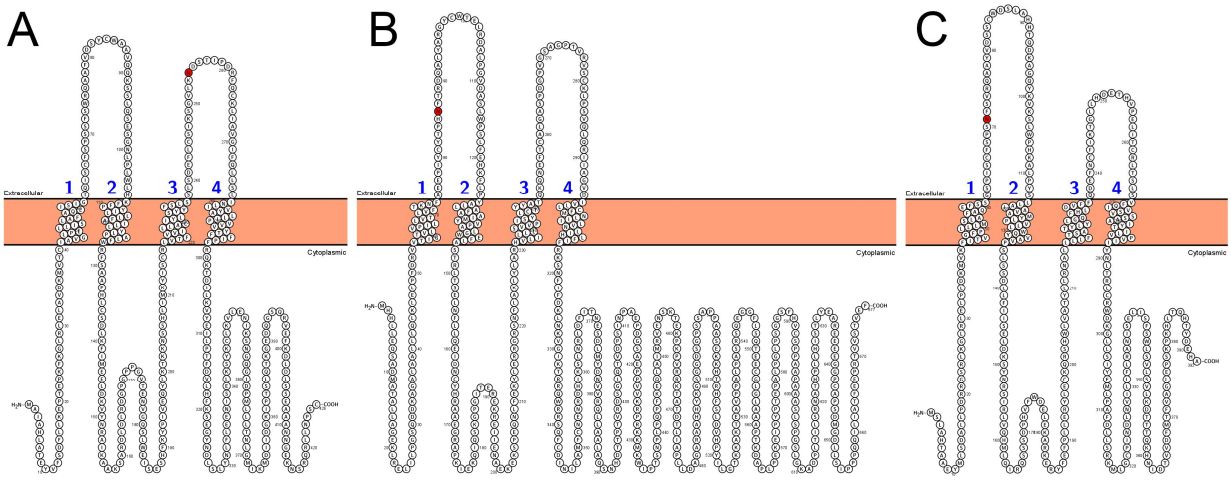

Figure 1.1 Topological representation of the three Pannexin family members (mouse). (A) Panx1, (B) Panx2, and (C) Panx3 show similar topological structures with four transmembrane domains (as indicated by the numbers), two extracellular loops, and cytoplasmic N terminal, C terminal, and loop. The N-glycosylation modification is labeled in red for each Pannexin member, with Panx1 glycosylated on N254, Panx2 on N86, and Panx3 on N71. Structures were visualized using the Protter open-source tool (Omasits et al., 2014).

1.1.2. Pannexin-1 channel function

Panx1 has been extensively characterized as an adenosine-5'-triphosphate (ATP) release channel and studied for its implications in the inflammatory processes and ischemic cell death. Panx1 has been shown to release ATP into the extracellular environment through its interaction with purinergic receptors, which can act as recruiting signals for phagocytes in apoptotic cells (Li et al., 2018; Chekeni et al., 2010). In these apoptotic cells, caspase proteins can cleave the C terminal tail (at residues 376-379) of Panx1, resulting in an activated channel that allows for the release of intracellular ATP. ATP release via Panx1 has also been shown to play a role in mucociliary lung clearance, olfactory sensory neurons, activation of insulin-stimulated glucose uptake, potentiation of skeletal muscle contraction, and the regulation of vasoconstriction (Ransford et al., 2009; Krick et al., 2016; Kurtenbach et al., 2014; Adamson et al., 2015; Riquelme et al., 2013;

Billaud et al., 2011). Its role in inflammatory response has also been explored. Panx1 is thought to promote inflammasome activation in response to injury, causing the extracellular release of pro-inflammatory cytokines interleukin 1 beta via the P2X7 receptor (Pelegrin and Surprenant, 2006). Furthermore, it has been shown to participate in acute inflammation by regulating the adhesion and emigration of leukocytes through the venous endothelium (Lohman et al., 2015). Panx1's involvement in epilepsy was proposed due to the elevated expression of Panx1 in animal models and human patients with increased seizure activity (Mylvaganam et al., 2010; Jiang et al., 2013; Li et al., 2017). As epilepsy and seizure activity leads to increased extracellular concentrations of potassium, it is reasonable to believe that Panx1, a channel that is largely regulated by elevated extracellular potassium (as described in the next section), would have a role in epilepsy. Another factor that leads to an increased susceptibility to seizures is the involvement of glutamate (DiNuzzo et al., 2014). Glutamate release has been previously shown to be regulated by Panx1 in astrocytes (Wei et al., 2016), suggesting that Panx1 participates in epileptic activity.

1.1.3. Pannexin-1 regulation at a protein level

Since its discovery, numerous methods of activation of the Panx1 channel have been proposed. Some methods have been explored more than others, and some have had conflicting data. Further, each method's exact mechanism of action remains poorly understood.

As previously mentioned, one of the widely believed mechanisms of regulation of Panx1 channels is extracellular potassium. An increase in extracellular potassium, either through potassium chloride (KCl) or potassium gluconate application, has been shown to

activate Panx1 channels (Jackson et al., 2014). Another mechanism of Panx1 activation is increased intracellular calcium levels (Locovei et al., 2006; Kurtenbach et al., 2013). In addition to calcium activation, Locovei et al. showed that ATP can also regulate Panx1 channels via P2Y receptors (Locovei et al., 2006). Interestingly, not only does ATP activate Panx1, but it can also inhibit Panx1 activity, depending on the concentration (Qiu et al., 2009). Further, besides playing a role in the activation of Panx1, ATP has been shown to cause Panx1 internalization, leading to a decrease in the channels at the cell surface (Boyce et al., 2015). Mechanical stimulation also influences Panx1 activity, as seen in oocytes (Bao et al., 2004) and neurons (Xia et al., 2012). Panx1 channels also seem to be sensitive to the environment's pH. An increasingly basic environment can activate zebrafish Panx1 channels, as seen with dye uptake experiments (Kurtenbach et al., 2013). Finally, post-translational modifications play a significant role in regulating Panx1 activity (and trafficking). This type of regulation will be covered in the next section.

1.1.4. Pannexin-1 post-translational modifications

Post-translational modifications have been shown to affect Panx1 in two major ways: trafficking/localization and functionality. Some common post-translational protein modifications include phosphorylation, acetylation, glycosylation, methylation, and ubiquitylation (Walsh et al., 2005). This section summarizes the post-translational modifications that have been shown in Panx1. A topological representation of the mouse Panx1 maps the post-translational modifications on a single subunit of the channel (**Figure 1.2**).

1.1.4.1. Glycosylation

As previously briefly mentioned, one of the original post-translational modifications identified for Panx1 is N-glycosylation. N-glycosylation is a modification that occurs during the trafficking stages of many eukaryotic membrane proteins and is essential for protein folding, trafficking, and stabilization (Cheung and Reithmeier, 2007). As the name suggests, the modification consists of adding an oligosaccharide to an asparagine residue. Generally, N-glycosylated membrane proteins are synthesized and undergo the first glycosylation modification in the ER, from where they travel to the cis Golgi to be trimmed to a high-mannose oligosaccharide. Next, the modification is further processed to a complex oligosaccharide in the medial Golgi. From there, it travels to the trans Golgi and finally the membrane. This modification gives Panx1 its distinct three-band expression pattern on western blots, with the highest band representing the complex, mature state, the middle band representing the high-mannose state, and the lowest band representing the unglycosylated form of Panx1 (Penuela et al., 2009). These glycosylation modifications were confirmed by treatment with both N-Glycosidase F and Endoglycosidase H (Endo H). The state of Panx1 glycosylation is associated with specific localization patterns within the cell. The unglycosylated core protein undergoes its first modification to the high-mannose state in the ER, at which point it is sensitive to Endo H treatment. Then, it is further modified to the complex glycosylated form in the Golgi apparatus, from where it is ready to move to the plasma membrane (Boassa et al., 2007). A mutational analysis where the glycosylation residue N254 of Panx1 was mutated to glutamine confirmed the lack of glycosylation. This mutation diminished plasma membrane localization and channel activity (Penuela et al., 2007; Penuela et al., 2009).

These studies also demonstrated that the glycosylation deficient Panx1 mutant could be partially rescued to the cell surface when co-expressed with the wild type (WT), glycosylated Panx3. However, this is not to say that the unglycosylated Panx1 form is not present on the cell surface. A subpopulation of the unmodified Panx1 is detectable at the membrane, as seen by the cell surface biotinylation assay (Gehi et al., 2011).

1.1.4.2. Phosphorylation

Following glycosylation, phosphorylation has been the next rising post-translational modification of interest in the Panx1 field. Several residues have been shown to be phosphorylated, mainly located in the cytoplasmic loop or the cytoplasmic tail. Interestingly, multiple studies identified the Src family kinases (SFKs) in regulating Panx1 activity. As previously mentioned, Panx1 proteins can interact with purinergic receptors. The P2X7 receptor is involved in the activation of Panx1, with Src kinase taking part in this signal transduction pathway (Iglesias et al., 2008). The research group proposed that Src kinase activates Panx1 via phosphorylation in response to P2X7 receptor stimulation. They show that by inhibiting Src kinase with a known blocker, PP2, Panx1 activation in response to treatment with BzATP is attenuated.

Further, Src kinases were also shown to be involved in Panx1 activation through NMDA receptor (NMDAR) activation in response to anoxic conditions (Weilinger et al., 2012). Here, the group identified the exact residue that undergoes phosphorylation modification: Y308, located in the C terminal tail of Panx1. Under anoxic conditions, NMDA activates Src kinase, as seen by the increase in the phosphorylated activated form of the kinase. This activated kinase can then regulate the Panx1 opening, and the inhibition of the kinase via PP2 treatment attenuated the opening of Panx1 in response

to anoxia. The group used an interfering peptide against the Y308 region of Panx1 to show that this residue is required to activate the channel during anoxia, even with an activated Src kinase. Although the phosphorylation of Y308 was at this point speculation, it was later confirmed in a study that demonstrated that NMDARs, Src kinase, and Panx1 form a signaling complex in response to ischemia or stroke (Weilinger et al., 2016). Using a phospho-specific antibody against pY308 of Panx1, the group showed that Src kinase indeed phosphorylates Panx1, and this modification is absent in cells lacking Src kinase or cells treated with PP2. They concluded that this complex's formation during excitotoxicity depends on the phosphorylation of this residue.

The cytoplasmic loop of Panx1 has also been shown to be a substrate for phosphorylation by Src kinase. In the venous endothelial cells, Src kinase can activate Panx1 as part of the TNF-a receptor signalling pathway (Lohman et al., 2015). In vascular inflammation, the TNF-a receptor is activated, which leads to the recruitment of Src kinase that phosphorylates and activates Panx1 ATP release, showing that Panx1 channels play a role in promoting leukocyte adhesion and emigration during inflammation. Using a phospho-specific antibody against a highly conserved residue in the cytoplasmic loop of Panx1, Y198, the research group showed that Src kinase phosphorylated Panx1 during this signaling pathway. The overexpression of Src kinase in Human Umbilical Vein Endothelial Cells (HUVECs) increased Y198 phosphorylation, whereas the inhibition of Src using i-Src showed a decrease in its phosphorylation state. To show that this phosphorylation event was part of the TNF-a signalling, they treated cells with TNF-a and observed an increase in phosphorylation of Y198. The same could not be said when cells were also treated with PP2 Src kinase inhibitor.

Aside from Src kinase's role in regulating Panx1 activity, there has been evidence leading to its role in regulating Panx1 trafficking. The Y150 residue, located in the cytoplasmic loop of Panx1, has been proposed to be a phosphorylation target for Src kinases (Nouri-Nejad et al., 2021). In melanoma cancer tumors, the Y150F mutant form of Panx1 was identified. As the Phenylalanine residue cannot undergo phosphorylation modification, it would mean that this mutation prevents phosphorylation. The Y150F mutant also showed to lack the complex N-glycosylation modification, resulting in increased intracellular expression. The group demonstrated that this residue was subject to phosphorylation by ectopically expressing Panx1, immunoprecipitation it, and performing mass spectrometry to identify phosphorylated peptides. They then treated cells with PP2 Src inhibitor and saw that although the total levels of Panx1 remained the same, the high mannose Gly1 species were decreased in wild-type Panx1 as opposed to no change in Y150F mutant. This experiment and the presence of a consensus sequence for Src kinase phosphorylation at Y150 show evidence that Src kinase does phosphorylate this residue; however, further exploration is needed to confirm this.

There has also been evidence of serine/threonine phosphorylation events that regulate Panx1 activity. S206, located in the cytoplasmic loop, was predicted to be phosphorylated by protein kinase G (PKG) in Human Embryonic Kidney 293 (HEK293) cells exposed to nitric oxide (Poornima et al., 2015). The research group showed that nitric oxide activated PKG, reducing Panx1 activity. This reduction was abolished when treating cells with KT5823, a PKG inhibitor. When treating cells with sodium nitroprusside, a nitric oxide donor, an increase of serine phosphorylation in immunoprecipitated Panx1 was observed. Using in silico predictions, S206 was identified as a potential candidate for

PKG phosphorylation. The S206A mutant abolished the nitric oxide inhibition, leading to the conclusion that this residue is the phosphorylation target for PKG.

Phosphorylation has also been predicted to inhibit Panx1 activity in response to mechanical stretch via PKA. T302 and S328, located in the C terminal tail of Panx1, have been proposed to be phosphorylated by PKA (Lopez et al., 2020). The research group used adenosine and cAMP analog treatment of HeLa cells transfected with Panx1 to show that the channel's activity is reduced in DAPI uptake assays. This reduction was prevented when pre-treating cells with PKI, a PKA inhibitor, suggesting that the Panx1 inhibition was due to a phosphorylation event by PKA. S302 and S328 were the predicted sites for PKA phosphorylation. Upon mutating these residues to alanine, the effects of cAMP treatment were diminished. Further, the phospho-mimicking mutations to aspartate resulted in a loss of activation of Panx1 in response to mechanical stretch, as seen with DAPI uptakes.

Another potential serine/threonine phosphorylation event occurs on S394 in the C terminal tail (Lopez et al., 2021). This residue is believed to be phosphorylated by CaMKII. Using HeLa cells, the research group showed that the S394A mutant lost its ability to uptake DAPI in response to membrane stretch, whereas S394D, the phospho-mimicking mutant, regained this activity. They also showed that the activation of Panx1 in response to membrane stretch requires active CaMKII by treating HeLa-transfected Panx1 cells with Calmodulin antagonist W7 and CaMKII inhibitor KN62. S394 was identified initially via *in silico* prediction as a CaMKII phosphorylation site. Interestingly, the S394D mutant resulted in internalized expression of Panx1, showing a vesicular distribution. The authors believe this is due to the active Panx1 interaction with P2 receptors, resulting in

internalization (Boyce et al., 2015). They treated cells with a P2 receptor blocker, suramin, to overcome this internalization. They showed that the S394D mutant resulted in higher DAPI uptake in suramin-treated cells compared to WT Panx1. However, it is important to note that this study used rat Panx1 constructs, whereas the S394 residue is not conserved in human Panx1.

1.1.4.3. S-nitrosylation and oxidation

S-nitrosylation is a post-translational modification whereby a nitric oxide moiety binds to a cysteine residue via a covalent interaction. This modification is reversible and can affect a protein's functionality and activity. Interestingly, nitric oxide has been shown to have a role in ischemia, a condition associated with Panx1. One of the first pieces of evidence of Panx1 having this post-translational modification was observed using nitric oxide donor and nitric oxide synthase inhibitors in hippocampal neurons (Zhang et al., 2008). The research group found that nitric oxide may have a role in regulating the opening of Panx1. Following this, a study showed that Panx1 undergoes S-nitrosylation in HEK293T cells using nitric oxide donors (Lohman et al., 2012). They found that these donors attenuated Panx1 activity, as seen in electrophysiological and ATP release assays. Furthermore, the researchers identified two cysteine residues that undergo this modification: C40 and C346. By mutating these residues to alanine, they saw that the nitric oxide donor treatment no longer inhibited Panx1 activity, suggesting that this S-nitrosylation plays an important role in inhibiting Panx1 channels. Further evidence of C346 residue impacting channel activity was seen in a separate study, where the mutagenesis of C346 to a serine resulted in a constitutively active channel (Bunse et al., 2010).

A terminal cysteine residue of Panx1, C426, has been shown to undergo oxidation and thereby inhibiting the channel activity (Krick et al., 2016). Using human airway epithelial cells, the research group showed that treatment with IFN-y resulted in the up-regulation of dual oxidase 2, which increases H2O2 levels, leading to the temporary Panx1 inhibition via oxidation of C426.

1.1.4.4. Other post-translational modifications

As the C terminal tail is often a central hub for post-translational modifications and interaction sites due to its highly divergent nature, it is no surprise that a CT deficient Panx1 mutant results in diminished trafficking capabilities. The Panx1Δ307 mutant showed a reduced expression at the cell surface, as demonstrated by immunoblotting and immunolocalization studies (Gehi et al., 2011). Further, a study showed that the proximal region of the Panx1 CT, R299-D378, is vital for cell surface localization (Epp et al., 2019). They used Panx1 CT deletion mutants to demonstrate that while a whole CT deletion affects the cell surface localization, a deletion from residue 379 and onwards does not. They describe a leucine-rich repeat motif (LRR) at residues S328-K348 within the proximal region of the CT, which is required for the proper localization of Panx1.

The C terminal tail is also vital for the Panx1 channel function. There has been evidence of the C terminal tail cleavage by caspase 3, 7, and 11 at the D379 residue of the human Panx1 (D378 of mouse Panx1) (Spagnol et al., 2014; Sandilos et al., 2012; Yang et al., 2015; de Gassart and Martinon, 2015; Chekeni et al., 2010). Cleavage of this region results in a leaky, constitutively active channel. This type of post-translational modification is non-reversible and, therefore, could result in cell death due to this constitutive activity.

Ubiquitination is one of the modifications that have not yet been extensively explored in Panx1. The formation of ubiquitin chains, or polyubiquitination, often leads to the proteolysis and degradation of the tagged protein (Guo and Tadi, 2021). A study that characterized the ubiquitinome in HCT116 cells identified two residues of human Panx1 that are subject to ubiquitination: K380 and K409, both located in the C terminal tail (Kim et al., 2011). However, more research is needed to explore the full extent of these modifications.

There has also been recent evidence of acetylation modification of Panx1 channels at several lysine residues identified by mass spectrometry: K140, K321, K374, K381, and K409 (Chiu et al., 2021). The research group found that of these, K140 and K409 are constitutively acetylated and that the K140 residue is likely most important for the regulation of channel activity. The channel's activity depends on the deacetylation of K140 by alpha-1-adrenergic receptor (α1D-AR), Gαq, and a non-canonical RhoA-mammalian diaphanous (mDia)-HDAC6 signaling pathway.

.

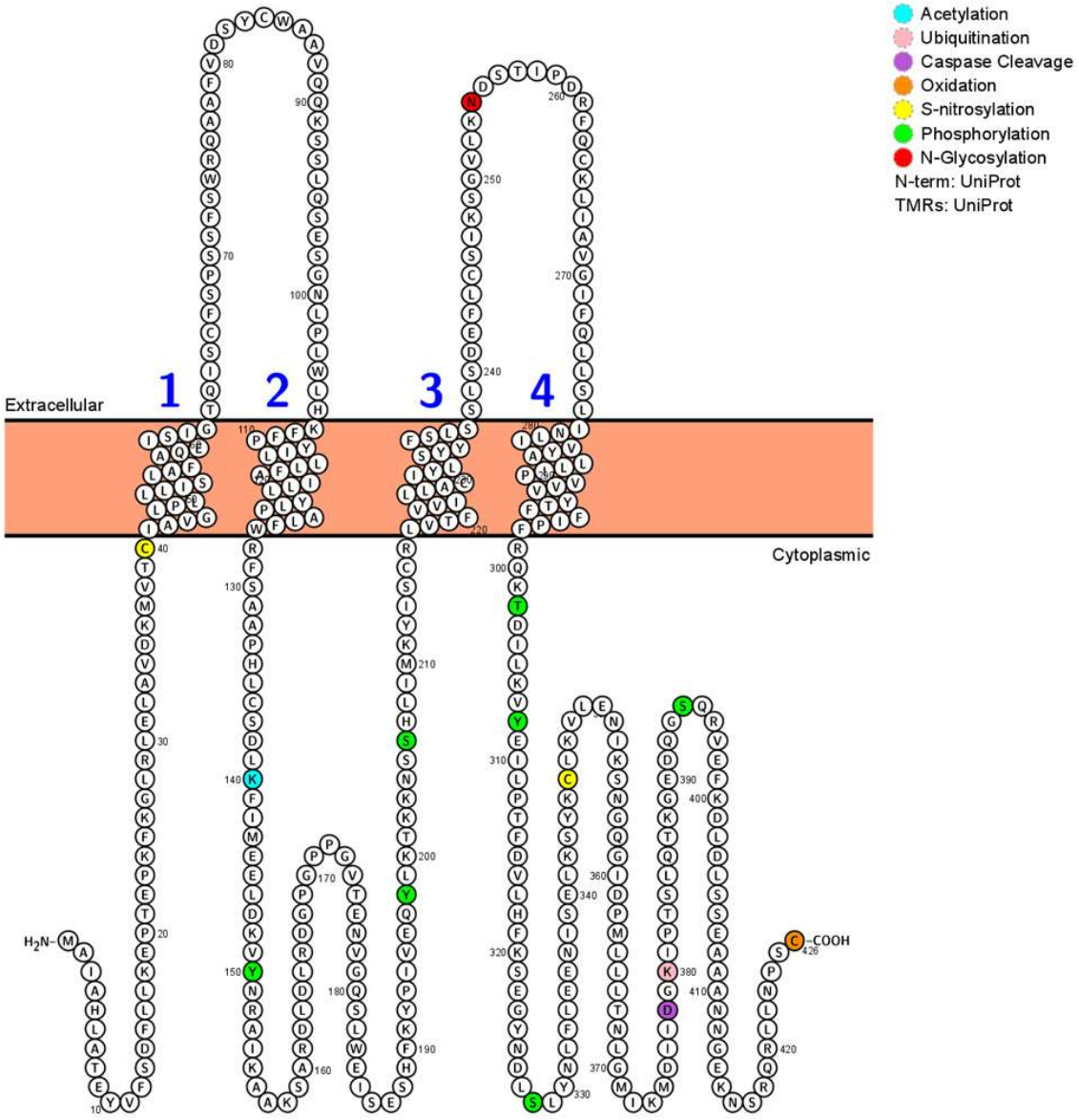

Figure 1.2. Topological representation of the mouse Panx1 subunit with the investigated and proposed post-translational modifications. Protein topological structure and labeled PTMs were visualized using the Protter open-source tool (Omasits et al., 2014)

1.1.5. Pannexin-1 structure

Since its discovery, Panx1 was assumed to form hexameric channels, similar to the gap junction protein family of Connexins. However, as previously discussed, Panx1s do not form gap junction channels, likely due to the glycosylation post-translational

modification required for proper protein trafficking, which prevents docking to Panx1 channels in adjacent cells. Therefore, although topologically similar, Panx1s and Connexins are not functionally the same, and it is no surprise that Panx1s do not form hexametric channels with recent discoveries.

In 2020, multiple research groups independently found that Panx1s form homomeric heptameric channels (Deng et al., 2020; Jin et al., 2020; Michalski et al., 2020; Qu et al. 2020; Ruan et al., 2020). These research groups used cryo-electron microscopy (cryo-EM) to determine the resolution structures of *Homo sapiens* and *Xenopus tropicalis* Panx1. These studies used different versions of Panx1: truncated C terminal tail, removal of residues from the cytoplasmic loop, mutated Panx1 at the caspase cleavage site (D376E/D379E), and the full-length protein. The results show that the structures from the various studies were similar, with the extracellular and transmembrane domains nearly identical (Mim et al., 2021).

The dimensions of the Panx1 channel can provide us with insight into its functional properties. The channel was found to be ~105-110 Å long and ~100 Å wide (**Figure 1.3A**). The regions around the intracellular and extracellular boundaries are composed of mainly positively charged residues, which is in line with the known function of Panx1 for transporting negatively charged molecules like chloride ions and ATP. The extracellular domain also functions as the size restrictive region, with a diameter of ~9 Å at the narrowest site (at residue W74 highlighted in green) (**Figure 1.3B**), which is large enough to pass ATP molecules (Jin et al., 2020). However, the exact dynamics and sizes of the Panx1 structure in its active or inactive conformations remain to be investigated. It is

possible that the pore size changes as the channel gets activated and can even have multiple open conformations to allow the passage of various molecules.

.

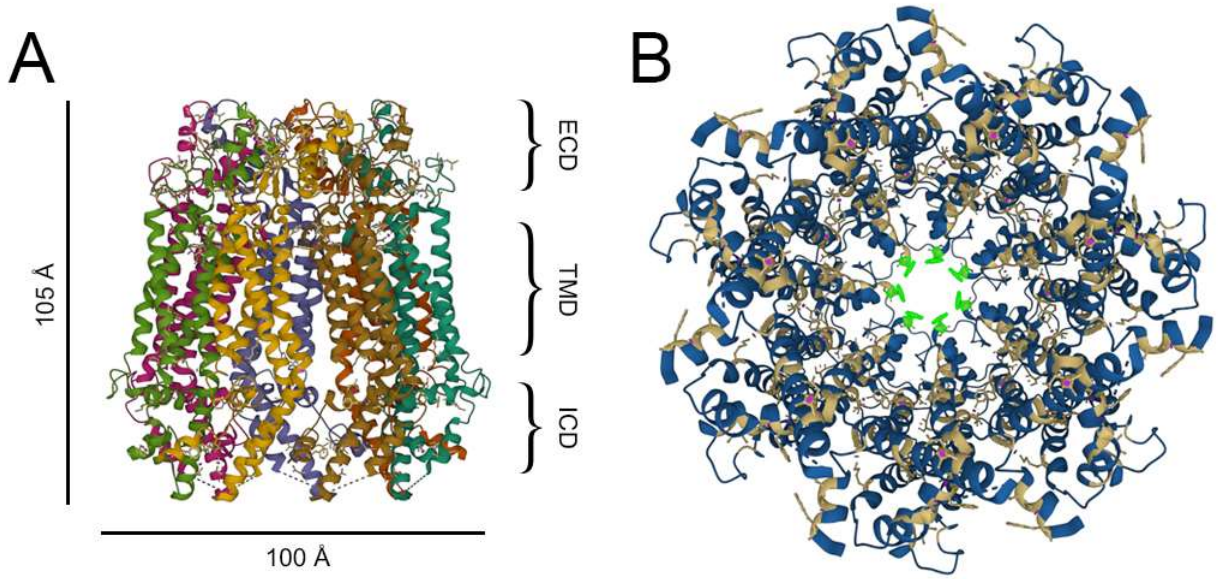

Figure 1.3. Structure and size of the human Panx1 channel. (A) Size of the Panx1 channel with the seven individual subunits represented by the different colours. (B) The Panx1 pore shows the narrowest region at the W74 residue highlighted in green. ECD: extracellular domain, TMD: transmembrane domain, ICD: intracellular domain. Images were created using Mol Viewer (Sehnal et al., 2021), PDB ID#6M66 (DOI: 10.2210/pdb6M66/pdb) (Jin et al., 2020) from RCSB PDB rcsb.org (Berman et al., 2000).*

1.2. Zebrafish Pannexins

The zebrafish model is a beneficial organism to study various biological attributes, including brain function both physiologically and at a cellular level. Specifically, the zebrafish model can be used in research focusing on early development, as fertilization and growth occur externally, and the embryo and larvae are transparent. In neurobiology, this model also serves as a tool for studying the biological basis of learning and memory through various behavioural tests (Blaser and Vira, 2014; Gerlai, 2016). Although there

are undeniable similarities in the zebrafish neurobiology compared to the mammalian model, the fish model is a simplified version (Blaser and Vira, 2014). However, this simplification is useful when elucidating complex biological mechanisms that can eventually transfer to mammalian system research. Further, the combination of transparent embryo development and the faster growth period gives the zebrafish model an edge in the field of genetic manipulation (Sertori et al., 2016). Genome editing techniques such as zinc finger nucleases (ZFNs), transcription activator-like effector nucleases (TALENs), and clustered regularly interspaced short palindromic repeats (CRISPR) can be applied to the zebrafish model for studying specific neurological pathways from a molecular and cellular to the behavioural level.

The evolution of zebrafish has created multiple replicate genes via the Teleost whole-genome duplication events. The first two events occurred 400-600 million years ago, and the third occurred 320-350 million years ago (Bond et al., 2012). Although one of the duplicated genes can be inactivated over time, some copies will remain if there is a selective advantage in both genes (Force et al., 1999). It is believed that the Panx1 gene was duplicated in zebrafish during the third whole genome duplication event. This event resulted in two functional Panx1 genes: *Panx1a*, located on chromosome 15, and *Panx1b*, located on chromosome 5 (Bond et al., 2012). Only one copy of both *Panx2* and *Panx3* genes was identified in the zebrafish genome.

The expression patterns of these Pannexin genes differ. At the transcription level, Panx2 is expressed in the eye and the brain, Panx3 has the highest expression in the skin, brain, fin, and gills, Panx1a has ubiquitous expression, and Panx1b is mainly expressed in the brain and the eye (Bond et al., 2012; Prochnow et al., 2009; Zoidl et al.,

2008). Interestingly, while both Panx1a and Panx1b are expressed in the retina of the zebrafish eye, the localization patterns are distinct. Panx1a protein expression was detected in the outer retina, part of the outer plexiform layer, via immunohistochemistry (Prochnow et al., 2009). This suggests that the protein is expressed in the horizontal cells and was also proven using a knockout Panx1a −/− larvae zebrafish model (Safarian et al., 2020). Contrastingly, Panx1b expression was detected in the inner nuclear layer and the ganglion cell layer of the retina of the adult zebrafish (Kurtenbach et al., 2013). This was confirmed in the knockout Panx1b −/− adult zebrafish model (Safarian et al., 2021).

The distinct expression patterns suggest different roles for each Panx1 zebrafish ohnologues. Indeed, key differences were observed in the specific ohnologue knockout zebrafish models. In two separate studies, Safarian et al. characterized the Panx1a and Panx1b knockout zebrafish (Safarian et al., 2020; Safarian et al., 2021). The survival rate of Panx1a knockout larvae did not differ from the wild-type TL fish, while the Panx1b knockout model had a significantly lower rate. Further, while the Panx1a knockouts were anatomically normal, a portion of the Panx1b knockout larvae showed malformations that included swimming bladder edemas, ventricular hypertrophy, irregularly shaped yolk sacs, and abnormal spinal curvature. These anatomically malformed larvae did not survive past 5/6 days post fertilization. The larvae that survived to adulthood had no issues with fertility and reproduction for both knockout models. It is also worth noting that although the mammalian mouse model showed a compensatory role of Panx3 in the Panx1 knockout model (Whyte-Fagundes et al., 2018), no compensation was detected for either of the zebrafish knockout models. The main findings of these knockout studies suggest that Panx1a is involved in dopaminergic signaling and that the knockout model

has altered visuomotor behaviour, as seen in the swimming behaviour tests in the dark. In contrast, Panx1b was also determined to be involved in locomotion and visual motor functions and regulate the circadian clock system. The Panx1b knockout model lacked leftward locomotion under low light conditions.

Since most of this thesis focuses on the Panx1a ohnologue, a sequence alignment between the zebrafish and the human Panx1 is shown below (**Figure 1.4**). A comparison between the known/predicted phosphorylation residues of the mouse Panx1 and the corresponding conserved residues on the zebrafish Panx1a protein are summarized in **Table 1.1.**

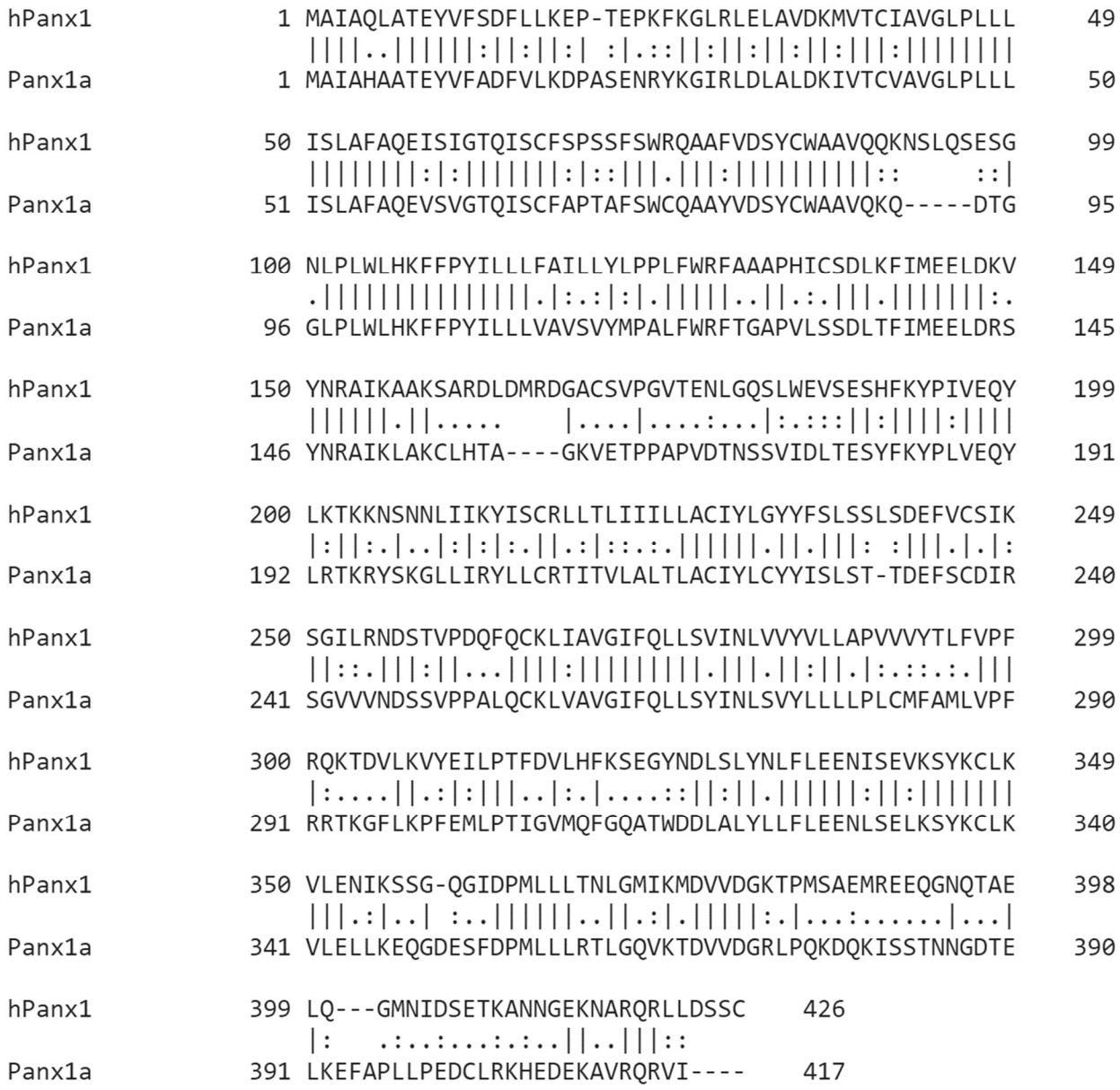

Figure 1.4. Sequence comparison of the zebrafish Panx1a and human Panx1. Sequence alignment between hPanx1 and Panx1a shows a similarity score of 72.6%, an identity score of 55.2%, and a gap score of 4.4%. Alignment was performed using Pairwise Sequence Alignment with EMBOSS Needle (Madeira et al., 2022).

Table 1.1. Known/predicted phosphorylation sites of the mouse Panx1 compared to the conserved or non-conserved residues on the zebrafish Panx1a.

Mouse Panx1	**Zebrafish Panx1a**
Y150	Conserved (Y146)
Y198	Conserved (Y191)

S206	Conserved (S198)
T302	Not conserved
Y308	Not conserved
S328	Not conserved
S394	Not conserved

1.3. Hypothesis and research objectives

As the zebrafish model provides feasibility in handling/reproduction, genetic manipulation, and neurobiological characterization during early development, it is useful for studying the Panx1 channel function. However, research on the zebrafish Panx1 is limited, requiring further investigation into similarities and differences between the mammalian and the Teleost Panx1. With the growing evidence of post-translational modifications affecting the function and trafficking of the mammalian Panx1, I hypothesize that the zebrafish Panx1a can undergo phosphorylation modifications contributing to its regulation and trafficking.

The main aims of this research were as follows:

1. To identify key residues and novel phosphorylation post-translational modifications of the zebrafish Panx1a and understand their role in the trafficking and function of the protein.
2. To explore the kinase interactome of Panx1a, establish evidence of physical interaction, and determine the functional consequences of the relationship between the two proteins.

These aims are addressed using the Neuro 2a cell line to overexpress fluorescently tagged Panx1a wild-type and mutant constructs. The first aim is addressed in Chapters 3 and 4, and the second aim is addressed in Chapters 4 and 5.

Chapter 3 was published in *Biomolecules* journal (Timonina et al., 2020), titled “Role of an Aromatic–Aromatic Interaction in the Assembly and Trafficking of the Zebrafish Panx1a Membrane Channel”. This chapter addresses the hypothesis that a key conserved residue, Y205, is involved in the stabilization and trafficking of Panx1a. The research in this chapter explores the consequences of mutating this residue and its effects on the localization of the channel. This study also examines whether this residue is subject to phosphorylation or has an alternative function in regulating Panx1a.

Chapter 4 is titled “Exploring the Panx1a interactome and phosphorylation in transfected Neuro 2a cells”. In this chapter, I hypothesize that Panx1a can interact with kinases and is phosphorylated for the proper functioning of the channel. By purifying overexpressed Panx1a, I identify novel phosphorylation residues and interacting partners of the protein, which address both aims 1 and 2. Using mutagenesis, I explore the functional role of several residues to understand how phosphorylation modifications may impact the zebrafish Panx1a. Using *in silico* kinase prediction tools, based on the identified phosphorylation residues, I investigate the interaction between ERK2 and Panx1a. I also explore the consequences of kinase pharmacological treatment on the expression of Panx1a.

Chapter 5 is titled “The trafficking and localization of the zebrafish Panx1a are regulated via interaction with CaMKIIa”. The hypothesis for this chapter is that Panx1a interacts with CaMKIIa, a kinase pulled down and identified in the mass spectrometry screen in Chapter 4. This section focuses on the second aim as I explore the interaction with CaMKIIa and determine the effects of overexpression of the kinase on Panx1a localization and function. I address this hypothesized interaction by using co-

immunoprecipitation (CoIP) and Förster Resonance Energy Transfer Analysis (FRET) techniques. I explore the functional consequences by utilizing CaMKIIa mutants for Panx1a dye uptake assays and localization studies.

.

Chapter 2. Material and Methods

This section combines the materials and methods used in all chapters of this thesis. Although some methods overlap different studies, some procedures have slight modifications. Such changes are outlined and noted within each subsection of this chapter.

2.1. Experimental Methods

2.1.1. Plasmid construction and mutagenesis

The full-length *Danio rerio* Panx1a (NM_200916.1, aa 1-416), *Danio rerio* Panx1b (NM_001100030.2, aa 1-422), *Rattus norvegicus* CaMKIIa (NM_012920.1, aa 1-478), *Mus musculus* Panx1 (NM_019482, aa 1-426), or isoform 2 of *Mus musculus* Cav-1 (NM_001243064, aa 1-147), were cloned into pEYFP-N1, pECFP-N1, pDsRed2-monomer, pEGFP-N1, pdTomato-His-N1, or His-N1 expression vectors. Organelle markers for ER (calreticulin) and Golgi apparatus (galactosyltransferase) were tagged with DsRed2 as previously described (Siu et al., 2016). Panx1a and CaMKIIa mutants were generated as previously described (Siu et al., 2021) or by site-directed mutagenesis using the Q5 Hot Start Site-Directed Mutagenesis kit (New England Biolabs, Inc., Boston, MA, USA) according to the manufacturer's protocols. Oligonucleotides were designed using the NEBaseChanger tool (**Table 2.1**) and synthesized by Integrated DNA Technologies (IDT, Coralville, IA, USA). All plasmid constructs were sequence verified (Eurofins MWG Operon LLC, Huntsville, AL, USA).

2.1.2. Cell culture and transfection

Neuro 2a cells (ATCC®, CCL-131, Manassas, VA, USA) were cultured in DMEM supplemented with 10% FBS, 1% penicillin and streptomycin, and 1% non-essential

amino acids (Thermo Fisher Scientific, Rockford, IL, USA) at 37 °C and 5% CO2. ~3,000,000 cells were seeded for 10cm plates, ~800,000 cells for 6cm plates, ~25,000 cells for 35mm glass-bottom dishes (MatTak Corporation, Ashland, MA, USA) and 24-well plates.

Cells were transiently transfected using Effectene™ Transfection Reagent Kit (Qiagen Inc., Valencia, CA, USA) according to the manufacturer's protocol. For each construct, 2000ng DNA was used in 10cm plates, 1000ng for 6cm plates, and 200ng for 35mm glass-bottom dishes and 24-well plates (except for triple transfected cells, where 100ng was used for each construct). All experiments were performed 48h post-transfection.

2.1.3. Western blot

Protein samples were separated by 10% sodium dodecyl-sulfate polyacrylamide gel electrophoresis (SDS-PAGE) at 100-150V for 1.5h. Gels were transferred to nitrocellulose membranes using the Trans-Blot Turbo Transfer System (Bio-Rad Inc., Mississauga, ON, Canada) at 1.3A and 2.5V for 7mins. Membranes were blocked with Odyssey Blocking Buffer (LI-COR Biosciences, St. Lincoln, NE, USA) or Intercept® (PBS) Protein-Free Blocking Buffer (LI-COR Biosciences) for one hour at RT and incubated with primary antibodies overnight at 4°C. Primary antibodies used were as follows: rabbit-anti-His (1:1000, Bethyl Laboratories Inc.) for detection of dTomato-His and His tagged constructs, rabbit-anti-GFP (1:500, Santa Cruise Biotechnologies, Dallas, TX, USA) for detection of EYFP tagged constructs, mouse-anti-GFP (1:250) for detection of EYFP and ECFP tagged constructs, mouse-anti-mCherry (1:200) for detection of dsRed tagged constructs, and mouse-anti-β-Actin (1:1500, Sigma-Aldrich Chemie GmbH, Munich, Germany) for detection of β-Actin. The secondary antibodies used were: donkey-anti-

rabbit iRDye 680 and goat-anti-mouse iRDye 800 (1:15000, LI-COR Biosciences). Protein detection was performed using the Odyssey® CLx Infrared Imaging System (LI-COR Biosciences).

2.1.4. His60 Ni Gravity Column pull down

Neuro 2a cells were transfected with dTomato-His tagged constructs using three 10cm plates per construct. The pull-down was performed according to the manufacturer's protocol. Briefly, cells were lysed under native conditions using His60 Ni xTractor™ Buffer (Clontech Laboratories Inc.) supplemented with Halt™ Protease and Phosphatase Inhibitor Cocktail (Thermo Scientific). The lysates were loaded into the His60 Ni Gravity Columns (Clontech Laboraties Inc.) and incubated at 4°C for 1 hour with rotation. Columns were washed, and proteins were eluted using the supplied buffers.

2.1.5. Mass spectrometry

Samples were purified using His60 Ni Gravity Columns, and eluted samples were sent to SPARC BioCentre Molecular Analysis at The Hospital for Sick Children, Toronto, Ontario, for sample processing and protein identification. For every 15ug of protein, each sample was reduced with 10mM DTT for 1h at 60°C and alkylated with 20mM iodoacetamide for 45mins at RT in the dark. Digestion was performed with Trypsin (Pierce) and Chymotrypsin (Promega) using 0.5ug per sample at a proteinase:protein ratio of 1:30-1:50 overnight at 37°C. Each digested sample was desalted with manual c18 ZipTip, lyophilized using a speed vac, and resuspended in 0.1% formic acid. Protein identification was performed by EASY-nLC 1200 nano-LC system with 75um x 50cm PepMax RSLC EASY-Spray column filled with 2uM C18 beads (ThermoFisher, San Jose, CA, USA), pressure 900 Bar, at 60°C using the Thermo Scientific Orbitrap Fusion Lumos

Tribrid mass spectrometer. PEAKS Studio 10.6 build 20201221 and Scaffold software were used for protein identification with the following search parameters:

- Parent Mass Error Tolerance: 50 ppm
- Fragment Mass Error Tolerance: 0.02 Da
- Enzyme: Trypsin, Chymotrypsin
- Max Missed Cleavages: 3
- Fixed Modifications:
    - Carbamidomethylation: C (+57.02)
- Variable Modifications :
    - Oxidation : M (+15.99)
    - Deamidation : N, Q (+ 0.98)
    - Acetylation: peptide N-term (+42.01)
    - Phosphorylation (STY): 79.97

Each sample was analyzed in three biological replicates, and the identified proteins were pooled. A minimum of 2 peptides had to be identified in a single replicate to be considered a hit. All proteins co-precipitating with dTomato-His empty vector control were removed from the Panx1a-dTomato-His interactors. The resulting list of proteins was subject to analysis using PANTHER Classification System.

2.1.6. Co-Immunoprecipitation

For interaction studies, Neuro 2a cells were double transfected with dTomato-His tagged constructs as the bait and ECFP tagged constructs as the prey on 10cm plates. For experiments using Brefeldin A (BFA) treatment, cells were incubated with 5ug/mL BFA (Sigma-Aldrich) for 19h before lysing. Cells were lysed using Pierce™ IP Lysis buffer

(Thermo Fisher Scientific, Rockford, IL, USA) supplemented with HALT™ Protease Inhibitor Cocktail (Thermo Fisher Scientific, Rockford, IL, USA) for 5mins at 4°C. Lysates were centrifuged at 15xG for 10mins at 4°C, and the resulting supernatants were collected. 50uL of Dynabead™ Protein A (ThermoFisher) were incubated with 7ug of anti-His antibody (Bethyl Laboratories Inc., Montgomery, TX, USA) for 15mins at RT with rotation. The lysates were then incubated with the antibody conjugated Dynabeads for 1h at RT with rotation. Samples were washed once with lysis buffer and three times with PBS-tween. The proteins were eluted from the beads by heating the samples in 1X Laemmli sample buffer at 95°C for 5mins and were subjected to western blot analysis.

2.1.7. Förster Resonance Energy Transfer Analysis (FRET)

For interaction studies, Neuro 2a cells were double transfected with DsRed tagged constructs as the acceptor fluorophores, and ECFP or EYFP tagged constructs as the donor fluorophores on glass coverslips in 24-well plates for FRET analysis using the acceptor bleach protocol (Siu et al., 2016). Cells were fixed with 4% PFA for 15 minutes, and coverslips were mounted using ProLong™ Gold Antifade Mountant (ThermoFisher) or Fluoroshield TM (Sigma-Aldrich). Imaging was done using the Zeiss LSM 700 confocal microscope using the Plan-Apochromat 63x/1.4 Oil DIC M27 objective, according to the previously established protocol (Siu et al., 2016). DsRed tagged proteins were recorded and photobleached with the 555nm laser at 100% intensity. The resulting change in ECFP or EYFP fluorescence was recorded with the 405nm or 488nm laser, respectively. The bleaching was terminated upon reaching 10% of the DsRed baseline fluorescence intensity. FRET efficiency was calculated using the following formula:

$$FRETeff = (Dpost – Dpre)/Dpost$$

where Dpost is the average intensity after bleaching, and Dpre is the average intensity before bleaching. The calculated threshold FRET value for 10nm distance was 1.7% for the DsRed and ECFP and 1.4% for DsRed and EYFP pairs based on the reference distances (5.1nm for DsRed/ECFP and 4.9nm for DsRed/EYFP) (Muller et al., 2013).

2.1.8. Fluorescence Recovery After Photobleaching (FRAP)

Neuro 2a cells were grown on 35mm glass-bottom dishes and transfected with fluorescently tagged WT or mutant Panx1a to assess cell surface dynamics. Cells were incubated in DMEM lacking phenol red for 30 min prior to experimentation. Dishes were placed into a 37 °C live-cell imaging chamber, and time-lapse imaging was performed using a Zeiss 700 confocal microscope using the Plan-Apochromat 63x/1.4 Oil DIC M27 objective. Regions of interest (ROIs) were selected at the membrane of single cells with no neighboring cells. ROIs were photobleached at 488nm at 100% laser strength. Images were taken every one second for 50 seconds post bleaching. Recovery was calculated using the following equation:

$$F = (Ft - F0)/(Fi - F0)$$

where F is the normalized fluorescence at a given time point, Ft is the fluorescence intensity at t seconds, F0 is the fluorescence intensity upon bleaching, and Fi is the fluorescence intensity immediately prior to bleaching.

2.1.9. Dye uptake assay

Neuro 2a cells were transfected with fluorescently tagged constructs on 35mm glass-bottom dishes to assess the functionality of Panx1a. Cells were incubated in DMEM lacking Phenyl red 48 hours post-transfection for 30 minutes before imaging using the Zeiss 700 confocal microscope using EC Plan-Neofluar 40x/1.30 Oil M27 objective. Cells

were treated with 10uM EtBr immediately prior to recording. Images were taken at a 512x512 pixel resolution at either 30 seconds or 1-minute intervals for either 5 or 10 minutes (as described in independent figures). For experiments that used double-transfected cells, only cells expressing both proteins were used for analysis. Dye uptake was measured by normalizing the EtBr channel to the EYFP channel.

2.1.10. Total Internal Reflection Fluorescence (TIRF)

Neuro 2a cells were double transfected with EYFP and DsRed tagged constructs on 35mm glass-bottom dishes. Imaging was done using the Zeiss Observer Z1 spinning-disk microscope using Zeiss 100X (Plan-Apochromat, DIC, M27, 1.46) oil immersion lens and Photometrics Evolve™512 camera, as previously described (Brown et al., 2019). Images were recorded at a 512x512 pixel resolution for 1min at 1sec intervals. Imaris (Zurich, Switzerland) software was used to track vesicle size and displacement of EYFP tagged constructs co-expressed with DsRed tagged constructs.

2.1.11. Cell surface biotinylation assay

Neuro 2a cells were double transfected with fluorescently tagged constructs on 6cm plates. Cells were labeled with 0.25 or 0.5mg of membrane-impermeable EZ-Link™ Sulfo-NHS-Biotin (Thermo Fisher) per plate for 30mins at room temperature. Plates were washed with PBS, and the reaction was quenched with 50mM glycine buffer three times for 5 minutes each. Cells were collected in PBS, washed, and lysed in NP40 lysis buffer for 30 minutes or with Pierce IP Lysis buffer (Thermo Fisher) for 5 minutes supplemented with HALT™ Protease Inhibitor Cocktail (Thermo Fisher) at 4°C. The resulting lysates were incubated with 90uL of prewashed Dynabeads™ MyONE™ Streptavidin C1 (Invitrogen) overnight at 4°C with rotation. Beads were washed twice with 2% SDS in

dH20, once with 0.1% deoxycholate, 1% Triton X-100, 500 mM NaCl, 1 mM EDTA, 50 mM Hepes pH 7.5, once with 250 mM LiCl, 0.5% NP-40, 0.5% deoxycholate, 1 mM EDTA, 10 mM Tris; pH 8.1, and twice with 50 mM Tris, 50 mM NaCl pH 7.4. The proteins were eluted from the beads by heating the samples in 1X Laemmli sample buffer at 95°C for 5mins and were subjected to western blot analysis.

2.1.12. Immunofluorescence, confocal microscopy, and co-localization

For immunofluorescence, transfected cells were fixed with 100% methanol for 10 min at RT. Cells were blocked in PBS containing 2% BSA for 1h at RT. Next, the primary antibody dilution containing rabbit anti-His (1:1000) (Bethyl Laboratories Inc.) in PBS with 0.1% BSA was applied for 1h at RT. Cells were then incubated with 2ug/mL of secondary antibody dilution containing Alexa Fluor 568 goat anti-rabbit (Thermo Fisher Scientific, Rockford, IL, USA) in PBS with 0.1% BSA for 1h at RT. Lastly, cells were washed in PBS and mounted with Fluoroshield™ (Sigma-Aldrich).

For imaging fluorescently tagged proteins, Neuro 2a cells were transfected with fluorescently tagged constructs on coverslips in 24-well plates. Cells were fixed with 4% PFA for 15-30 minutes at RT and mounted with either Fluoroshield™ (Sigma-Aldrich) or ProLong™ Gold Antifade Mountant (ThermoFisher). Imaging was done using the Zeiss LSM 700 confocal microscope. Zeiss ZEN Black was used to control imaging parameters. For co-localization, only cells expressing all proteins of interest were chosen, and the Pearson's R Value between the fluorescent channels was determined using ImageJ software.

2.1.13. Quantitative Real-Time PCR

Total RNA was extracted 48h post-transfection using RNeasy Plus Mini Kit (Qiagen) according to the manufacturer's protocol from Neuro 2a cells, with or without 5ug/mL BFA treatment for 19h. A total of 1ug of RNA was used to synthesize cDNA using the ReadyScript cDNA Synthesis Kit (Sigma-Aldrich). qPCR was performed using the SsoFast EvaGreen Supermix (Bio-Rad) with the oligonucleotide pairs described (**Table 2.2**). Quantification of 18s rRNA served as an internal standard. Each assay was performed in triplicate in three independent experiments using the CFX Connect Real-Time PCR Detection System (Bio-Rad). Relative gene expression values were calculated using the Relative Expression Software Tool (REST) (Pfaffl et al., 2002), with the EYFP-transfected cells serving as the control group.

2.1.14. PhosphoProtein purification

Neuro 2a cells were transfected with Panx1a-EYFP on two 10cm plates and were collected in PBS. Cells were centrifuged, and the cell pellets were subjected to phospho-purification using a PhosphoProtein Purification kit (Qiagen Inc.) according to the manufacturer's protocol. Briefly, cells were lysed using the provided lysing buffers and centrifuged at 10 x G for 30mins. 35mg of protein was loaded into the column and allowed to pass through. The captured phosphorylated proteins were eluted with the provided buffers, and samples were mixed with 1X Laemmli sample buffer for western blot analysis.

2.1.15. Pharmacology

Neuro 2a cells were treated with BFA (5ug/mL) for 19h prior to experimentation. BFA was used to block the transport between the ER and Golgi compartments. Cells were

treated with Ionomycin (Sigma-Aldrich) (2μM) in combination with 2 mM [Ca2+]E for 5 minutes prior to experimentation. Ionomycin increases the intracellular concentration of calcium. Kinase inhibitors/activators used were as follows: MAPK inhibitor PD98059 (Sigma-Aldrich) (10uM) for 3 hours, GSK3 inhibitor SB415286 (Sigma-Aldrich) (25uM) for 24 hours, PKA inhibitor H-89 (Sigma-Aldrich) (30uM) for 3 hours, AMPK activator Metformin 1,1-Dimethylbiguanide hydrochloride (Sigma-Aldrich) for 24 hours, and CaMKIIa inhibitor KN-93 (50uM) for 5 minutes prior to experimentation. Concentrations was chosen based on the published literature in Neuro 2a cells (Choi et al., 2011; Dickey et al., 2011; Gupta et al., 2011; Namsi et al., 2018; Siu et al., 2021).

2.1.16. Statistical analysis

Statistical analysis and graphical generation were performed using MATLAB R2018b, GraphPad Prism 8 or 9, and REST. Co-localization, dye uptake, and western blot quantification data were generated using ImageJ. The sample size (n) is indicated for each analysis, with all experiments conducted in replicates of n>3. Normally distributed data were confirmed with the Shapiro-Wilk normality test and were analyzed using two-tailed t-tests. Non-normal distributed data were analyzed by the two-tailed Mann-Whitney U test or Kruskal-Wallis test.

2.2. General Materials

2.2.1. Biosafety

The research project in this thesis was performed in accordance with federal, provincial, and institutional regulations for the containment Level 2 laboratories located at the Life Science Building (LSB), Department of Biology.

2.2.2. Organisms

2.2.2.1. Bacterial strains

Escherichia coli (*E. coli*) DH5α (Invitrogen, Burlington, Canada)
Genotype: F– Φ80lacZΔM15 Δ (*lac*ZYA-*arg*F) U169 *rec*A1 *end*A1 *hsd*R17 (rK–, mK+) *pho*A *sup*E44 λ– *thi*-1 *gyr*A96 *rel*A1

E. coli NEB 5-alpha competent (New England Biolabs, Whitby, Canada)
Genotype: *fhu*A2 Δ(*arg*F-*lac*Z) U169 *pho*A *gln*V44 Φ80 Δ(*lac*Z)M15 *gyr*A96 *rec*A1 *rel*A1 *end*A1 *thi*-1 *hsd*R17

2.2.2.2. Eukaryotic cells

Neuroblastoma 2a cells (Neuro 2a cells) were derived from *Mus musculus*, developed by Klebe and Ruddle in 1967 from a strain A albino mouse spontaneous tumour. Neuro 2a cells used in this thesis were generously provided by Dr. David C. Spray (Albert Einstein College, NY, USA).

2.2.3. Commercial kits

Site-directed mutagenesis	Q5® Site-directed Mutagenesis Kit (New England Biolabs)
QIAquick Gel Extraction Kit	Gel Elution of DNA fragments (QiaGen)
Ligation Kit	CloneJETTM PCR Cloning Kit (Thermo Scientific)
Plasmid DNA Purification	QIAPrep Spin Miniprep Kit (QiaGen)
Re-ligation of vector DNA	Rapid DNA Ligation Kit (Thermo Scientific)
Restriction Digestion	Fast digestion Top Fermentas Kit (Thermo Scientific)
His-tagged protein purification	His60 Ni Gravity Column Purification Kit (Takara)
Phosphorylated protein purification	PhosphoProtein Purification Kit (Qiagen)
Magnetic beads for CoIP	Dynabeads™ Protein A for Immunoprecipitation (Thermo Scientific)

Magnetic beads for cell surface biotinylation	Dynabeads™ MyOne™ Streptavidin C1 (Thermo Scientific)
Biotin for cell surface biotinylation	EZ-Link™ Sulfo-NHS-Biotin, No-Weigh™ Format (Thermo Scientific)
Transfection reagent	Effectene Transfection Reagent (Qiagen)

2.2.4. Oligonucleotides for mutagenesis

Table 2.1. Oligonucleotide primers used for mutagenesis.

Gene	Mutation	Forward Primer	Reverse Primer
panx1a	Y205A	ACTGATCCGCGCCCTTCTTTGCC	AATCCTTTAGAGTAGCGC
	R204Y:Y205R	ATTACTGATCtACCGCCTTCTTTGCCGCAC	CCTTTAGAGTAGCGCTTG
	I203Y:R204I:Y205R	CCGCCTTCTTTGCCGCACCATC	ATGTACAGTAATCCTTTAGAGTAGCG
	W123A	AGCGTTGTTTGCGCGGTTTACAG	GGCATGTAAACTGACACTG
	Y205F	ACTGATCCGCTTCCTTCTTTGCC	AATCCTTTAGAGTAGCGCTTG
	Δ320-417	GTCATCAAGGATCCACCG	AAGATCATCCCAGGTCGC
	Δ148-159	GGAAAAGTAGAAACACCGC	GTTGTAGGAACGGTCCAG
	Δ154-165	CCAGCTCCAGTGGATACA	AGCCAATTTGATGGCTCTG
	Δ184-195	CGCTACTCTAAAGGATTAC	AAAATAGCTCTCGGTGAG
	Δ191-198	AAAGGATTACTGATCCGC	CTGCTCCACCAGAGGATA
	Δ290-296	CTGAAGCCTTTCGAGATG	TGGAACCAACATGGCAAAC
Camk2a	T286A	CAGACAGGAGGCCGTGGACTGCC	TGCATGCAGGAGGCCACAG
	T286D	CAGACAGGAGGACGTGGACTGCCTG	TGCATGCAGGAGGCCACA
	F293A	CCTGAAGAAGGCCAATGCCAGGAGG	CAGTCCACGGTCTCCTGT
	K42M	GTATGCTGCCATGATTATCAACACCAAGAAGCTC	TCCTGGCCAGCCAGCACC
	D135N	GGTGCATCGCAACCTGAAGCCTG	ACCCCCATCTGGTGACAG
	R296A	GTTCAATGCCGCGAGGAAACTGAAGGG	TTCTTCAGGCAGTCCACG
	T305A:T306A	AGCCATCCTCGCCGCTATGCTGGCCA	CCCTTCAGTTTCCTCCTGGCATTG
	H477Y	CGTCCTGCCGTATCGAATTCTGC	GAGGGCGCCCCAGATCTG

2.2.5. Oligonucleotides for RT-qPCR

Table 2.2. Oligonucleotide primers used for RT-qPCR. Primers were designed for detected ER stress markers as described (Oslowski and Urano, 2011).

Gene	Forward Primer	Reverse Primer
ATF4	GGGTTCTGTCTTCCACTCCA	AAGCAGCAGAGTCAGGCTTTC
CHOP	CCACCACACCTGAAAGCAGAA	AGGTGAAAGGCAGGGACTCA
EDEM	CTACCTGCGAAGAGGCCG	GTTCATGAGCTGCCCACTGA
BiP	TTCAGCCAATTATCAGCAAACTCT	TTTTCTGATGTATCCTCTTCACCAGT
sXBP1	CTGAGTCCGAATCAGGTGCAG	GTCCATGGGAAGATGTTCTGG
usXBP1	CAGCACTCAGACTATGTGCA	GTCCATGGGAAGATGTTCTGG
tXBP1	TGGCCGGGTCTGCTGAGTCCG	GTCCATGGGAAGATGTTCTGG

2.2.6. Solutions and media

2.2.6.1. Solutions for cell culture

10% Formalin	Sigma-Aldrich

Trypsin	Sigma-Aldrich
PBS (phosphate buffered saline)	Sigma-Aldrich
Penicillin and Streptomycin	BioShop
FBS (fetal bovine serum)	Gibco
NEA (non-essential amino acids)	Sigma-Aldrich
Dulbecco's Modified Eagle Medium (DMEM)	Sigma-Aldrich
Mounting media: Fluoroshield with DAPI	Sigma-Aldrich
Mounting media: ProLong™ Gold antifade reagent	Invitrogen

2.2.6.2. Solutions for bacteria culture

LB Media	1% bacto tryptone, 0.5% yeast extract, 0.5% NaCl, 50µL/mL of kanamycin or 100µL/mL of ampicillin
LB agar	LB medium (1% agar), 50µL/mL of kanamycin or 100µL/mL of ampicillin
SOC media	2% bacto tryptone, 0.5% bacto yeast extract, 10mM NaCl, 2.5 mM KCl, 10mM MgCl2, 10mM MgSO4, 20 mM glucose

2.2.6.3. Solutions for biological methods

DNA Loading Buffer	10x FastDigest Green buffer (Fermentas)
1x TAE Gel Loading Buffer	40mM Tris, 20mM acetic acid, 1mM EDTA
Laemmli Sample Buffer	2% SDS, 10% glycerol, 5% βmercaptoethanol, 0.1% Orange G, 50mM Tris-HCl, pH 6.8
Laemmli Running Buffer	192mM glycine, 0.1% SDS, 25mM Tris-HCl pH 8.3
Blocking Solution (western blot)	Odyssey Blocking Buffer (Li-Cor Bioscience)

Blocking Solution (western blot)	Intercept Blocking Buffer (Li-Cor Biosciences)
PBS (phosphate buffered saline)	130mM NaCl, 28mM KCl, 10mM Na2HPO4, 1.8mM KH2PO4, pH 7.4
Protease and Phosphatase inhibitor	Halt™ Protease and Phosphatase Inhibitor Cocktail (Thermo Scientific)
Protease inhibitor	Halt™ Protease Inhibitor Cocktail (100X) (Thermo Scientific)

2.2.7. Software

Image Processing	ImageJ, Adobe Photoshop
DNA Analysis	SnapGene
Image acquisition	ZEN 2010, ZEN Black (Carl Zeiss)
Statistical Analysis	Prism 8. Prism 9, MATLAB R2018b, REST
DNA and Protein concentration	Nanodrop2000 a280
Protein sequence alignment	EMBOSS Needle
Proteomic analysis	Panther Classification System
Mass spectrometry analysis	Scaffold

Chapter 3. Role of an Aromatic-Aromatic Interaction in the Assembly and Trafficking of the Zebrafish Panx1a Membrane Channel

Ksenia Timonina[1], Anna Kotova[1], and Georg Zoidl[1,2] *

Affiliations:

[1]Department of Biology, York University, Toronto, ON M3J 1P3, Canada
[2]Department of Psychology, York University, Toronto, ON M3J 1P3, Canada

Timonina, K., Kotova, A., & Zoidl, G. (2020). Role of an aromatic–aromatic interaction in the assembly and trafficking of the zebrafish panx1a membrane channel. *Biomolecules*, *10*(2), 272.

Acknowledgements

We would like to thank Logan Donaldson for critical discussions and advice regarding the structural aspects of the study.

Author contributions

Designed the study and wrote the manuscript (K.T., G.Z.); executed experiments (K.T., A.K.); analyzed data (K.T., A.K.). All authors have read and agreed to the published version of the manuscript.

Declarations

The authors declare no conflict of interest.

Copyright

3.1. Abstract

Pannexin-1 (Panx1) is a ubiquitously expressed hexameric integral membrane protein known to function as an adenosine triphosphate (ATP) release channel. Panx1 proteins exist in unglycosylated core form (Gly0). They undergo critical post-translational modifications forming the high mannose glycosylation state (Gly1) in the endoplasmic reticulum (ER) and the complex glycosylation state (Gly2) in the Golgi apparatus. The regulation of transition from the ER to the cell membrane is not fully understood. Using site-specific mutagenesis, dye uptake assays, and interaction testing, we identified two conserved aromatic residues, Trp123 and Tyr205, in the transmembrane domains 2 and 3 of the zebrafish Panx1a protein. Results suggest that both residues primarily govern the assembly of Panx1a subunits into channels, with mutant proteins failing to interact. The results provide insight into a mechanism enabling regulation of Panx1 oligomerization, glycosylation, and trafficking.

3.2. Introduction

Pannexin-1 (Panx1) is an integral membrane glycoprotein forming a large pore membrane channel ubiquitously in the mammalian central nervous system (CNS) (Bruzzone et al., 2003; Ray et al., 2005; Vogt et al., 2005). The protein shares sequence homology with the invertebrate gap junction proteins called innexins (Dahl and Muller, 2014). Panx1 is a hexameric voltage-gated and mechanosensitive channel involved in calcium and ATP signaling, and it is sensitive to extracellular pH changes (Ambrosi et al., 2010; Bao et al., 2004; Dahl, 2015; Wang and Dahl, 2018). Due to glycosylation modifications, Panx1 exists in three forms: the unmodified nonglycosylated state (Gly0), the high mannose state (Gly1) formed in the endoplasmic reticulum (ER), and the

complex glycosylated state (Gly2) formed in the Golgi apparatus (Boassa et al., 2008; Penuela et al., 2007; Penuela et al., 2009). The addition of large glycosylation complexes is discussed as a reason preventing Panx1 from forming gap junctions. These modifications enable Panx1 to exchange small molecules between extracellular and intracellular environments (Sosinsky et al., 2011). A glycosylation-deficient mutant of mouse Panx1^{N254Q} demonstrated limited membrane localization, with only a subpopulation reaching the cell surface (Penuela et al., 2007; Penuela et al., 2009). Despite Panx1's limited capacity to form gap junctions, they are topologically similar to the gap junction protein family of connexins and innexins (Dahl and Muller, 2014; Ambrosi et al., 2010; Scemes et al., 2007). A single Panx1 subunit has four transmembrane domains, two extracellular loops, a cytoplasmic loop, and intracellular amino and carboxyl terminals. The exact structure and folding of the protein remain unknown as the structure of Panx1 at an atomic resolution has not yet been established.

Previously, a zebrafish (*Danio rerio)* Panx1 ortholog (Panx1a) has been described and found to form functional membrane channels in the Neuroblastoma 2a (Neuro 2a) cell line (Kurtenbach et al., 2013; Prochnow et al., 2009). Due to a teleost whole-genome duplication event that occurred between 320 and 350 million years ago, a Panx1a ohnologue exists (panx1b) (Bond et al., 2012). Panx1a and panx1b show distinct tissue expressions, glycosylation patterns, and electrophysiological gating properties (Kurtenbach et al., 2013). This study will focus on the Panx1a ohnologue.

Electrophysiological gating properties and multiple factors regulating the Panx1 channel, as well as complex pharmacology, have been described (Dahl et al., 2013; Whyte-Fagundes and Zoidl, 2018). Panx1 blockers include carbenoxolone, mefloquine,

and flufenamic acid, which also act on gap junction proteins. Potassium and glutamate can activate Pannexins. Studies across multiple fields demonstrated that Panx1 is a major molecular hub interacting with many signaling pathways. To address the complex life cycle of Panx1, we explored the role of an aromatic–aromatic interaction between amino acids W123 and Y205 in the cytoplasmic loop of Panx1a near transmembrane (TM) domains 2 and 3, respectively. Aromatic–aromatic interactions have been previously shown to be important in TM–TM association of membrane proteins (Gebhardt et al., 2011; Johnson et al., 2007). The forces of these interactions help strengthen oligomerization and suggest a role in folding and stabilization. Both W123 and Y205 are highly conserved between various membrane channels and gap junction proteins. Mutation analysis of Panx1a paired with co-localization and protein interaction studies led to the conclusion that the two aromatic residues are vital for the structural stabilization and interaction of Panx1a TM domains before insertion into the cell membrane. Outcomes of this study are relevant to understand how Panx1 proteins mature and traffic to the cell membrane.

3.3. Results

3.3.1. Mutation of aromatic amino acids alters trafficking of Panx1a to the cell membrane

Sequence alignment of multiple Pannexin orthologs and paralogs, as well as the distant invertebrate relative INX-6, revealed that aromatic amino acids W123 and Y205 of Panx1a were conserved (**Figure 3.1A**). W123 and Y205 were located at the border of the predicted cytoplasmic loop and transmembrane domains 2 and 3, respectively (**Figure 3.1B**). The two amino acid residues aligned with the invertebrate INX-6 Y192 and

W126. Previous work of Oshima et al. (Oshima, 2017; Oshima et al., 2016) showed that the Y192 of INX-6 was in close proximity to W126, leading us to propose that this also applies to the aromatic residues in Panx1a. A topological comparison of orthologs and paralogs of Panx1a and the distant invertebrate ortholog INX-6 showed that aromatic residues tyrosine and tryptophan appeared in similar positions (**Supplementary Figure 3.1**).

In Neuro 2A cells, the membrane localization of EYFP-tagged Panx1a was compromised when mutating either Y205 or W123, thus identifying them as amino acids required for cell surface localization (**Figure 3.1C**). Substitution of these amino acids with an alanine residue resulted in disruption of membrane localization of Panx1a, showing retained cytoplasmic expression. A positional shift of Y205 either one or two amino acids upstream of its original position resulted in a similar phenotype as the alanine substitution. These mutants were denoted R204Y:Y205R and I203Y:R204I:Y205R. A double alanine mutant at both Y205 and W123, denoted Y205A:W123A, also revealed cytoplasmic expression. The subcellular localization of mutants indicated that the position for this aromatic amino acid was critical.

The efficient membrane trafficking of Panx1a requires N-glycosylation. A western blot analysis determined the state of glycosylation for the aromatic mutants. The Y205A, R204Y:Y205R, I203Y:R204I:Y205R, W123A, and Y205A:W123A mutants showed a loss of the complex glycosylation (Gly2) form of the protein. All mutants still expressed the high mannose glycosylation form (Gly1) (**Figure 3.1D**).

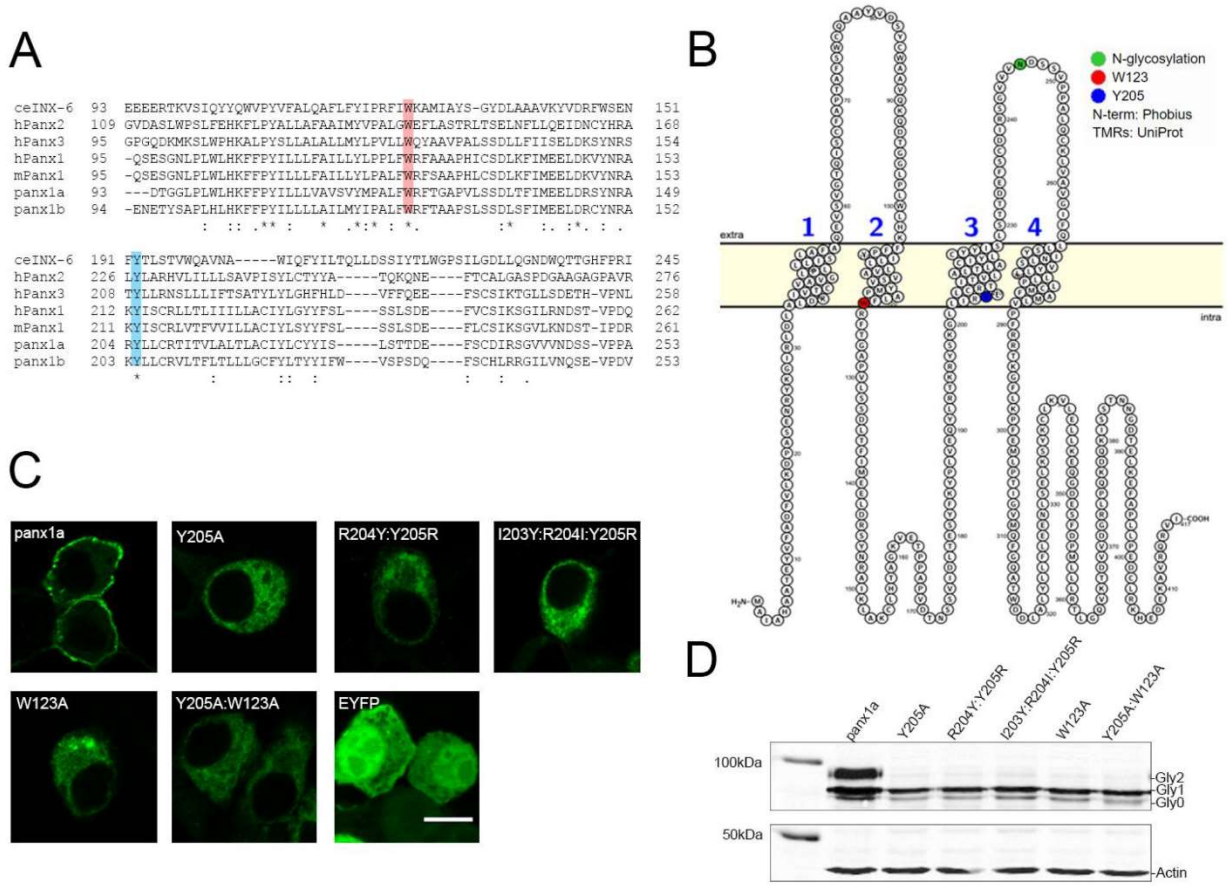

Figure 3.1. Expression and localization of Panx1a WT and mutants in Neuro 2a cells. (A) Sequence alignment of Panx1a with Pannexin orthologs and paralogs and the Caenorhabditis elegans INX-6 protein. (B) Topological representation of a Panx1a subunit showing the positions of both aromatic residues at the transmembrane and intracellular loop borders. The image was generated using Protter (Omasits et al., 2014) (C) Localization of EYFP-tagged wild type Panx1a and mutants in transfected Neuro 2a cells. Scale bar: 10µm. (D) Western blot analysis of transfected EYFP-tagged Panx1a and mutants. The three bands correspond to nonglycosylated Panx1a (Gly0), the high mannose glycosylation (Gly1), and the complex glycosylation (Gly2) forms. Expressed proteins were detected using an anti-GFP antibody and an anti-ß-actin antibody as the control.

3.3.2. Y205 phosphorylation is not required for membrane expression

The possibility of Y205 being a site for tyrosine phosphorylation in Panx1a was tested by replacement with the aromatic amino acid phenylalanine, which cannot be phosphorylated. Unlike Y205A, the EYFP-tagged Y205F mutant localization was similar

to wild type Panx1a (**Figure 3.2A**). Western blot analysis also showed that the Y205F mutant was efficiently glycosylated (**Figure 3.2B**), whereas Y205A was not. This was shown by the presence of the complex glycosylation variant of the Panx1a protein. It was concluded that the presence of aromatic amino acids, but not phosphorylation of Y205, was required for membrane localization. The localization was confirmed by a cell surface biotinylation assay, where the Y205F mutant was biotinylated at the cell surface and pulled down with streptavidin (**Figure 3.2C**). Cells transfected with EYFP alone were used as a control, showing that the bands were specific to Panx1a-EYFP. ß-actin, serving as endogenous quality control, was not detected in the biotinylated samples, indicating that biotin had not penetrated the membrane.

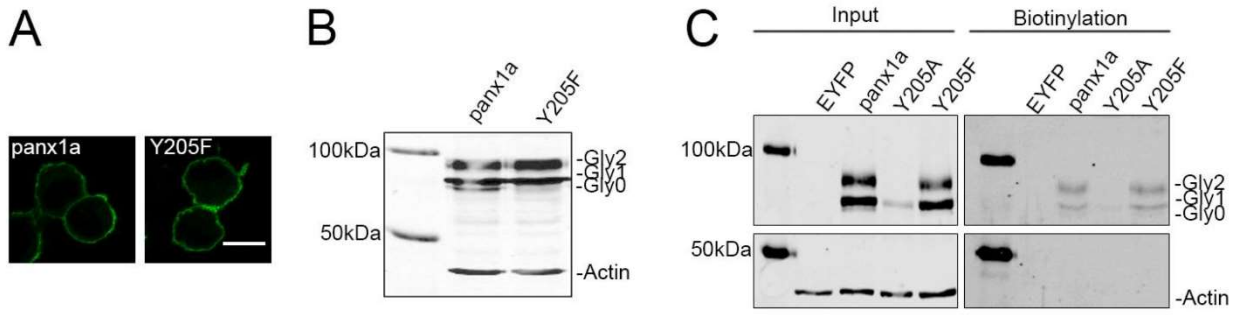

Figure 3.2. Comparison of the Panx1a Y205F and Y205A mutants. (A) Neuro 2a cells transfected with WT Panx1a-EYFP (left) and the Y205F-EYFP mutant (right) both showed membrane localization. Scale bar: 10µm. (B) Western blot analysis revealed similar glycosylation patterns when the Y205F mutant was compared to WT Panx1a. (C) Cell surface biotinylation assay showing that Y205F was present at the membrane of transfected Neuro 2a cells. Cell lysates after NP40 buffer lysis (Input) showed expression of both intracellular (ß-actin; Y205A) and membrane proteins (Panx1a; Y205F). The streptavidin pull-down fractions (Biotinylation) showed that all intracellular proteins were depleted, with Panx1a and Y205F found in the protein fraction from the cell surface. ß-actin served as an internal control, showing no bands in the biotinylation fraction. Expressed proteins were detected using an anti-GFP antibody and an anti-ß-actin antibody as the control.

3.3.3. The Y205F mutation restores Panx1a channel function and cell surface transport

A dye uptake assay and Fluorescent Recovery After Photobleaching (FRAP) analysis were used to assess the channel function and the cell surface dynamics of Panx1a and mutants. As expected, both Y205A and W123A mutants were unable to uptake EtBr due to the lack of transport to the cell membrane. Fluorescent images showed the dye uptake at 0 (start) and 10 min (endpoint) post-treatment with EtBr (**Figure 3.3A**). Only the wild type and Y205F mutant showed dye uptake above baseline. When dye uptake was quantified, a significant difference in total EtBr uptake between WT (43.67 ± 20.00, n = 17) and both Y205A and W123A mutants was detected (Y205A: 0.60 ± 0.19, n = 14, p = < 0.0001; W123A: 4.99 ± 1.40, n = 13, p = < 0.0001) (**Figure 3.3B**). Both mutants showed similar dye uptake to the EYFP control (EYFP: 4.79 ± 0.97, n = 13, p = < 0.0001), which was considered to represent baseline uptake of EtBr. The Y205F mutant showed no significant difference in total dye uptake when compared to wild type Panx1a (Y205F: 36.99 ± 15.13, n = 16, p = 0.38). The general trend of the dye uptake over the course of 10 min was similar for wild type and the Y205F mutant (**Figure 3.3C**).

Next, we assessed the cell surface diffusion dynamics of Y205F and wild type Panx1a using FRAP. Images showed EYFP tagged wild type Panx1a and Y205F expressing cells prior to bleaching, at bleaching, and recovery 5 s and 50 s post bleaching (**Figure 3.3D**). The average percent recovery 50 s post bleaching showed no significant difference between wild type Panx1a and Y205F (WT: 56.70 ± 20.04, n = 35; Y205F: 52.28 ± 11.96, n = 33; p = 0.43) (**Figure 3.3E**). The general trend in recovery at a five-second interval was the same for both wild type and mutant proteins (**Figure 3.3F**). These

results proved that the aromatic amino acid tyrosine could be substituted for phenylalanine at position 205 without disruption of channel mobility. Together with the dye uptake assay, these results showed that the Y205F mutant demonstrates wild type properties.

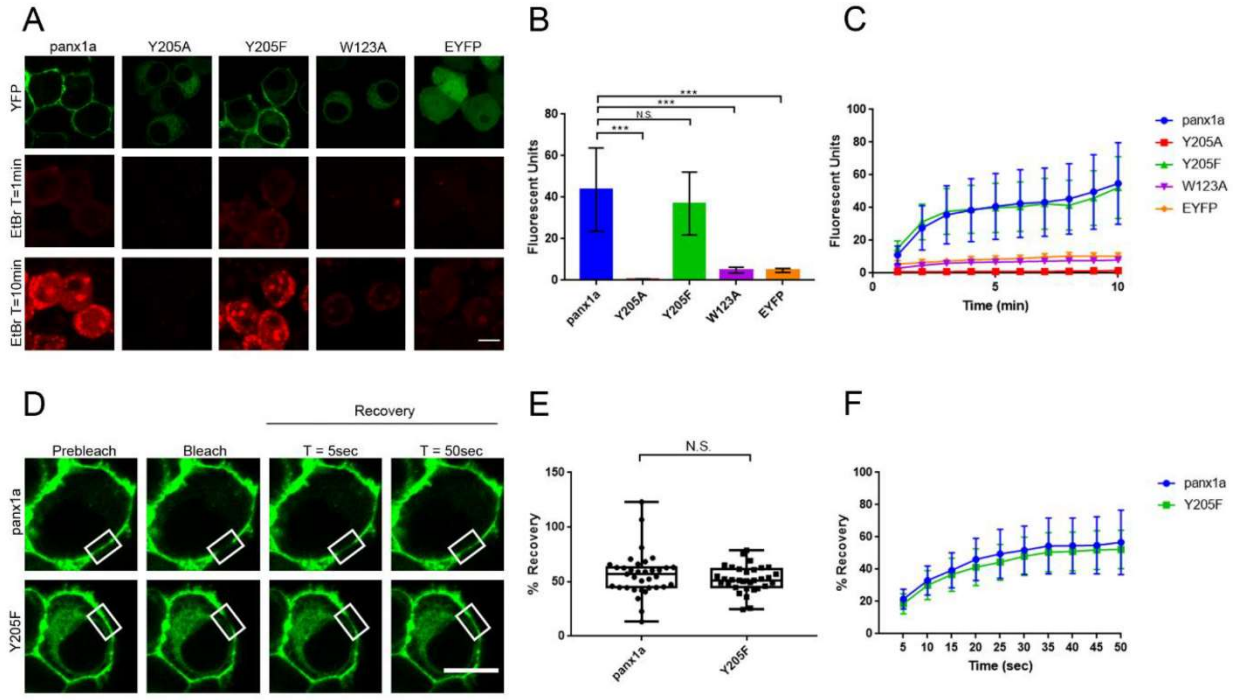

*Figure 3.3. Functional analysis of the Y205F mutant using dye uptake assay and Fluorescence Recovery After Photobleaching (FRAP). (A) Fluorescent images are showing dye uptake of Panx1a WT and mutants 10 min after EtBr application. EYFP-transfected cells were used as a negative control. Scale bar: 10μm. (B) Total EtBr fluorescence measured 10 min post dye application shown as a bar graph. Wild type Panx1a: n = 17, Y205A: n = 14, Y205F: n = 16, W123A: n = 13, EYFP: n = 13. (C) EtBr fluorescence measured throughout the 10 min with one-minute intervals. (D) FRAP analysis of WT Panx1a and Y205F mutant showing selected regions (white rectangles) pre bleaching, immediately after bleaching, and recovery 5 s and 50 s post bleaching. Scale bar: 10um. (E) Total % recovery, 50 s post photobleaching. Wild type Panx1a: n = 35, Y205F: n = 33. (F). % recovery measured throughout 50 s with five-second intervals. Error bars show the standard deviation of the mean. ***p < 0.001, N.S., not significant.*

3.3.4. Y205A Is Retained in Intracellular Compartments but Does Not Induce ER Stress

First, we confirmed that the complex glycosylation of zebrafish Panx1a was added in the Golgi apparatus by treating Panx1a-EYFP transfected Neuro 2a cells with BFA. Previous studies have shown that 21 h treatment of 5ug/mL BFA disrupts the trafficking of rodent Pannexin-1 between the ER and Golgi (Boassa et al., 2008). This was evidenced by Western blot showing a partial or complete decrease of the Gly2 form of the protein and a slight increase of the Gly1 form. Here, a 19h treatment with 5ug/mL BFA established a Panx1a localization similar to the one reported for the mammalian Pannexin-1 (**Figure 3.4A, B**). The localization of the Y205A-EYFP mutant was not affected by BFA treatment.

To test whether Y205A is retained in the intracellular compartments, co-localization studies with organelle and vesicle biomarkers were performed. Neuro 2a cells were double transfected with Panx1a-EYFP WT and either Sec24D-mCherry (COP II marker), Cav-1-His (Caveolin-1 marker), calreticulin-DsRed (ER marker), or galactosyltransferase-DsRed (Golgi apparatus marker) (**Figure 3.4C**). The same was done with the Y205A-EYFP mutant (**Figure 3.4D**). Panx1a co-localized significantly with Cav-1, which was evident by the significant localization in the cell membrane. The Y205A mutant was visually co-localized most with the ER and Sec24D markers and less with the Golgi and Cav-1 markers. The quantification of co-localization showed Panx1a co-localized significantly more with Cav-1 than Sec24D (Sec-24D: 0.61 ± 0.20, n = 34; Cav-1: 0.71 ± 0.12, n = 36; p = 0.018), and with ER than Golgi biomarkers (ER: 0.43 ± 0.23, n = 29; Golgi: 0.24 ± 0.19, n = 35; p = 0.0003) (**Figure 3.4E**). In contrast, the Y205A mutant co-

localized significantly more with Sec24D than Cav-1 (Sec24D: 0.86 ± 0.055, n = 30; Cav-1: 0.60 ± 0.15, n = 31; p < 0.0001), and with ER than Golgi markers (ER: 0.94 ± 0.07, n = 20; Golgi: 0.51 ± 0.12, n = 20; p < 0.0001), suggesting that trafficking of Y205A out of the ER was impaired (**Figure 3.4F**).

Next, ER stress was ruled out by quantitative real-time PCR of established biomarkers (**Figure 3.4G**). The mRNA levels of five different ER stress markers were quantified: ATF-4, CHOP, EDEM, BiP, and XBP1 (spliced (s), unspliced (us), and total(t)). We used Neuro 2a cells treated with 5ug/mL BFA for 19h as the “stress” group and EYFP-transfected cells as the control group. The BFA-treated “stress” cells showed significant upregulation of all stress genes tested compared to the EYFP-transfected cells (ATF-4: p < 0.001, CHOP: p < 0.000, EDEM: p < 0.000, BiP: p < 0.000, sXBPI: p < 0.000, usXBPI: p = 0.019). Except for one upregulated gene, expression of Y205A did not affect cell stress markers (BiP: p = 0.005). Overexpression of both wild type and mutant Panx1a caused no significant difference in the expression levels of stress genes when compared to EYFP-expressing cells.

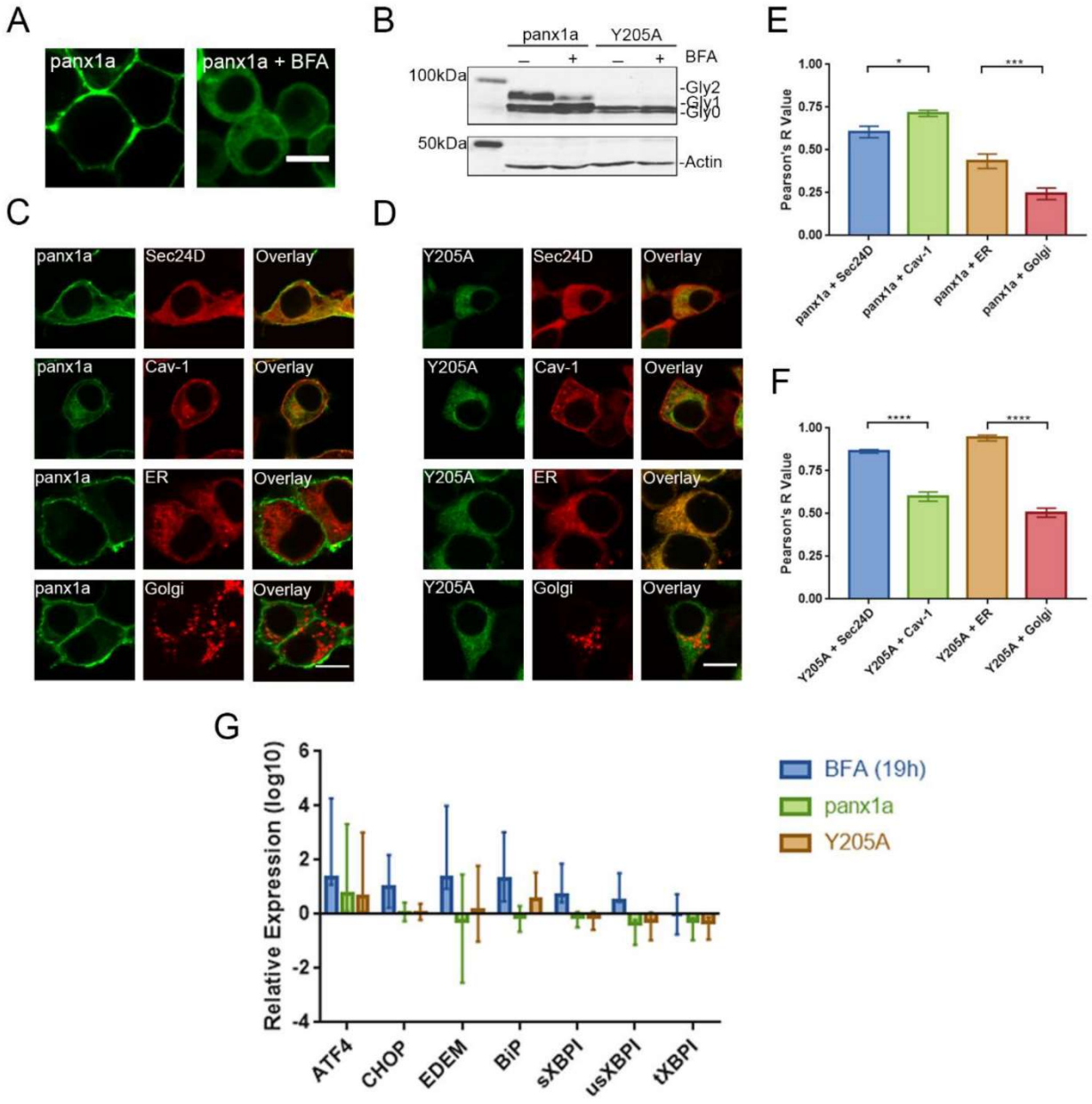
A
panx1a
panx1a + BFA
B
panx1a
Y205A
BFA
100kDa
-Gly2
-Gly1
-Gly0
50kDa
-Actin
C
panx1a
Sec24D
Overlay
Cav-1
ER
Golgi
D
Y205A
E
Pearson's R Value
panx1a + Sec24D
panx1a + Cav-1
panx1a + ER
panx1a + Golgi
F
Y205A + Sec24D
Y205A + Cav-1
Y205A + ER
Y205A + Golgi
G
Relative Expression (log10)
ATF4
CHOP
EDEM
BiP
sXBPI
usXBPI
tXBPI
BFA (19h)
panx1a
Y205A

*Figure 3.4. Expression of Brefeldin A (BFA)-treated cells, co-localization with cellular markers, and ER stress analysis of Panx1a and the Y205A mutant. (A) Images of Panx1a-EYFP transfected Neuro 2a cells treated with 5ug/mL BFA for 19h showed a reduction of cell membrane localization. Scale bar: 10μm. (B) Western blot analysis showed that treatment with 5ug/mL BFA for 19h caused a decrease in the Gly2 state and an increase in the Gly1 state of the wild type Panx1a protein. No effect was detected for the Y205A mutant. Proteins were detected using an anti-GFP antibody. ß-actin served as a protein loading control. (C, D) Co-localization of EYFP-tagged Panx1a and the Y205A mutant with mCherry-tagged Sec24D (COP II vesicle marker), His-tagged Cav-1 (Caveolin-1 marker), DsRed-tagged calreticulin (ER marker), and DsRed-tagged galactosyltransferases (Golgi apparatus marker). His-tagged Cav-1 was detected using an anti-His antibody and Alexa Fluor 568 secondary antibody. (E, F) Co-localization quantification of the wild type and mutant Panx1a with the vesicle and organelle markers. Error bars show standard error of the mean. WT Panx1a + Sec24D: n = 34, WT Panx1a + Cav-1: n = 36, WT Panx1a + ER: n = 29, WT Panx1a + Golgi: n = 35, Y205A + Sec24D: n = 30, Y205A + Cav-1: n = 31, Y205A + ER: n = 20, Y205A + Golgi: n = 20. (G) Real-time qPCR analysis of ER stress genes. Neuro 2a cells were transfected with EYFP alone, Panx1a-EYFP, and Y205A-EYFP. When indicated, cells were treated with 5ug/mL BFA for 19h. 18s rRNA was used as the reference gene. EYFP-transfected cells were used as the control group. Data were collected in three independent experiments in triplicate for each gene. All data were relative to the EYFP control group. ****$p < 0.0001$, ***$p < 0.001$, *$p < 0.05$.*

3.3.5. Trafficking of Y205A to the cell surface cannot be rescued by WT Panx1a

Double transfection of WT Panx1a-DsRed with Y205A-EYFP did not rescue the observed localization phenotype. The intracellular retention of the mutant remained (**Figure 3.5A**). However, with the evident co-localization of mutant and WT proteins in the cytoplasm, we proceeded to test whether the two proteins interacted.

Förster Resonance Energy Transfer (FRET) experiments determined the proximity between Panx1a WT and the Y205A mutant. Panx1a-DsRed and Panx1a-EYFP had a FRET efficiency above the threshold of 0.014 at the cell membrane. We concluded that the channels had assembled in a compact state after insertion into the cell membrane (0.06 ± 0.03, n = 103) (**Figure 3.5B**). As expected, the intracellular FRET efficiency

between Panx1a-DsRed and Panx1a-EYFP was significantly lower than at the cell membrane. This was explained as reflecting the increased compactness when Panx1a channels were assembled from protein monomers (0.03 ± 0.02, n = 100; p = < 0.0001). No significant difference in FRET efficiency was detected between the intracellular Panx1a-DsRed and Panx1a-EYFP pair when compared to Panx1a-DsRed paired with Y205A-EYFP mutant (0.03 ± 0.02, n = 63; p = 0.25), or pairs of mutants Y205A-DsRed and Y205A-EYFP (0.03 ± 0.03, n = 50; p = 0.71), suggesting neither combination had the ability to reach a compact state. To complement these results, we also calculated the FRET distance based on the FRET efficiencies (**Supplementary Figure 3.2**).

The FRET experiment did not allow us to conclude the ability of wild type and mutant proteins to interact. This question was addressed using a His60 Ni column pull-down assay. The Panx1a-dTomato-His protein pulled down Panx1a-EYFP efficiently (**Figure 3.5C**). The Y205A-dTomato-His protein showed a faint signal corresponding to Panx1a-EYFP, suggesting that the ability to interact was drastically reduced. The negative control, dTomato-His paired with Panx1a-EYFP protein lysates, did not pull-down wild type Panx1a subunits excluding dTomato-His as interaction partner with either Panx1a or EYFP.

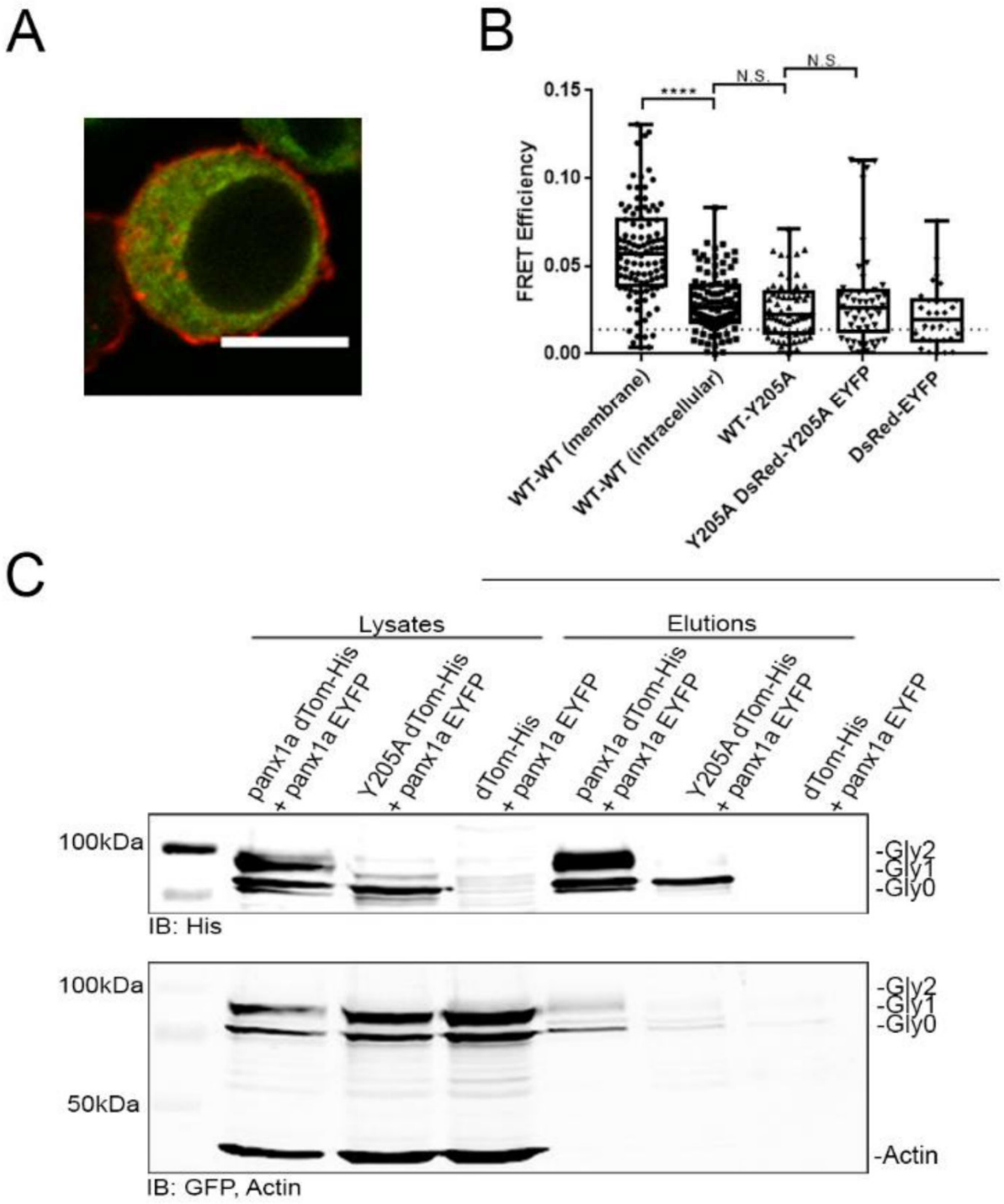
A
B
C
FRET Efficiency
0.15
0.10
0.05
0.00
****
N.S.
N.S.
WT-WT (membrane)
WT-WT (intracellular)
WT-Y205A
Y205A DsRed-Y205A EYFP
DsRed-EYFP
Lysates
Elutions
panx1a dTom-His + panx1a EYFP
Y205A dTom-His + panx1a EYFP
dTom-His + panx1a EYFP
100kDa
-Gly2
-Gly1
-Gly0
IB: His
50kDa
-Actin
IB: GFP, Actin

*Figure 3.5. Interaction studies of Panx1a and the Y205A mutant using FRET and pull-down assay. (A) Fluorescent image showing a Neuro 2a cell transfected with Panx1a-DsRed and Y205A-EYFP. Scale bar: 10μm. (B) FRET efficiencies. WT–WT (membrane) (n = 103) indicates Panx1a-DsRed interaction with Panx1a-EYFP using selected cell membrane regions as a positive control. WT–WT (intracellular) (n = 100) indicates Panx1a-DsRed interaction with Panx1a-EYFP using selected regions inside the cell. WT-Y205A (n = 63) indicates Panx1a-DsRed interaction with Y205A-EYFP inside the cell. Y205A-Y205A (n = 50) indicates Y205A-DsRed interaction with Y205A-EYFP inside the cell. DsRed-EYFP indicates DsRed interaction with EYFP inside the cell as the negative control. The dotted line represents the FRET efficiency threshold of 1.4%. (C) His60 Ni pull-down using cells double-transfected with Panx1a-dTomato-His and Panx1a-EYFP, Y205A-dTomato-His and Panx1a-EYFP, or dTomato-His with Panx1a-EYFP. Cell lysates on the left show expression levels before pull down. Elutions on the right show proteins recovered by pull down. Anti-GFP and anti-His antibodies detected eluted proteins. An anti-ß-actin antibody served as a loading control. ****p < 0.0001, N.S., not significant.*

3.4. Discussion

3.4.1. Panx1a requires aromatic amino acid residues for folding and stabilization

The highly conserved aromatic amino acid residues located on the intracellular side of transmembrane domain 2 (TM2) and 3 (TM3) were identified by sequence alignment with human Pannexin proteins and the INX-6 channel. Presently, only the high-resolution crystal structure of INX6 has been reported. The mutation of either the Y205 or the W123 residues resulted in the retention of the protein. Since the two residues are in close proximity to each other, as seen with the INX-6 channel, it is possible that they interact by aromatic–aromatic interactions similar to those reported previously (Johnson et al., 2007). We suspect that this interaction is needed for protein structure by enhancing the helix–helix association in a membrane environment. To prove this, we created mutants in which the aromatic residue was moved one or two residues upstream of the

205 position. Our data show that the position of the tyrosine residue is critical. When Y205 was mutated to another aromatic residue, phenylalanine, membrane localization was restored.

Many integral membrane proteins contain transmembrane domains made up of bundles of lipid-bilayer-spanning alpha helices. The TM alpha-helices are generally composed of a core of mostly hydrophobic amino acids, with basic and aromatic amino acids at each end of the helix. This arrangement is suggested to play a unique role in membrane protein interactions with water/lipid interfaces, anchoring the proteins into the membrane through an interaction of their aromatic rings with the lipid head groups (Killian and Heijne, 2000; Cowan et al., 1992; Ulmschneider and Sansom, 2001). Previously, aromatic–aromatic interactions have been shown to stabilize the transmembrane domains of the K^+ channel (Gebhardt et al., 2011). The study explores the implications of these interactions for both channel function and stabilization. Similarly, a pore-blocking hydrophobic motif at the cytoplasmic aperture of the closed-state Nav1.7 channel was found (Lampert et al., 2008). However, a scanning cysteine-alanine mutagenesis (SCAM) analysis of the mouse Panx1 protein expressed in the *Xenopus laevis* oocyte model (Wang and Dahl, 2010) has shown that replacing W127 and F220 with the amino acid cysteine had only minor effects on irreversible current inhibition with no loss-of-channel function after treatment with 100μM maleimidobutyryl-biocytin (MBB).

3.4.2. Lack of the aromatic amino acid residues disrupts trafficking and limits post-translational processing of Panx1a

Here, we present results that provide insight into the post-translational processing of Panx1a and the relevance for trafficking. The presence of the high mannose

glycosylation form (Gly1) on western blots indicated the ability to undergo limited post-translational modification. Both W123A and Y205A mutant proteins still underwent the first modification step towards complex glycosylation (Gly2). N-glycosylation of rodent or human Pannexin-1 at amino acid position N254 and the corresponding position N246 in zebrafish Panx1a is considered necessary for trafficking to the cell membrane (Boassa et al., 2008; Penuela et al., 2007; Kurtenbach et al., 2013). When lacking this N-glycosylation motif, both Gly1 and Gly2 forms were missing, and cell surface transport was limited (Penuela et al., 2007; Penuela et al., 2009; Kurtenbach et al., 2013; Prochnow et al., 2009).

The co-localization analysis revealed that the Y205A mutant was more abundant in the ER than the Golgi. Previous research has shown that the transport of Panx1 between the ER and Golgi is mediated via COP II vesicles (Bhalla-Gehi et al., 2010). When we tested the co-localization of Y205A with Sec24D, a COP II protein, a strong co-localization was found. Panx1 has also previously been shown to co-localize with the scaffolding protein Cav-1 (Delalio et al., 2018), which is the main component of the caveolae plasma membranes found in many cell types. Here, only the wild type Panx1a protein co-localized efficiently, with significantly less co-localization of the Y205A mutant. The reduced co-localization with Cav-1 and lack of complex glycosylation implied that the Y205A mutant was not trafficking efficiently past the Golgi stage. This assumption was tested by blocking trafficking between ER and Golgi with BFA treatment. Similar to previous reports (Boassa et al., 2008), the spatial differences of intracellular Panx1 trafficking correlated with Golgi blockage by BFA treatment.

3.4.3. The Y205A trafficking deficiency was not caused by ER stress

The accumulation of integral membrane proteins like Panx1a can occur upon transient overexpression, causing ER stress when misfolded or when otherwise altered proteins trigger a cellular stress response. The RT qPCR analysis tested whether ER stress was a confounding factor in this investigation. Transcriptional regulation of Atf-4, CHOP, EDEM, BiP, and XBP1 is known as an indicator of ER stress and the unfolded protein response (UPR) (Oslowski and Urano, 2011). Brefeldin-A treatment reliably upregulated the Atf-4, CHOP, EDEM, and BiP transcripts in Neuro 2a cells. In the case of XBP1, we also used primers for the spliced, unspliced, and total XBP1 mRNA. When the XBP1 mRNA is spliced, it produces a transcriptionally active basic leucine zipper transcription factor that participates in regulating other ER stress genes. The spliced XBP1 was significantly upregulated after BFA treatment, validating our model. Both overexpression of the Y205A mutant or the wild type Panx1a failed to cause transcriptional activation of ER stress genes. We excluded ER stress response as a primary cause of trafficking deficiencies of the Y205A mutant. Other types of protective or destructive stress responses, such as apoptosis, necrosis, pyroptosis, or autophagic cell death, were not investigated since transfected cells appeared healthy when the experimental endpoints were reached.

3.4.4. The Y205A mutation disrupted the oligomerization state of the Panx1a channel assembly

FRET tests and pull-down experiments tested the interaction between Y205A-EYFP and WT Panx1a-DsRed protein pairs. In contrast to wild type:wild type pairs, the low FRET efficiency detected between wild type:Y205A, as well as Y205A:Y205A pairs,

suggested that the mutant protein failed to form higher-order complexes. Consistently, the pull-down experiment demonstrated that the interaction between wild type and mutant proteins was low or even nonexistent.

3.5. Conclusions

This study identified two critical aromatic amino acids, W123 and Y205, that together help Panx1a proteins to oligomerize and efficiently traffic to the cell membrane. Based on the high-resolution structure of the INX-6 channel (Oshima et al., 2016), it is reasonable to speculate that the aromatic–aromatic interaction between Y205 and W123 contributes to Panx1a channel folding or assembly. These findings provide new insights into the life cycle of Pannexins by complementing a growing body of distinct molecular mechanisms and requirements, enabling regulation of Panx1 oligomerization, glycosylation, and trafficking.

3.6. Supplementary materials

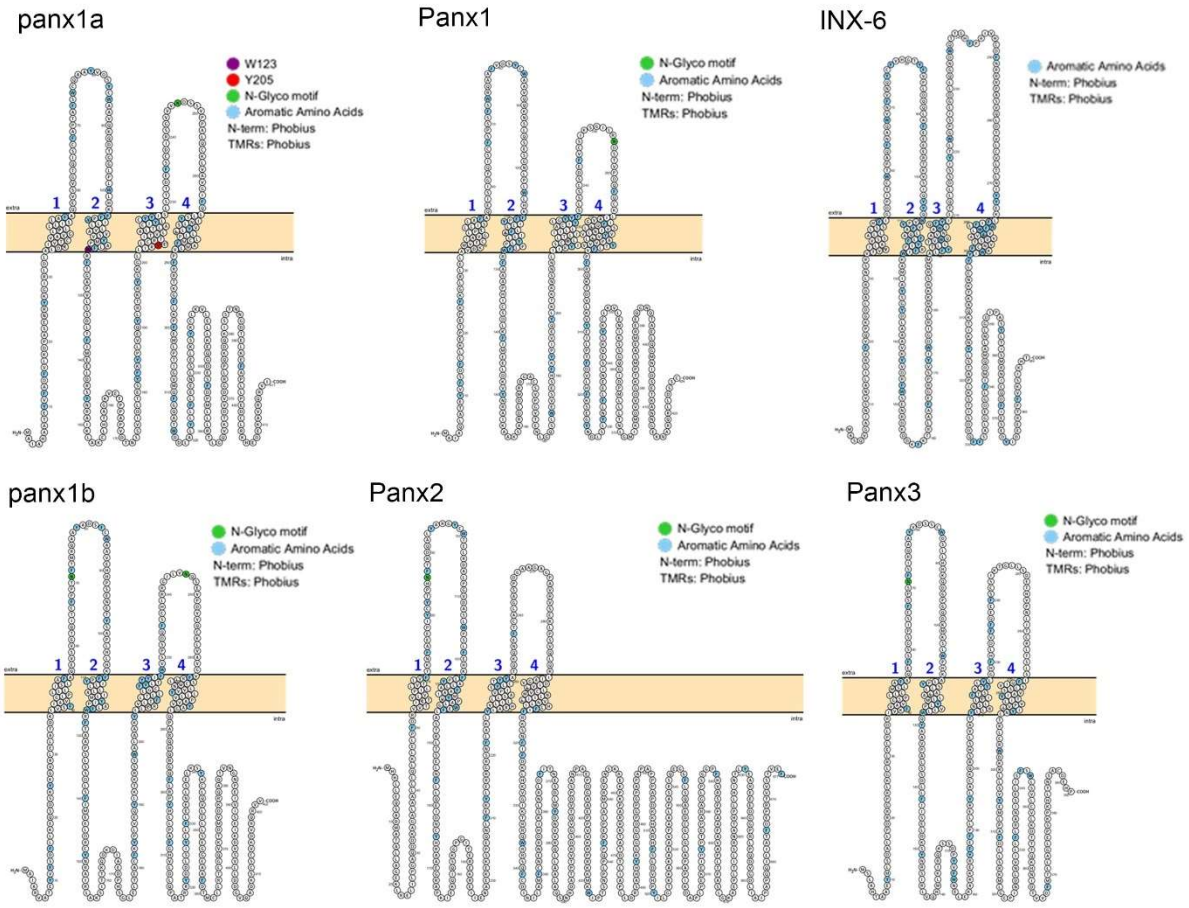

Supplementary Figure 3.1. Topological comparison of Panx1a with its ohnologue panx1b, human Pannexin orthologs, and the C. elegans INX-6 protein. The aromatic residues W123 and Y205 are highlighted in Panx1a in purple and red, respectively. Aromatic residues (tyrosine, tryptophan, and phenylalanine) are highlighted in blue. Images were generated using the interactive Protter tool (Omasits et al., 2014).

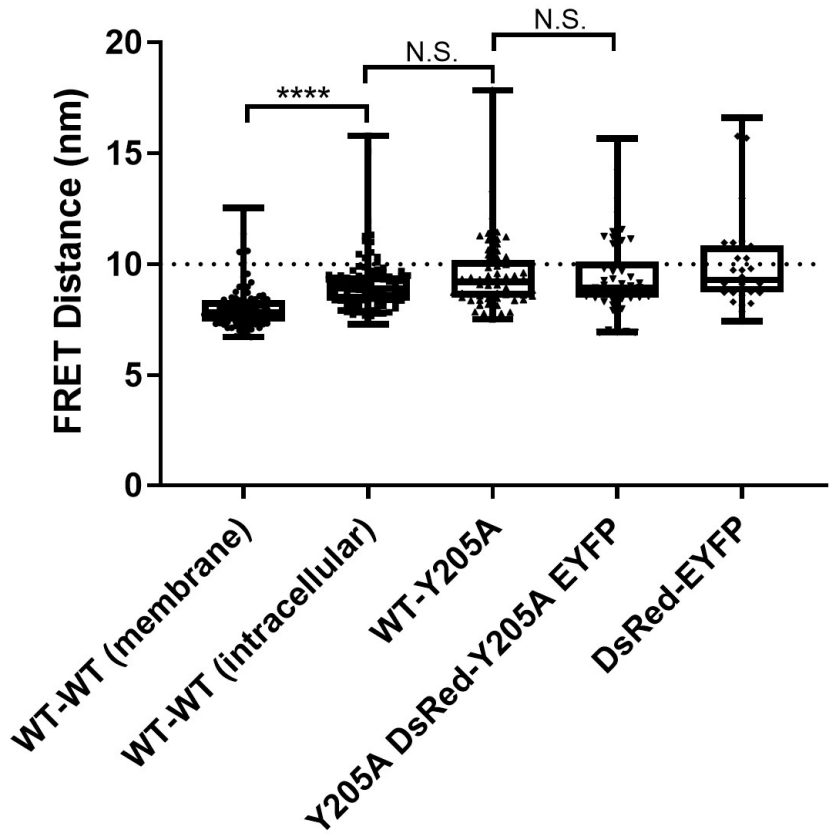

*Supplementary Figure 3.2. FRET distance graph shows the FRET distance using the reference distance between DsRed and EYFP pair (4.9nm). WT-WT (membrane) indicated Panx1a-DsRed interaction with Panx1a-EYFP using selected cell membrane regions as a positive control. WT-WT (intracellular) indicated Panx1a-DsRed interaction with Panx1a-EYFP using selected regions inside the cell. WTY205A indicated Panx1a-DsRed interaction with Y205A-EYFP using selected regions inside the cell. Y205A-Y205A indicated Y205A-DsRed interaction with Y205A-EYFP inside the cell. Note that only WT:WT pairs in the cell membrane showed proximity indicating a compact assembly of Panx1a monomers in channels. DsRed-EYFP pairs serve as negative control. The dotted line represents the FRET distance threshold of 10nm. ****p < 0.0001.*

Chapter 4. Exploring the Panx1a interactome and phosphorylation in transfected Neuro 2a cells

4.1. Introduction

Currently, the interactome of Panx1 and its related family members is understudied. A substantial amount of work is required to understand the full extent of Pannexins and their role in cellular signaling via interactions with other proteins. Recent studies have explored phosphorylation's role in channel activity and trafficking. However, modern research has only just begun scratching the surface of understanding the complexity of Panx1 signaling.

Some of the prominent Panx1 interactors identified are Caspase 1 and purinergic receptors. Panx1 has been shown to interact with Caspases, whereby the channel gets activated in apoptotic cells via the cleavage of its C terminal (Kim et al., 2015; Sandilos et al., 2012). The purinergic receptor family proteins are also known interactors of Panx1 (Li et al., 2011; Silverman et al., 2009; Pelegrin and Suprenant, 2006). Purinergic receptors have been shown to activate Panx1, and together they influence cell signaling via calcium propagation, apoptosis via ATP release, and induction of seizures via regulation of acetylcholine 1 (M1) receptor, and inflammation-induced enteric neuron death (Pelegrin and Suprenant, 2006; Locovei et al., 2007; Iglesias et al., 2008; Kim and Kang, 2011; Gulbransen et al., 2012). Known and predicted interactors of the human and mouse Panx1 can be visualized by STRING database as shown below (**Figure 4.1 and Figure 4.2**) (Szklarczyk et al., 2019).

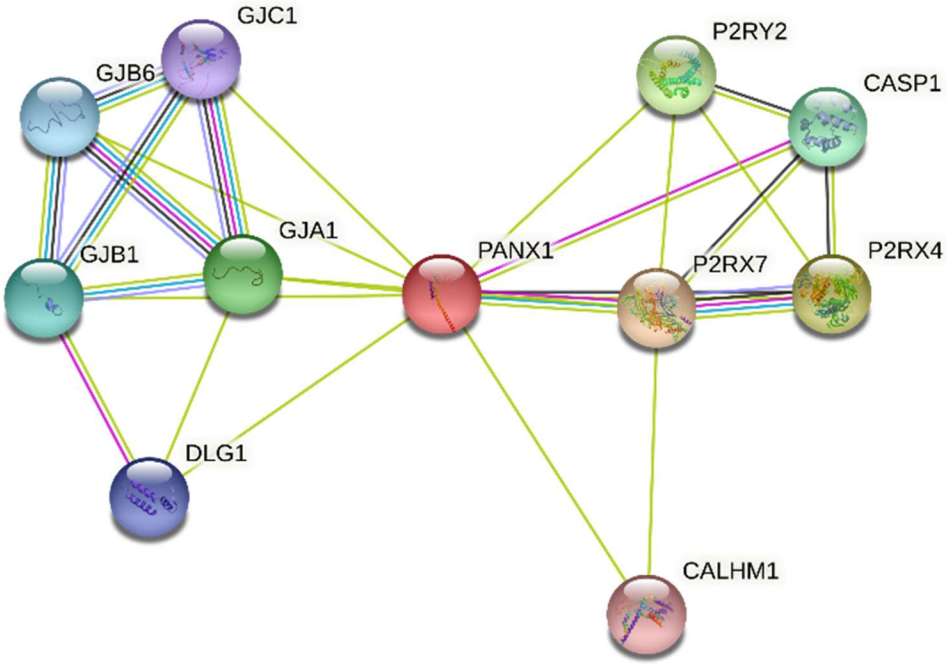

Figure 4.1. Interaction data of human Panx1 from STRING database. Edges represent protein-protein associations. Light blue edges: from curated databases (known interactions), pink edges: experimentally determined (known interactions), black edges: co-expression, yellow edges: text mining. Coloured nodes indicate query protein (red) and the first shell of interactors. Nodes that are filled contain known or predicted 3D structures of the proteins. Abbreviations: P2RX7: P2X purinoreceptor 7, P2RX4: P2X purinoreceptor 4, P2RY2: P2Y purinoreceptor 2, GJA1: Gap junction alpha-1 protein, CASP1: Caspase-1, GJB1: Gap junction beta-1, GJB6: Gap junction beta-6, DLG1: Disks large homolog 1, GJC1: Gap junction gamma-1, CALHM1: Calcium homeostasis modulator protein 1. Figure created using STRING database (Jensen et al., 2009).

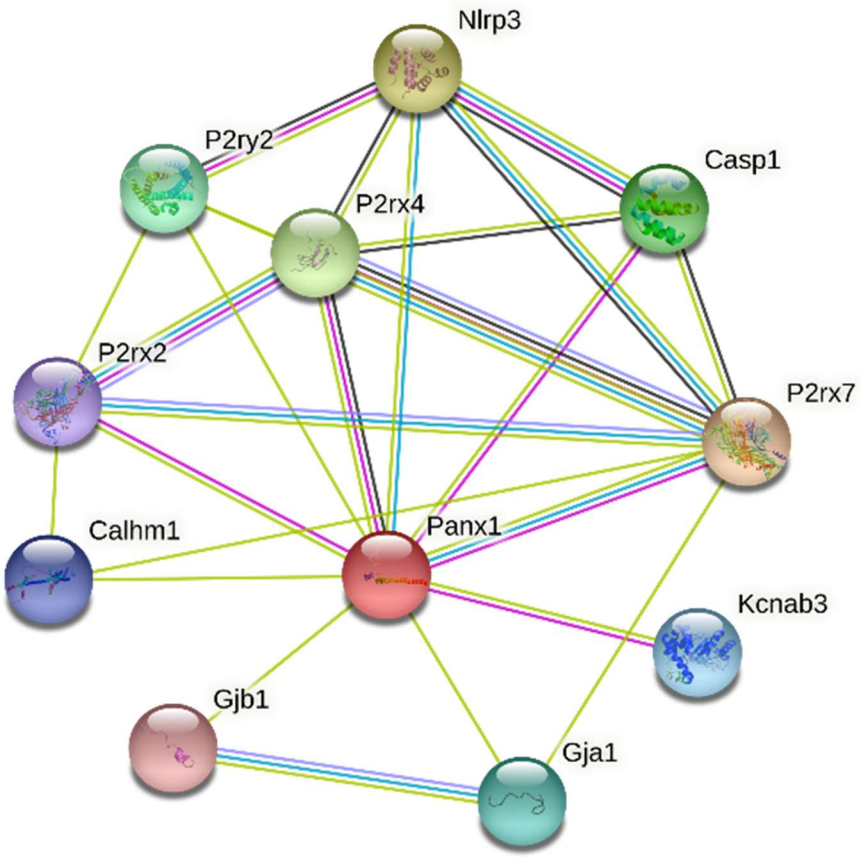

Figure 4.2. Interaction data of mouse Panx1 from STRING database. Edges represent protein-protein associations. Light blue edges: from curated databases (known interactions), pink edges: experimentally determined (known interactions), black edges: co-expression, yellow edges: text mining. Coloured nodes indicate query protein (red) and the first shell of interactors. Nodes that are filled contain known or predicted 3D structures of the proteins. Abbreviations: P2rx7: Purinergic receptor p2x, Nlrp3: NACHT, LRR and PYD domains-containing protein 3, P2rx4: Purinergic receptor p2x, ligand-gated ion channel 4, Casp1: Caspase-1, P2ry2: Purinergic receptor p2y, g protein-coupled 2, Gja1: Gap junction alpha-1, Kcnab3: Potassium voltage-gated channel shaker-related subfamily a, beta member 3, Calhm1: Calcium homeostasis modulator protein 1, P2rx2: P2X purinoreceptor 2, Gjb1: Gap junction beta-1. Figure created using STRING database (Jensen et al., 2009).

A few kinases have also been proposed to interact with Panx1 to modify the protein post-translationally. SFKs are the most established interacting kinases of Panx1. Research shows that SFKs activate Panx1 via phosphorylation of residues on both the

CL and CT at Y198 and Y308, respectively (Lohman et al., 2015; Weilinger et al., 2016). Furthermore, SFKs also regulate Panx1 trafficking via phosphorylation of the CL residue Y150 (Nouri-Nejad et al., 2021). Studies propose that serine/threonine kinases like PKG and CaMKII also modulate Panx1 in response to nitric oxide exposure (Poornima et al., 2015) and an increase in cytoplasmic calcium (Lopez et al., 2021), respectively.

In this chapter, we explore the interactome of the zebrafish Panx1a using Neuro 2a cells. With the ongoing and existing research on the mammalian Panx1, we want to determine how the zebrafish Panx1a compares and differs from its mammalian counterpart. Exploring the phospho-proteome of Panx1a will allow us to study Pannexins in a live animal model that provides the feasibility of use to better understand these membrane channels.

4.2. Results

4.2.1. Identification and In-silico analysis of Panx1a-interacting proteins

To explore the Panx1a interactome, we performed a His-column purification in combination with mass spectrometry. Neuro 2a cells were transfected with Panx1a-dTomato-His or dTomato-His empty vector control and were subjected to affinity purification using the His60 Ni Gravity Column 48 hours post-transfection. The resulting eluates were processed, and proteins were identified using LC-MS/MS and ran through PEAKS Studio 10.6 build 20201221 and Scaffold. The sample preparation and the protein and PTM identification were performed by SPARC BioCentre Molecular Analysis, The Hospital for Sick Children, Toronto, Canada. Proteins identified in the dTomato-His negative control samples were pooled and removed from the Panx1a interacting partners. The final list of identified interacting proteins is summarized in Appendix Table A.1.

The resulting Panx1a interactors were analyzed using the PANTHER database. Functional classification was performed based on the inputted accession numbers. PANTHER identified a total of 177 genes, of which 151 were classified into 11 different Molecular Function classes (**Figure 4.3A**), 296 into 12 different Biological Process classes (**Figure 4.3B**), and 145 into 20 different Protein classes (**Figure 4.3C**). Interestingly, the protein class with the highest number of gene hits was ‘protein modifying enzymes'. This class can be further divided into four categories: the non-receptor serine/threonine protein kinase (3 genes), protease (8 genes), protein phosphatase (1 gene), and ubiquitin-protein ligase (7 genes) (**Figure 4.3D**). The three non-receptor serine/threonine protein kinases identified were Citron Rho-interacting kinase (Cit), Calcium/calmodulin-dependent protein kinase type II subunit delta (CaMKIId), and Cyclin-dependent kinase 2 (Cdk2). In addition, other relevant protein interactors included A-kinase anchor protein 12 (Akap12) and Proto-oncogene tyrosine-protein kinase receptor Ret (Ret). Forty-one interacting proteins were also grouped into 29 different Pathways (**Figure 4.3E**).

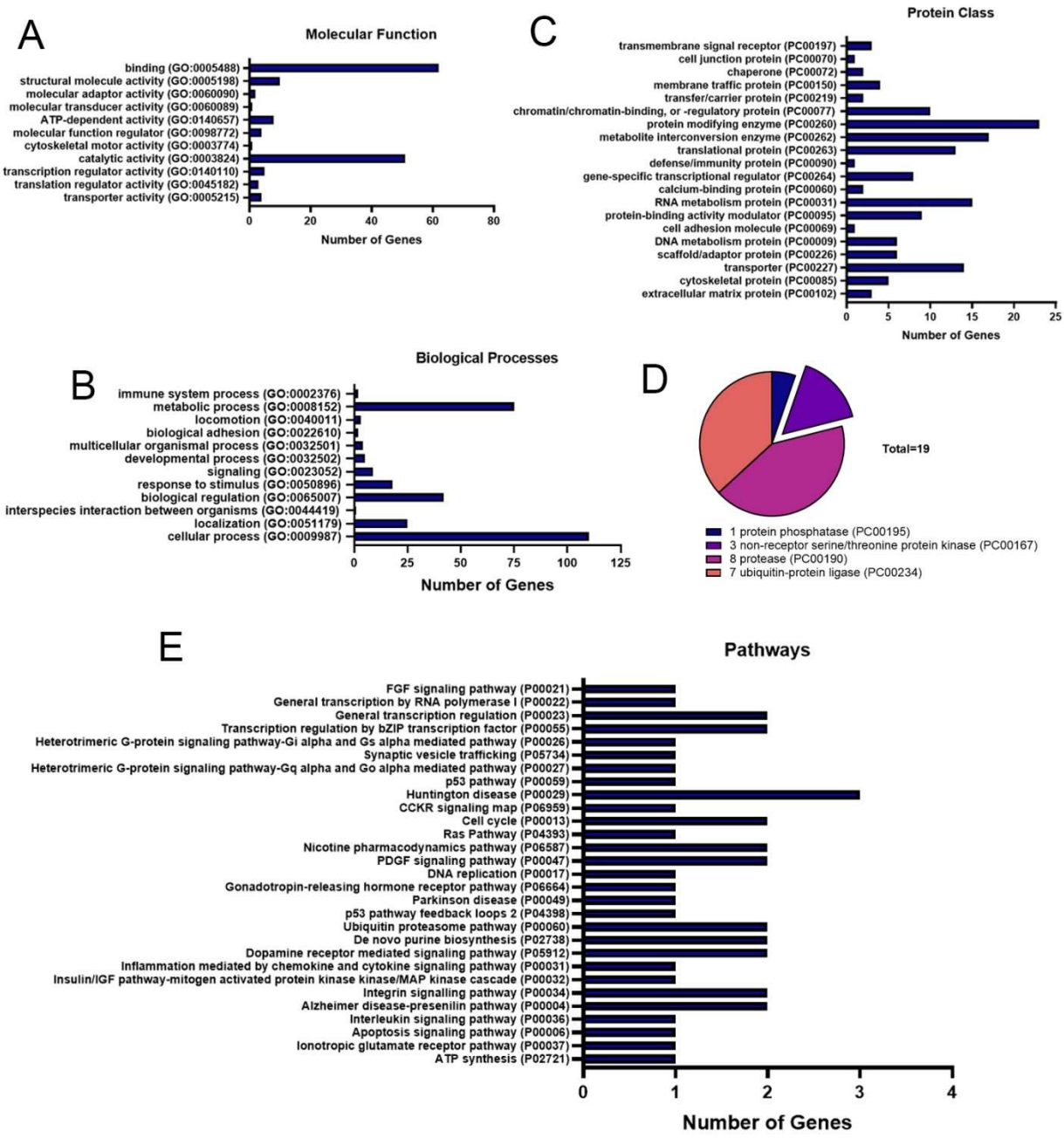

Figure 4.3. PANTHER classification of Panx1a interacting proteins in transiently transfected Neuro 2a cell line. A total of 177 genes were identified as interacting partners and were categorized into (A) Molecular Function, (B) Biological Processes, and (C) Protein Class. (D) Pie chart shows the distribution of 19 identified genes (out of 23) in the "protein modifying enzymes" protein class. (E) PANTHER pathways were identified by grouping 41 of the 177 protein hits.

4.2.2. Identification and characterization of novel Panx1a phosphorylation residues

We demonstrated that the overexpressed Panx1a-EYFP is phosphorylated in Neuro2a cells (**Figure 4.4A**). The PhosphoPurification column isolated intact proteins that contain phosphorylation modifications. Our western blot analysis showed bands corresponding to Panx1a in the phosphorylated fraction. The absence of b-Actin in the phosphorylated fraction indicates that the experiment was successful, and the column did not trap non-phosphorylated proteins.

We identified four phosphorylation sites in the intracellular loop of Panx1a from our mass spectrometry analysis. One residue, T164, showed a reliable site of phosphorylation. T158, T171, and S174 are also potential phosphorylation sites but with lower localization probability. We created point mutations to generate T164A, S174A, and S173A mutants. T164 was chosen based on its reliable detection, S174 was chosen as it is conserved in the human and mouse Panx1, and S173 was chosen since it is the neighbouring residue to S174.

First, we looked at the expression of these mutants by western blot and saw no visible differences compared to WT Panx1a (**Figure 4.4B**). We then used the dye uptake assay to test the functionality of these mutants compared to WT Panx1a. Neuro 2a cells were transfected with Panx1a-EYFP WT and mutants, and cells were treated with EtBr (10uM) for 5 minutes. There were no visible differences in the localization of each Panx1a construct. We used the total EtBr uptake values normalized to Panx1a expression to quantify these results (**Figure 4.4C**). Although there was no difference between WT Panx1a and T164A or S174A mutants (Panx1a: 2.46 ± 0.12, n = 106; T164: 2.56 ± 0.11,

n = 85, p = 0.72; S174: 2.37 ± 0.13, n = 73, p > 0.99), the S173A mutant showed a significant decrease in EtBr uptake (S173A: 1.32 ± 0.068, n = 112, p < 0.0001). Images show EtBr uptake before and after EtBr application (**Figure 4.4D**).

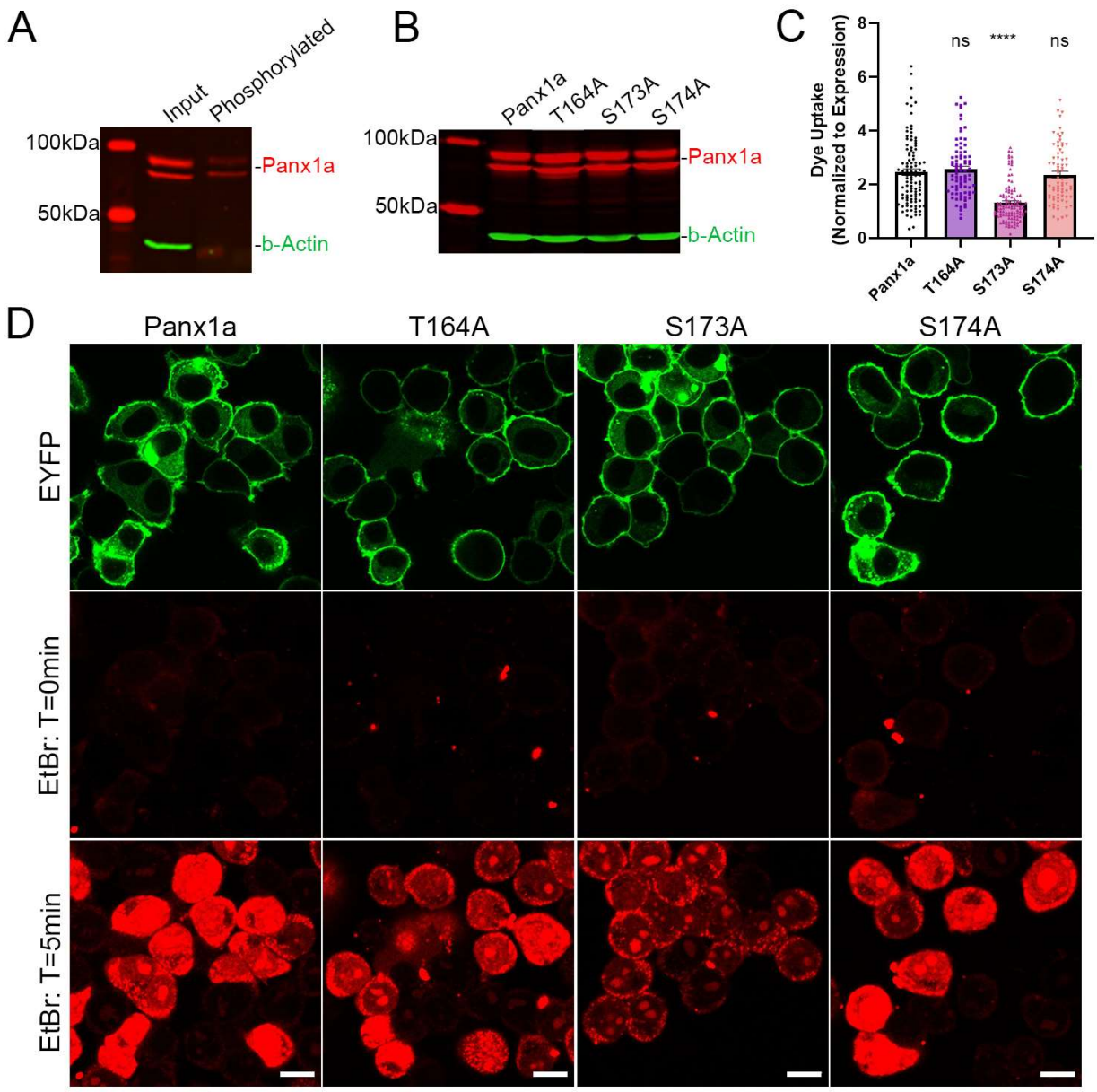
A
Input
Phosphorylated
100kDa
50kDa
-Panx1a
-b-Actin
B
Panx1a
T164A
S173A
S174A
100kDa
50kDa
-Panx1a
-b-Actin
C
Dye Uptake
(Normalized to Expression)
ns
****
ns
Panx1a
T164A
S173A
S174A
D
Panx1a
T164A
S173A
S174A
EYFP
EtBr: T=0min
EtBr: T=5min

*Figure 4.4. Characterization of phosphorylated residues in the intracellular loop of Panx1a. (A) Western blot analysis of phospho-purification of Neuro 2a cells transfected with Panx1a-EYFP. The input fraction represents the total lysate prior to phospho-protein purification. The phosphorylated fraction represents the intact eluted phospho-containing proteins. B-Actin served as the negative control. (B) Western blot analysis of cells transfected with Panx1a-EYFP WT and phosphorylation mutants. B-Actin served as the loading control. (C) Quantification of total dye uptake normalized to Panx1a-EYFP expression after 5 minutes as described in (D). (D) Dye uptake images of cells transfected with Panx1a-EYFP WT and phosphorylation mutants. The top panels show the subcellular localization and expression of the WT and mutated Panx1a proteins. Middle panels show the intracellular dye levels immediately after EtBr (10uM) application. The bottom panels show the dye uptake after 5 minutes of EtBr application. Scale bar: 10um. Panx1a was used as the control group for statistical analysis. ****p < 0.0001, ns not significant.*

4.2.3. Exploring the effects of kinase pharmacological agents on Panx1 activity

We were interested in exploring the effects of various kinase inhibitors on the activity of Pannexins. Previous studies have shown that Panx1a and Panx1b are more active in comparison to mouse Panx1 (mPanx1) (Kurtenbach et al., 2013). For this reason, we decided to test the dye uptake activity of all three Panx1s with various kinase treatments. We used three pharmacological agents: MAPK inhibitor PD98059, GSK3 inhibitor SB415286, PKA inhibitor H-89, and AMPK activator Metformin. For Panx1a, we did not observe any significant changes in dye uptake activity (Panx1a: 2.38 ± 0.17, n = 50; Panx1a/PD98059: 4.93 ± 0.96, n = 31, p = 0.36; Panx1a/SB415286: 2.32 ± 0.15, n = 31, p > 0.99; Panx1a/H-89: 6.57 ± 1.70, n = 25, p = 0.09; Panx1a/Metformin: 2.37 ± 0.20, n = 34, p > 0.99) (**Figure 4.5A**). Panx1b had significantly more dye uptake with PD98059 and H-89 treatments (Panx1b: 5.71 ± 0.89, n = 13; Panx1b/PD98059: 18.84 ± 2.60, n = 9, p = 0.005; Panx1b/SB415286: 7.69 ± 2.01, n = 8, p > 0.99; Panx1b/H-89: 32.24 ± 4.72, n = 8, p < 0.0001; Panx1b/Metformin: 4.94 ± 0.41, n = 8, p > 0.99) (**Figure 4.5B**). mPanx1 activity was significantly affected by H-89 and Metformin (mPanx1: 1.67 ± 0.13, n = 49; mPanx1/PD98059: 3.43 ± 0.76, n = 21, p > 0.99; mPanx1/SB415286: 1.48 ± 0.11, n =

19, $p > 0.99$; mPanx1/H-89: 4.06 ± 1.04, $n = 16$, $p < 0.004$; mPanx1/Metformin: 1.004 ± 0.11, $n = 23$, $p = 0.036$) (**Figure 4.5C**).

It is important to note that although there was no significant effect on dye uptake activity of Panx1a, the treatment of Neuro 2a cells with the various pharmacological agents affected Panx1a expression and cellular morphology (**Figure 4.5D**). The MAPK inhibitor, PD98059, resulted in a “dotty” vesicle-like expression of Panx1a. The GSK3 inhibitor, SB415286, caused the cells to be deformed, large, and have multiple nuclei. The PKA inhibitor, H-89, resulted in the differentiation of the cells with long, dendritic-like processes. The AMPK activator, Metformin, had no visible effect on Panx1a expression or cellular morphology.

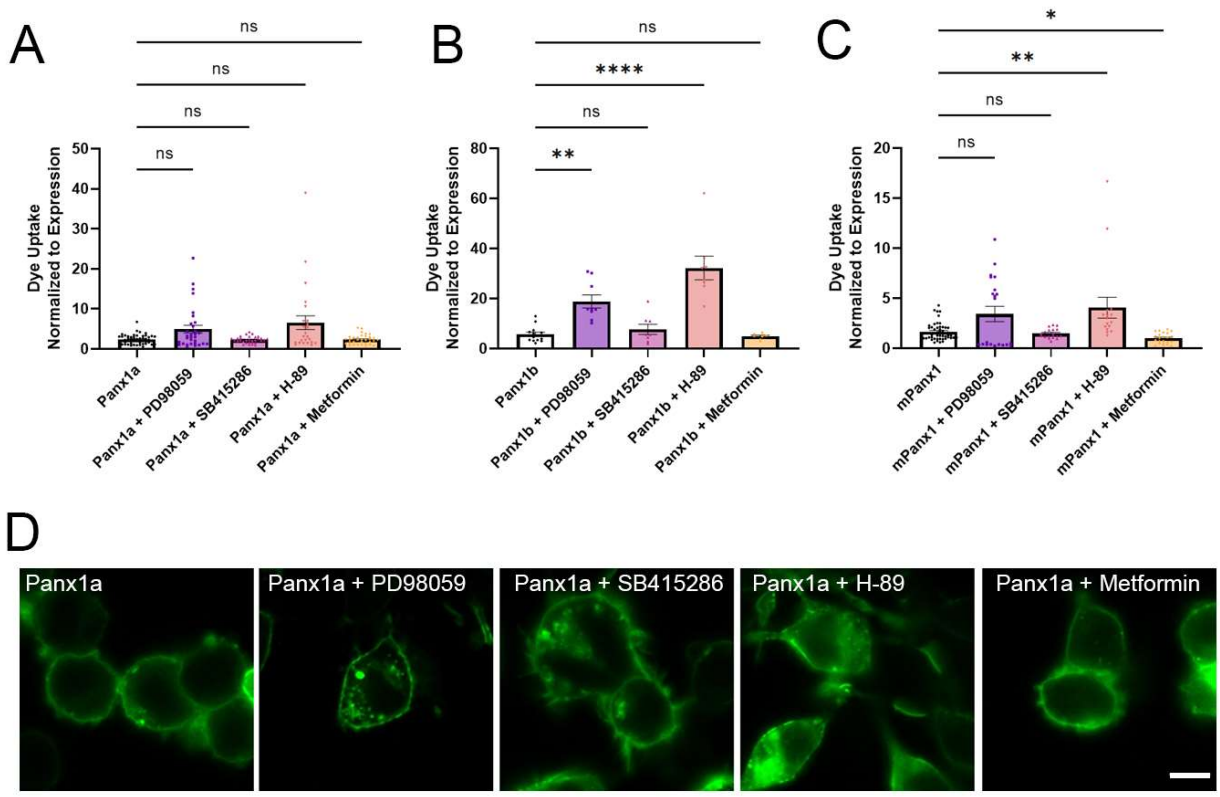

*Figure 4.5. Effects of kinase pharmacological agents on the dye uptake activity of different Panx1s. Quantification of (A) Panx1a, (B) Panx1b, and (C) mPanx1 dye uptake activity with or without treatment of PD98059 MAPK inhibitor, SB415286 GSK3 inhibitor, H-89 PKA inhibitor, and Metformin AMPK activator drugs. All Pannexins were tagged with EYFP. Sample sizes were the following: Panx1a: n = 50; Panx1a + PD98059: n = 31; Panx1a + SB415286: n = 31; Panx1a + H-89: n = 25; Panx1a + Metformin: n = 34; Panx1b: n = 13; Panx1b + PD98059: n = 9; Panx1b + SB415286: n = 8; Panx1a + H-89: n = 8; Panx1a + Metformin: n = 8. mPanx1: n = 49; mPanx1 + PD98059: n = 21; mPanx1 + SB415286: n = 19; mPanx1 + H-89: n = 16; Panx1a + Metformin: n = 23. (D) Images show the varying effects of each drug on the expression of Panx1a and cellular morphology. Scale bar: 10μm. N.S. not significant, *p < 0.05, **p < 0.01, ****p < 0.0001.*

4.2.4. Investigating ERK2 as the phosphorylating kinase of Panx1a

After identifying T164 as a site for phosphorylation, we were interested in determining which kinase is responsible for this modification event. We used the publicly available kinase prediction software NetPhos 3.1 as a starting point. A prediction score of 0.5 or greater indicates a positive prediction ('Yes' in the "Answer'

column). The top two kinases predicted for T164 were Cdk5 and MAPK(**Table 4.1**). As MAPK has been previously identified as a potential interactor of the mouse Panx1 protein (Frederiksen et al., 2019), we were particularly interested in this kinase.

Table 4.1 Predicted kinases for the identified phosphorylated residue T164 in the intracellular loop by NetPhos 3.1 Server.

Position	Context	Score	Kinase	Answer
164 T	GKVETPPAP	0.615	Cdk5	YES
164 T	GKVETPPAP	0.543	P38MAPK	YES
164 T	GKVETPPAP	0.496	GSK3	.
164 T	GKVETPPAP	0.481	Unsp	.
164 T	GKVETPPAP	0.427	CaM-II	.
164 T	GKVETPPAP	0.393	CKI	.
164 T	GKVETPPAP	0.377	Cdc2	.
164 T	GKVETPPAP	0.351	DNAPK	.
164 T	GKVETPPAP	0.288	CKII	.
164 T	GKVETPPAP	0.247	RSK	.
164 T	GKVETPPAP	0.245	ATM	.
164 T	GKVETPPAP	0.237	PKG	.
164 T	GKVETPPAP	0.130	PKC	.
164 T	GKVETPPAP	0.091	PKB	.
164 T	GKVETPPAP	0.081	PKA	.

ERK2 phosphorylates Threonine or Serine residues immediately followed by a Proline residue. Since this motif is common for multiple kinases, we searched for an ERK2-specific docking site. The second major docking site for ERK2 is the Docking site for ERK, FXFP (DEF) domain (Cargnello and Roux, 2011). The motif is characterized by an F-X-F-P sequence, where one of the Fs can be a Y and is positioned 6-20 amino acids downstream of the phosphorylation site. This motif is present in Panx1a at position 183-F-K-Y-P-186, downstream of T164 (**Figure 4.6A, B**).

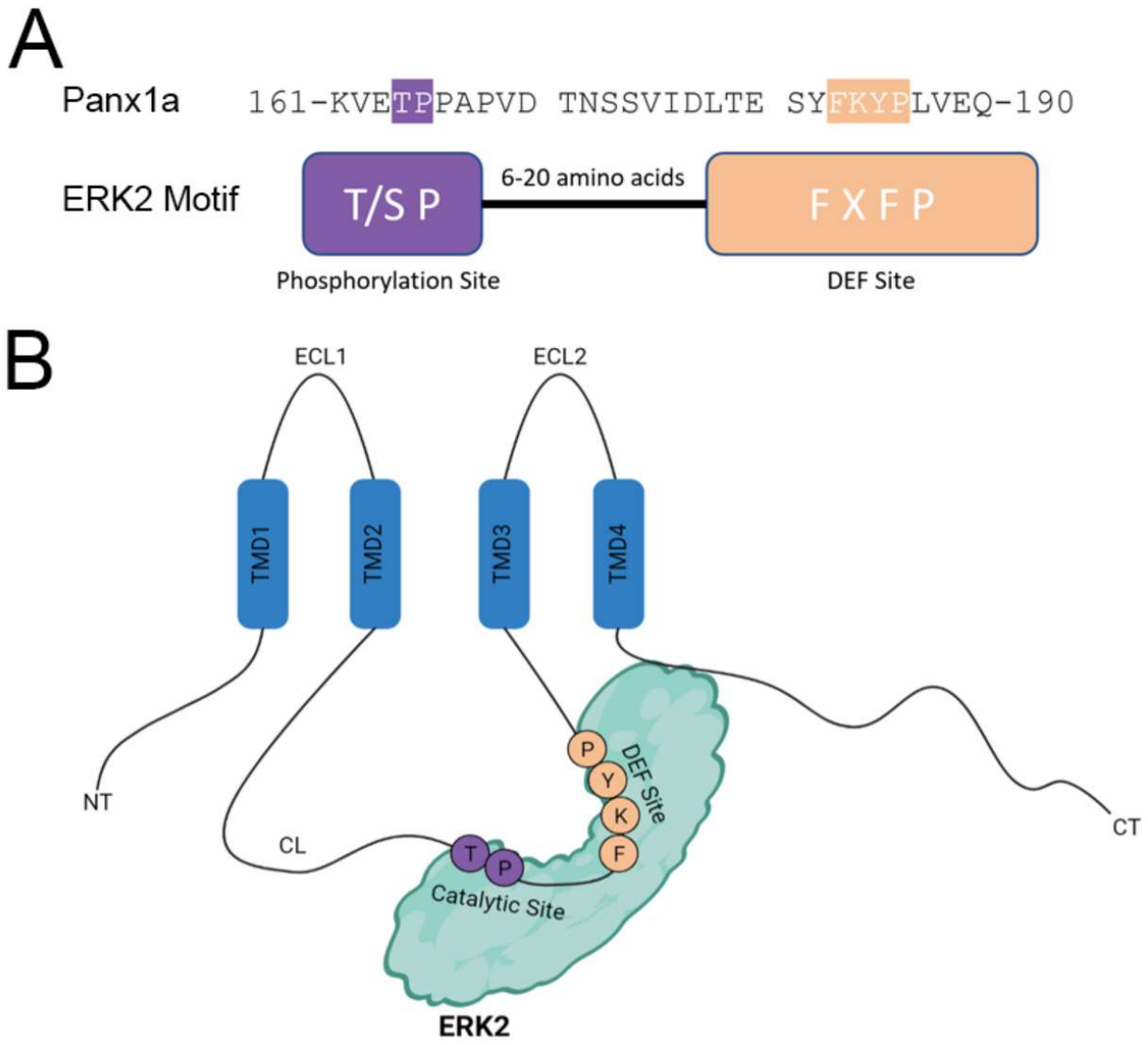

Figure 4.6. ERK2 binding motif – DEF site. (A) Portion of the Panx1a intracellular loop sequence (top) and the DEF ERK2 binding motif (bottom). (B) Topological representation of a single Panx1a subunit illustrating the binding of ERK2 to the cytoplasmic loop. Residues in purple represent T164-P165, and residues in orange represent F183-P186. DEF site: Docking site for ERK, FXFP (DEF) domain; NT: N Terminal Tail; ECL: Extracellular Loop; TMD: Transmembrane Domain; CT: C Terminal Tail; CL: Cytoplasmic Loop. Image was created with BioRender.com.

As kinase interaction can be challenging to detect, we overexpressed Panx1a-dTomato-His, ERK2-EGFP, and MEK1-Myc in the Neuro 2a cell line to conduct a co-immunoprecipitation assay. As a control, we used the dTomato-His empty vector co-

expressed with ERK2-EGFP and MEK1-Myc. Panx1a-dTomato-His was used as the bait protein and was pulled down using a rabbit anti-His antibody and Protein A Dynabeads™. A western blot analysis showed that ERK2 did not co-precipitate with Panx1a in this pull-down assay (**Figure 4.7A**). Both the experimental and the negative control did not show bands that correspond to ERK2-EGFP in the eluted fractions.

Establishing an interaction with a kinase through a Co-IP assay is not commonly done, considering that the interaction is innately transient. For this reason, we used FRET as a more sensitive approach for detecting potential interaction. A FRET efficiency of 1.2% was calculated using the Forster radius of 4.7nm for the EGFP/DsRed pair (Muller et al., 2013). Anything above 1.2% indicates that the two proteins are closer than 10nm apart, thereby potentially interacting. We overexpressed Panx1a-DsRed/ERK2-EGFP, Panx1a-DsRed/ERK2-EGFP/MEK1, and Panx1a-DsRed/ERK2-EGFP treated with PD98059. MEK1 was used as an activator for ERK2, and PD98059 was used as an ERK2 inhibitor. Our results show that there is no significant difference in FRET efficiency between Panx1a and ERK2 when co-expressed with MEK1 or treated with PD98059 (Panx1a/ERK2: 0.84 ± 0.13, n = 54; Panx1a/ERK2/MEK1: 1.66 ± 0.44, n = 22, $p > 0.99$; Panx1a/ERK2/PD98059: 0.99 ± 0.31, n = 17, $p > 0.99$) (**Figure 4.7B**). Only cells co-transfected with MEK1 showed a FRET efficiency above the threshold value of 1.2% between Panx1a and ERK2. DsRed and EGFP served as the negative control. Images show the expression of Panx1a-DsRed and ERK2-EGFP with no treatment (**Figure 4.7C**).

Finally, we measured ERK2 phosphorylation activity on Panx1a using the PhosphoProtein Purification Kit. Here, we overexpressed Panx1a-EYFP in Neuro 2a cells

and treated cells with PD98059. Panx1a was eluted in the phosphorylated fraction in equal amounts with or without the kinase inhibitor treatment (**Figure 4.7D**). Actin served as the negative control.

.

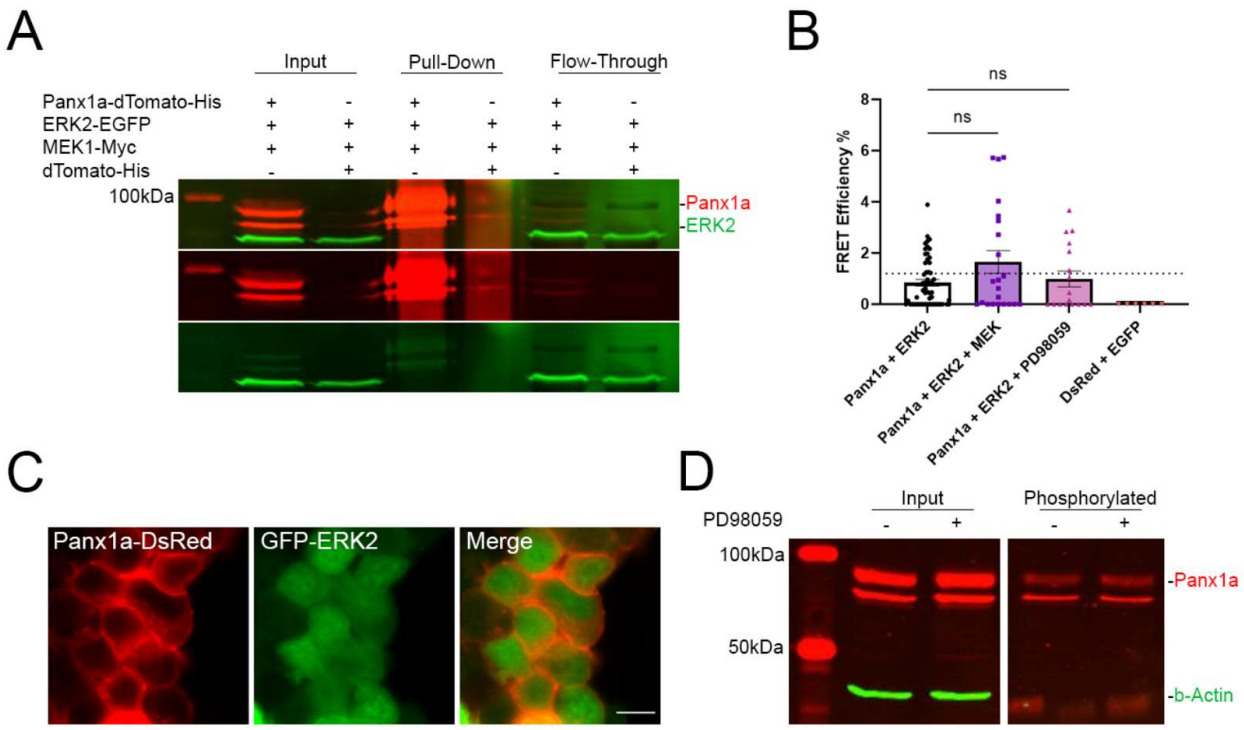

Figure 4.7. Exploring the interaction between Panx1a and ERK2. (A) Panx1a-dTomato-His was triple transfected with ERK2-EGFP and MEK1-Myc, and cells were subjected to co-immunoprecipitation. Input fractions represent the total lysates prior to immunoprecipitation with an anti-His antibody. Pull-Down represents the immunoprecipitated fractions. Cells triple transfected with dTomato-His empty vector, ERK2-EGFP, and MEK1-Myc were used as a negative control. Bottom: anti-GFP detection of GFP tagged proteins, middle: anti-His detection of dTomato-His tagged proteins, top: merged channels. (B) FRET analysis of Panx1a-DsRed and ERK2-EGFP alone, with MEK1, or with PD98059 ERK2 inhibitor. The dotted line represents the FRET efficiency threshold of 1.2%. The DsRed/EGFP pair was used as the negative control. Kruskal-Wallis multiple comparison significance test was used. Sample sizes were the following: Panx1a + ERK2: n = 54; Panx1a + ERK2 + MEK: n = 22; Panx1a + ERK2 + PD98059: n=17; DsRed + EGFP: n=6. (C) Images show Neuro 2a cells double transfected with Panx1a-DsRed and ERK2-EGFP. Scale bar: 10µm. (D) PhosphoProtein purification of Neuro 2a cells transfected with Panx1a-EYFP with or without PD98059 treatment. Panx1a-EYFP was detected using rabbit anti-GFP, and actin was used as the control. N.S. not significant.

4.3. Discussion

4.3.1. The zebrafish Panx1a membrane channel is post-translationally modified by phosphorylation

In this study, we successfully showed that Panx1a can undergo phosphorylation modifications when overexpressed in the Neuro 2a cell line. Although we were able to confidently identify at least one phosphorylated residue in the CL of Panx1a, there were challenges that we faced.

The percent coverage of the Panx1a protein in the mass spectrometry results was meager. At most, the peptides identified belonging to both Panx1a and dTomato-His (as this was a fluorescent-tagged protein) comprised 33.3% of the entire sequence. This low coverage means that there were substantial gaps in the protein coverage where we could not detect peptides. Any phosphorylated residues that might have been on these peptides were therefore not detected. Furthermore, the dynamic nature of the reversible phosphorylation modifications means that not all residues that undergo phosphorylation are consistently phosphorylated in all cell compartments. The purpose of these post-translational modifications is to allow the protein to be in a constant state of change, resulting in modulation of its biological function, trafficking between subcellular compartments, and participation in protein-protein interactions (Cohen, 2002). That said, detecting phosphorylation events on individual peptides makes it more complicated.

First, we showed that Panx1a undergoes phosphorylation modifications, as seen in the Phospho-Protein purification assay. We were able to detect a clear signal corresponding to Gly1 and Gly2 species. Interestingly, there was a visible preference for the Gly1 band in the phosphorylated fraction, indicating that phosphorylation events may

play an important role in its trafficking. We also identified multiple potential phosphorylated residues in our mass spectrometry analysis. The T164 residue was detected with high confidence for localization of the phosphorylation event. We also detected three other residues: T158, T171, and S174, all located in the cytoplasmic loop. These residues showed phosphorylation modification, but we could not confirm the location of each phosphorylation event. To conduct further analysis, we chose T164 residue for its high confidence detection, S174, as this residue is conserved in both mouse and human Panx1, and S173, considering that this residue is directly next to S174. Although the alanine mutants of these residues did not alter the expression of Panx1a, we did find it interesting that the S173A mutation had affected Panx1a function in the dye uptake assay, suggesting this residue requires phosphorylation for a fully functional channel. These results are an exciting look toward the future as we continue exploring Panx1a and its post-translational modifications.

4.3.2. Outcomes and challenges of identifying kinase interactors of Panx1a

An essential outcome of this study is the advancement toward identifying kinase interacting partners of the zebrafish Panx1a. The combined results from the interactors identified by mass spectrometry, the novel phosphorylated residues, and the pharmacological inhibition of multiple kinases lead us to explore two kinases: MAPK/ERK2, as discussed in this chapter, and CaMKIIa, which will be covered in the next chapter of this thesis.

ERK2 was the first kinase interactor we wanted to explore as this was the predicted kinase to phosphorylate residue T164. The sequence surrounding this site was a strong match for the second major ERK2 docking site known as the DEF site. In addition, the

results from the pharmacological treatment with PD98059, a MAPK inhibitor, showed an interesting expression pattern of Panx1a. We noticed a dotty, vesicular-like pattern of Panx1a expression upon treatment with this inhibitor. Although we did not detect a significant change in dye uptake activity of Panx1a expressing cells treated with PD98059, the results showed a slight upward trend of uptake in all three species of Panx1 (Panx1a, Panx1b, and mPanx1). An increase in the intracellular dotty expression of Panx1a may indicate that ERK2 has a role in the vesicular transport of Panx1a to the membrane.

When exploring a direct interaction between ERK2 and Panx1a, we were challenged by the fact that kinase interaction with their substrates is innately transient and weak, making it difficult to detect. We used FRET as a more sensitive assay for detecting interaction as it measures the distance between two proteins. A distance shorter than 10nm is considered close enough for two proteins to interact (Siu et al., 2016). Still, there was no evidence of an interaction between Panx1a and ERK2. However, the RAS-RAF-MEK-ERK signaling pathway has been well studied for many years and shows that MEK is an upstream activator of ERK2 (Macdonald et al., 1993). We decided to include MEK in our experiments to activate the overexpressed ERK2. In triple transfected cells expressing Panx1a, ERK2, and MEK1, we saw an increase in FRET efficiency between Panx1a and ERK2. This result indicated an interaction between Panx1a and *activated* ERK2, although it is still far too weak to be detected by CoIP, as shown in our results.

We used the phosphorylation purification assay to explore changes in the phosphorylation state of Panx1a when treated with the MAPK inhibitor PD98059.

However, there was no visible change in the phosphorylated fraction between treated and untreated cells. We believe that this is due to the sensitivity issues of the assay. A slight decrease in phosphorylation of one residue on the protein would not be sufficient to detect via phospho-purification column and western blotting. Furthermore, other phosphorylation events on different residues of Panx1a may mask any decreased signal.

We believe that our results show a potential interaction between Panx1a and ERK2 which needs further exploration with more sensitive approaches. Future experiments can include the treatment of ERK2 activators and inhibitors in combination with mass spectrometry to detect interaction and changes in the phosphorylation status.

.

Chapter 5. The trafficking and localization of the zebrafish Panx1a are regulated via interaction with CaMKIIa

5.1. Introduction

Pannexins are large pore membrane channels that are involved in cellular communication. Three members belong to this integral membrane protein family: Panx1, Panx2, and Panx3 (Bruzzone et al., 2003). Panx1, the most studied of the three, is ubiquitously expressed in the central nervous system and is regulated by voltage, extracellular potential, extracellular ATP, intracellular calcium, and mechanical membrane stimulation (Michalski et al., 2018; Locovei et al., 2006; Beckel et al., 2014). They function as ATP release channels and allow small molecules to go in and out of the cell (Bao et al., 2004; Chekeni et al., 2010). Panx1s have implications for glucose uptake, apoptosis, pain induction, and ischemia (Chekeni et al., 2010; Bargiotas et al., 2011; Weaver et al., 2017; Adamson et al., 2015).

The cryo-EM structures of the human and frog Panx1s have recently revealed a heptameric assembly of the channel with a pore diameter of 8-9.4 Å. (Michalski, 2020; Deng et al., 2020; Jin et al., 2020, Mou et al., 2020, Qu et al., 2020; Ruan et al., 2020). It has been established that each subunit is composed of four transmembrane domains, two extracellular loops, one intracellular loop, and an intracellular N and C terminal (Shestopalov and Panchin, 2008). Each subunit also undergoes N-glycosylation and exists as three species: core unglycosylated (Gly0), high-mannose glycosylated (Gly1), and complex glycosylated (Gly2) (Penuela et al., 2007). These post-translational modifications regulate the cellular distribution of Pannexins and play a role in targeting the protein to the cell membrane (Boassa et al., 2007). Although the Gly2 species have been shown to be highly expressed at the cell surface, the Gly1 and Gly0 species are

also capable of reaching the membrane, but to a lesser extent (Penuela et al., 2009). Phosphorylation modifications have also been proposed to regulate Panx1 channel function by SFKs, PKG, and, recently, CaMKII (Weilinger et al., 2012; Lohman et al., 2015; Poornima et al., 2015; Lopez et al., 2021).

Knockout Panx1 animal models have linked the channels to a role in learning and memory, synaptic plasticity modulation, and visuomotor functions. Prochnow et al. showed that the lack of extracellular ATP in Panx1 knockout mice regulates postsynaptic NMDA receptor activation, which led to anxiety behaviour and impairment of object recognition and spatial learning (Prochnow et al., 2012). Furthermore, the lack of Panx1 in mice resulted in the modulation of NMDA receptor subtype expression, thereby influencing long-term potentiation and long-term depression (Gajardo et al., 2018). In knockout zebrafish models, the lack of Panx1a channels affected swimming behaviour in the dark and regulated expression of pre- and post-synaptic markers in the dopaminergic signaling pathway (Safarian et al., 2020).

As discussed in Chapter 4, we identified a CaMKII isoform, CaMKIId, as an interactor of Panx1a in the mass spectrometry screen. CaMKII exists as four isoforms, all of which have a role in learning and memory (Zalcman et al., 2018). Previously, we have shown that Panx1 signaling is involved in modulating the interaction between Connexin-36 (Cx36) and CaMKIIa (Siu et al., 2021). Although we did not identify CaMKIIa as the interacting subunit for Panx1a, this was not surprising. Neuro 2a cells have been shown to express lower levels of CaMKIIa, with the CaMKIId isoform having the highest expression (Ye et al., 2019). However, since CaMKIIa is the most extensively studied

isoform and is exclusively expressed in the brain, we were particularly interested in its effects on Panx1a.

In this present study, we explore the role of CaMKIIa as a regulator of the zebrafish Panx1a protein channel. Our findings show a strong interaction between the two proteins present in the early trafficking stages of Panx1a. We explore the effects of CaMKIIa mutants on the expression and function of Panx1a channels, showing that a constitutively active CaMKIIa kinase regulates Panx1a localization. The outcome of this study provides new evidence of kinase-based modulation of Panx1 channels and valuable insight into the consequences of this interaction.

5.2. Results

5.2.1. Panx1a and CaMKIIa interact in the Neuro 2a cell line

After identifying the CaMKIId isoform in our mass spectrometry screen, we performed sequence alignment between mouse CaMKIId and mouse CaMKIIa and found that the two were 90.2% similar and 83.2% identical (**Supplementary Figure 5.1A**). Since we are interested in the zebrafish Panx1 ortholog, we also performed a sequence alignment between the zebrafish and mouse CaMKIIa (**Supplementary Figure 5.1B**). We confirmed that the two proteins share most of their sequence with a 97.5% similarity and a 93.9% identity. This led us to explore the potential interaction between Panx1a and CaMKIIa.

Panx1a-EYFP was transiently co-expressed with CaMKIIa-ECFP in Neuro 2a cells. At 48 hours post-transfection, an increase in the intracellular localization of Panx1a-EYFP was observed (**Figure 5.1**). Cells that co-expressed Panx1a-EYFP and the empty

ECFP vector control showed the characteristic enrichment of Panx1a channels in the cell membrane.

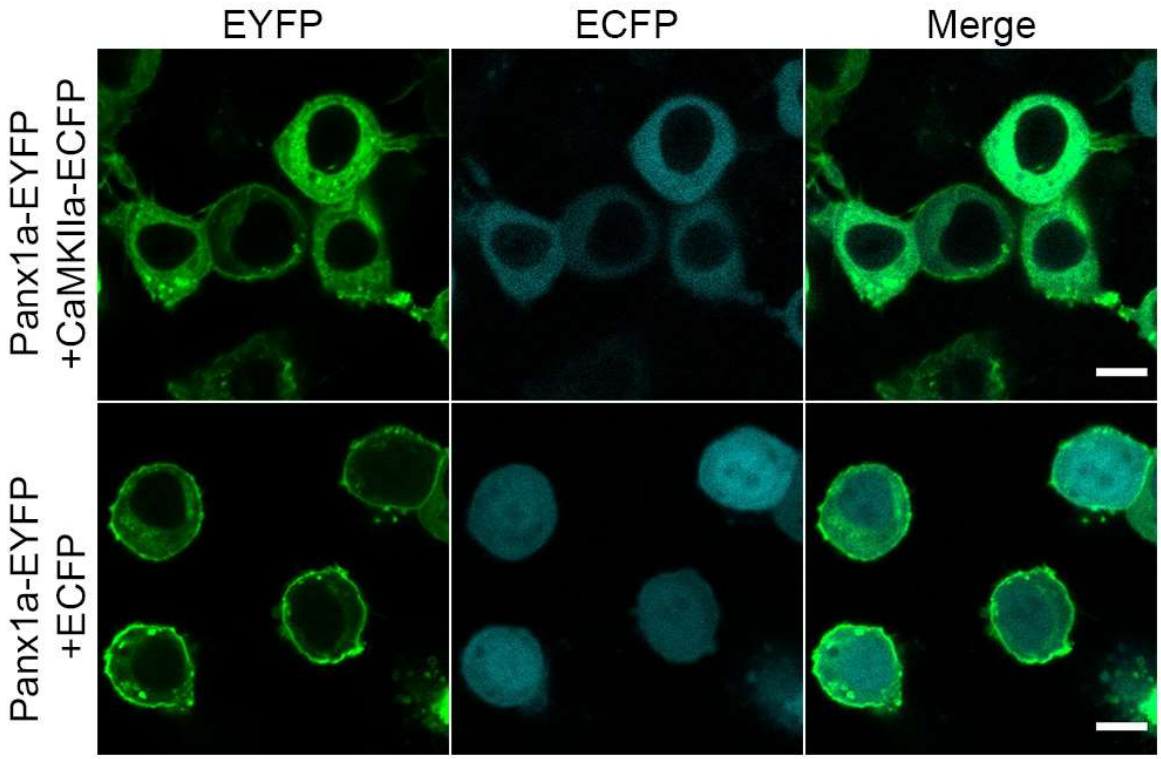

Figure 5.1. CaMKIIa overexpression affects Panx1a localization in transfected Neuro 2a cells. Images of cells transiently transfected with either Panx1a-EYFP and CaMKIIa-ECFP or Panx1a-EYFP and ECFP empty vector control demonstrate altered Panx1a localization. Scale bar: 10um.

The interaction of Panx1a with CaMKIIa was demonstrated by double transfecting Neuro 2a cells with combinations of CaMKIIa-ECFP and Panx1a-dTomato-His or CaMKIIa-ECFP and the dTomato-His empty vector control. CoIPs used anti-His antibody and Protein A Dynabeads™ to pull down Panx1a-dTomato-His and its interacting partners at 48 hours post-transfection. CaMKIIa-ECFP can be seen in the pull-down fraction of Panx1a-dTomato-His and CaMKIIa-ECFP double transfected cells (**Figure 5.2A**). Expression of dTomato-His empty vector control was insufficient for interaction

with CaMKIIa. Furthermore, the binding of CaMKIIa-ECFP to Panx1a-dTomato-His was significantly reduced when amino acids 320-417 of the 417 amino acid long wildtype protein were removed in Panx1aΔ320-417, suggesting that the carboxyterminal domain of Panx1a plays a role in the interaction (**Figure 5.2B**).

Further, the FRET analysis of Neuro2a cells co-expressing Panx1a-DsRed and CaMKIIa-ECFP with or without treatment of 2mM extracellular Ca2+ and 2uM ionomycin suggested that the interaction increased upon a rise in cytoplasmic calcium (**Figure 5.2C**). FRET efficiency was observed to be above the 1.7% threshold and was significantly increased after treatment with ionomycin and calcium (Untreated: 2.12 ± 0.31, n = 33; Ionomycin: 4.57 ± 0.63, n = 30, $p < 0.0013$), demonstrating proximity of the interacting proteins when intracellular calcium was increased.

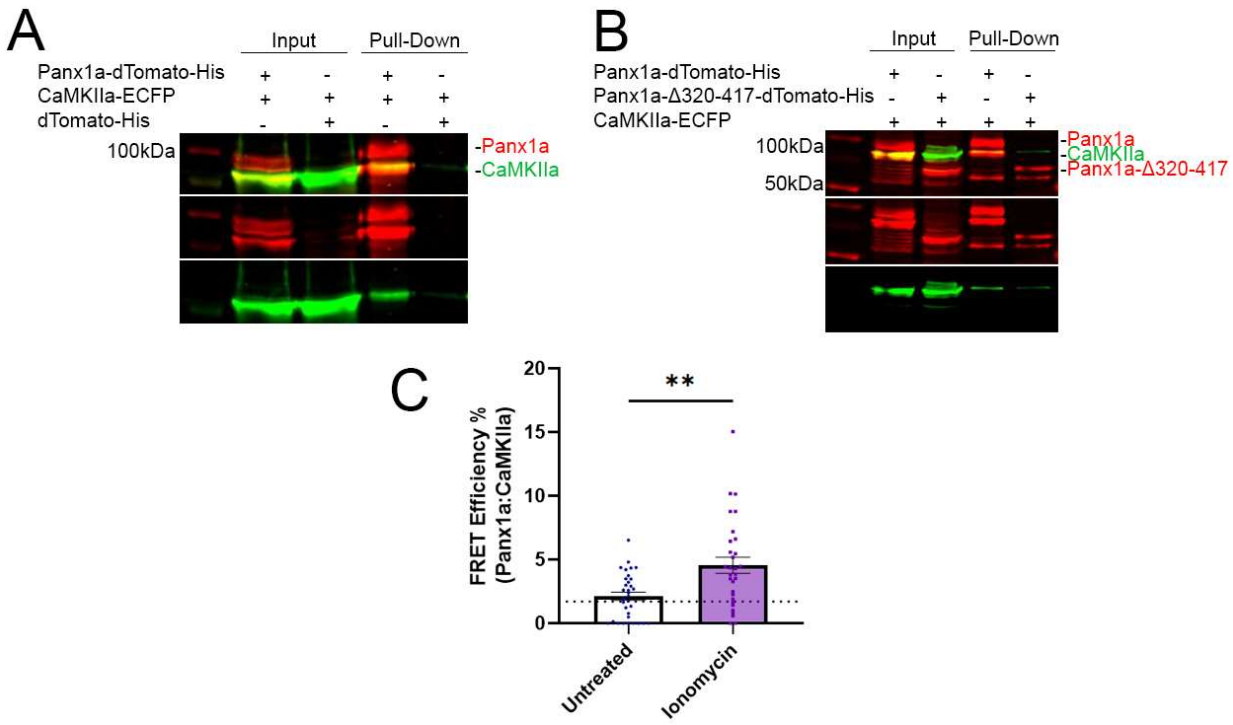

*Figure 5.2. CaMKIIa interacts with the zebrafish Panx1a in Neuro 2a cells that overexpress both proteins. (A) Panx1a-dTomato-His was double transfected with CaMKIIa-ECFP, and cells were subjected to co-immunoprecipitation. Input fractions represent the total lysates prior to immunoprecipitation with an anti-His antibody. Pull-Down represents the immunoprecipitated fractions. Cells double transfected with dTomato-His empty vector and CaMKIIa-ECFP were used as a negative control. (B) Panx1a-dTomato-His or Panx1a-Δ320-417-dTomato-His were double transfected with CaMKIIa-ECFP and were subjected to His purification. Input fractions represent the total lysates prior to pull-down with a His-60 Ni Gravity Column. Pull-Down represents the purified fractions. For both (A) and (B), bottom: anti-GFP detection of ECFP tagged proteins, middle: anti-His detection of dTomato-His tagged proteins, top: merged channels. (C) FRET analysis of the interaction between Panx1a-DsRed and CaMKIIa-ECFP in cells with or without increased intracellular calcium (2 mM [Ca2+]E (Myers et al., 2017) and 2 uM ionomycin). The dotted line represents the threshold of 1.7% (equals to 10 nm distance between FRET pairs). Mann–Whitney U (two-tailed) significance test was used. Sample sizes were the following: Untreated: n = 33; Ionomycin: n = 30. Error bars show SEM; **p < 0.01.*

We also tested the effects of KN-93, a CaMKII inhibitor, to determine if the interaction was affected. We did not see an increase or decrease in FRET upon

treatment with KN-93 (Untreated: 10.67 ± 0.83, n = 33; KN-93: 10.65 ± 0.75, n = 19, p = 0.48) (**Figure 5.3A**). Our CoIP results also showed that Panx1a and CaMKIIa still interact upon treatment with KN-93 (**Figure 5.3B**), in line with the FRET results.

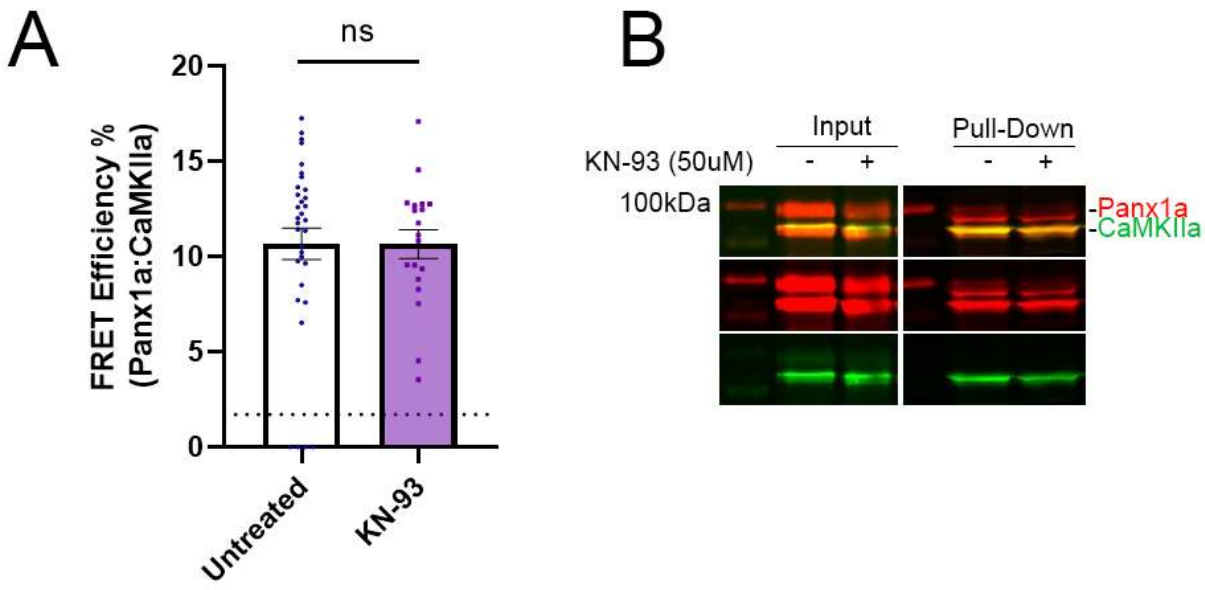

Figure 5.3. Treatment with KN-93, a CaMKIIa inhibitor, does not abolish the interaction between Panx1a and CaMKIIa. (A) FRET analysis of the interaction between Panx1a-DsRed and CaMKIIa-ECFP in cells with or without KN-93 treatment (50uM, 5 minutes). The dotted line represents the threshold of 1.7% (equals to 10 nm distance between FRET pairs). Mann–Whitney U (two-tailed) significance test was used. Sample sizes were the following: Untreated: n = 33; KN-93: n = 19. (B) Panx1a-dTomato-His was double transfected with CaMKIIa-ECFP either with or without KN-93 (50uM, 5 minutes) treatment and was subjected to co-immunoprecipitation. Input fractions represent the total lysates prior to immunoprecipitation with an anti-His antibody. Pull-Down represents the immunoprecipitated fractions. Bottom: anti-GFP detection of ECFP tagged proteins, middle: anti-His detection of dTomato-His tagged proteins, top: merged channels. Error bars show SEM; ns, not significant.

The homology of the zebrafish Panx1a ohnolog Panx1b is ≈ 70% (Bond et al., 2012; Kurtenbach et al., 2013). Therefore, we tested whether CaMKIIa can also bind Panx1b by replacing Panx1a-dTomato-His with Panx1b-dTomato-His in CoIP assays

(**Supplementary Figure 5.2**). The ability of Panx1b to interact with and pull down CaMKIIa like Panx1a suggested that this interaction is evolutionary conserved between the fish paralogs and Mammalia (Lopez et al., 2021).

5.2.2. Overexpression of CaMKIIa affects Panx1a localization and glycosylation status

CaMKII holoenzyme mechanisms that govern the roles in synaptic plasticity are well-characterized (Myers et al., 2017; Cook et al., 2021). Functional and structural mutants of CaMKIIa allow testing effects on Panx1a localization and function. We used CaMKIIA mutants that are suggested to increase kinase activity (T286D, F293A, and T305A:T306A), inhibit activity (K42M, D135N, T286A, and R296A), and prevent kinase oligomerization (H477Y). Here, the depletion of Panx1a from the cell membrane in the presence of CaMKIIa suggested that this interaction was required for post-translational N-glycosylation and transport to the cell membrane (Boassa et al., 2008; Penuela et al., 2007; Penuela et al., 2009; Gehi et al., 2011). We performed a western blot analysis of Panx1a co-expressed with the different CaMKIIa mutants (**Figure 5.4A**). The ratio of the three glycosylated forms of Panx1a, Gly0, Gly1, and Gly2, was quantified by normalizing the intensity of the Gly2 band to the Gly0 and Gly1 isoforms (**Figure 5.4B**). A significant decrease in the Gly2 isoform was detected when Panx1a was co-expressed with CaMKIIa compared to the ECFP vector control (ECFP: 1.28 ± 0.10, n = 4; CamkIIa (WT): 0.51 ± 0.07, n = 7, p = 0.0037). A similar decrease was observed when the CaMKII R296A mutant was co-expressed (R296A: 0.34 ± 0.054, n = 3, p = 0.0020). The remaining mutants showed no difference in the Gly2/Gly1/Gly0 ratio (K42M: 0.74 ± 0.069, n = 3, p = 0.20; D135N: 0.78 ± 0.12, n = 3, p = 0.42; T286A: 1.02 ± 0.11, n = 3, p > 0.99; T286D:

1.05 ± 0.018, n = 3, p > 0.99; F293A: 1.02 ± 0.17, n = 3, p > 0.99; T305A:T306A: 0.82 ± 0.04, n = 3, p = 0.46; H477Y: 1.18 ± 0.12, n = 3, p > 0.99). Images of Panx1a expression when co-expressed with the CaMKIIa mutants complement the results of this experiment (**Figure 5.4C**).

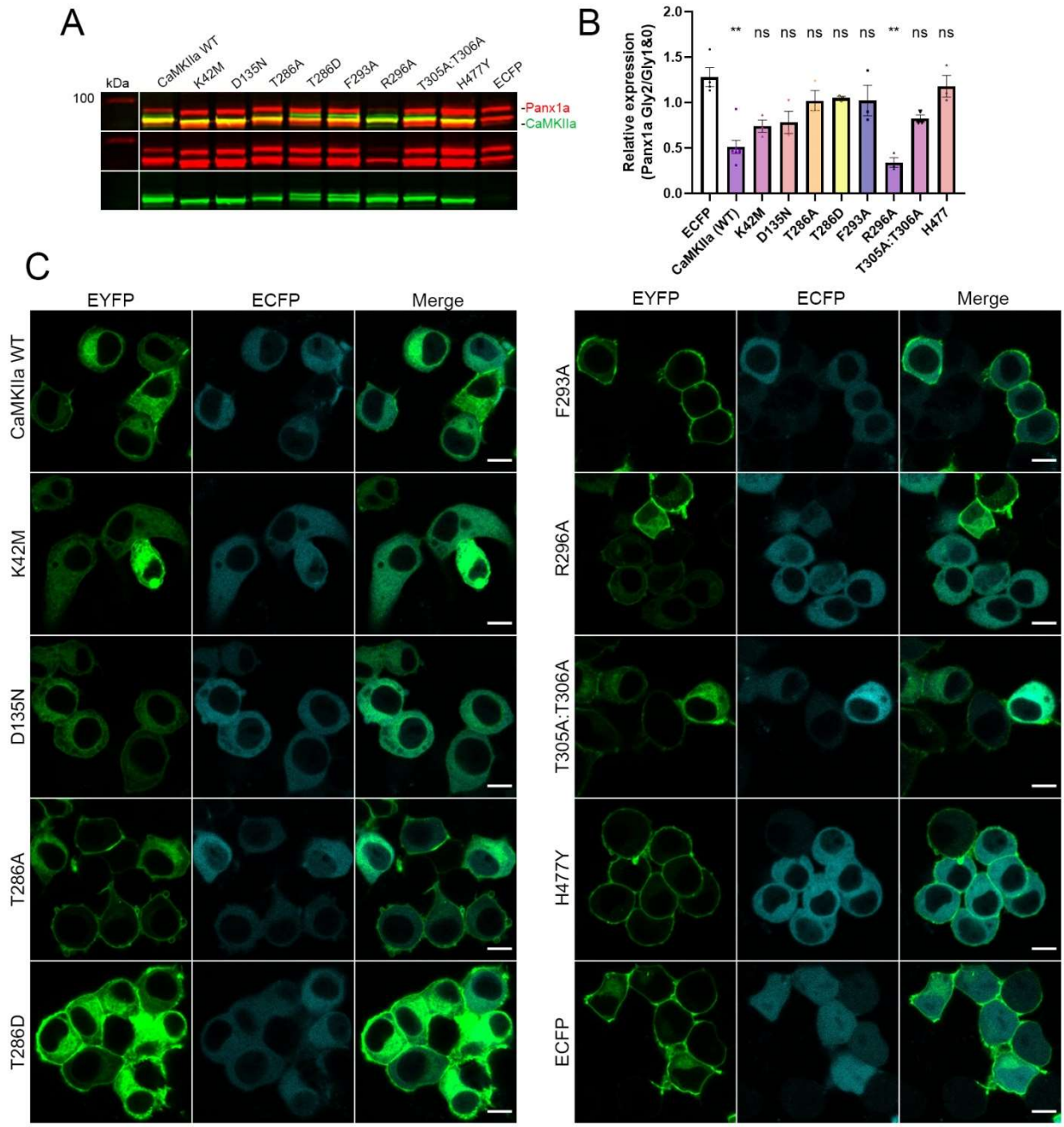
A
kDa
100
CaMKIIa WT
K42M
D135N
T286A
T286D
F293A
R296A
T305A:T306A
H477Y
ECFP
-Panx1a
-CaMKIIa
B
Relative expression (Panx1a Gly2/Gly1&0)
2.0
1.5
1.0
0.5
0.0
** ns ns ns ns ns ** ns ns
ECFP
CaMKIIa (WT)
K42M
D135N
T286A
T286D
F293A
R296A
T305A:T306A
H477
C
EYFP
ECFP
Merge
CaMKIIa WT
K42M
D135N
T286A
T286D
F293A
R296A
T305A:T306A
H477Y
ECFP

*Figure 5.4. Exploring the effects of functional and structural CaMKIIa mutants on the expression of Panx1a. (A) Western blot analysis of double transfected Neuro 2a cells showing changes in expression of Panx1a-dTomato-His with the indicated ECFP tagged CaMKIIa mutants. Bottom: anti-GFP detection of ECFP tagged proteins, middle: anti-His detection of dTomato-His tagged proteins, top: merged channels. (B) Quantification of Panx1a-Gly2 expression relative to that of Panx1a-Gly1+Panx1a-Gly0 when double transfected with the WT and mutant CaMKIIa constructs. ECFP was used as the control group for statistical analysis. Kruskal-Wallis multiple comparison significance test was used. Sample sizes were the following: ECFP: n = 4; CaMKIIa (WT): n = 7; K42M: n=3; D135N: n=3; T286A: n=3; T286D: n=3; F293A: n=3; R286A: n=3; T305A:T306A: n=3; H477Y: n=3. (C) Panx1a expression in Neuro 2a cells double transfected with Panx1a-EYFP and CaMKIIa-ECFP mutants. ECFP empty vector was used as a control. Scale bar = 10um. Error bars show SEM; **p < 0.01, ns not significant.*

FRET determined how CaMKIIa mutants influenced the interaction between Panx1a and CaMKIIa (**Figure 5.5A**). The Panx1a-DsRed/CaMKIIa-ECFP FRET pair and all mutants showed a mean FRET efficiency above the threshold of 1.7%. The FRET efficiency between Panx1a and the CaMKIIa mutants T286A, T286D, and H477Y exceeded the efficiency of WT CaMKIIa (CaMKIIa (WT): 7.82 ± 0.68, n = 41; T286A: 12.71 ± 0.70, n = 30, p < 0.0001; T286D: 10.99 ± 0.83, n = 25, p = 0.035; H477Y: 12.20 ± 0.76, n = 33, p = 0.0010). A hallmark feature of CaMKII is the generation of autonomous, Ca(2+)-independent activity by T286 autophosphorylation. The process requires ATP for the ATP-induced stabilization of Ca(2+)/calmodulin binding to the enzyme (Barcomb et al., 2014) and must be either further stimulated by Ca(2+)/CaM or supplemented with mutations of T305/T306 for enhancement of synaptic strength (Pi et al., 2010). The H477Y mutation prevents the assembly of the CaMKIIa holoenzyme (Chia et al., 2018). It is reasonable to speculate that the three mutants can bind Panx1a in a compact form. The remaining CaMKII2a mutants bind Panx1a without a compact state (K42M: 7.37 ± 0.84, n = 17, p > 0.99; D135N: 9.88 ± 0.88, n = 13, p > 0.99; F293A: 7.32 ± 0.71, n = 20,

p > 0.99; R296A: 9.23 ± 0.81, n = 31, p > 0.99; T305A:T306A: 12.20 ± 0.76, n = 33, p = 0.65).

To determine whether CaMKIIa influences the function of Panx1a, we used an EtBr dye uptake assay (**Figure 5.5B**). Cells were transfected with Panx1a-EYFP and CaMKIIa-ECFP constructs or ECFP empty vector control. As expected, the total dye uptake was reduced in cells expressing Panx1a and CaMKIIa WT compared to the empty vector control (ECFP: 3.29 ± 0.41, n = 14; CaMKIIa WT: 1.37 ± 0.25, n = 10, p = 0.14). Our results also indicate that the K42M, D135N, and T305A:T306A mutants all decreased Panx1a activity (K42M: 0.70 ± 0.18, n = 10, p < 0.0001; D135N: 1.28 ± 0.16, n = 10, p = 0.013; T305A:T306A: 1.35 ± 0.15, n = 10, p = 0.019). We saw no significant difference in dye uptake between T286A, T286D, F293A, R296A, and H477Y compared to ECFP empty vector control (T286A: 2.47 ± 0.64, n = 9, p = 0.81; T286D: 2.45 ± 0.43, n = 9, p > 0.99; F293A: 1.37 ± 0.15, n =10, p = 0.051; R296A: 1.91 ± 0.31, n = 9, p = 0.83; H477Y: 4.52 ± 0.23, n = 9, p > 0.99).

We confirmed that Panx1a was still expressed at the membrane in cells co-expressing CaMKIIa by cell surface biotinylation assay. Here, Neuro 2a cells were double transfected with Panx1a-EYFP and CaMKIIa-DsRed or DsRed empty vector. We could detect Panx1a in both samples; however, there appeared to be an increase in the Gly1 state in the biotinylated fraction in cells co-expressing CaMKIIa (**Figure 5.5C**). Actin served as the internal control, showing no detection in the biotinylated fractions.

.

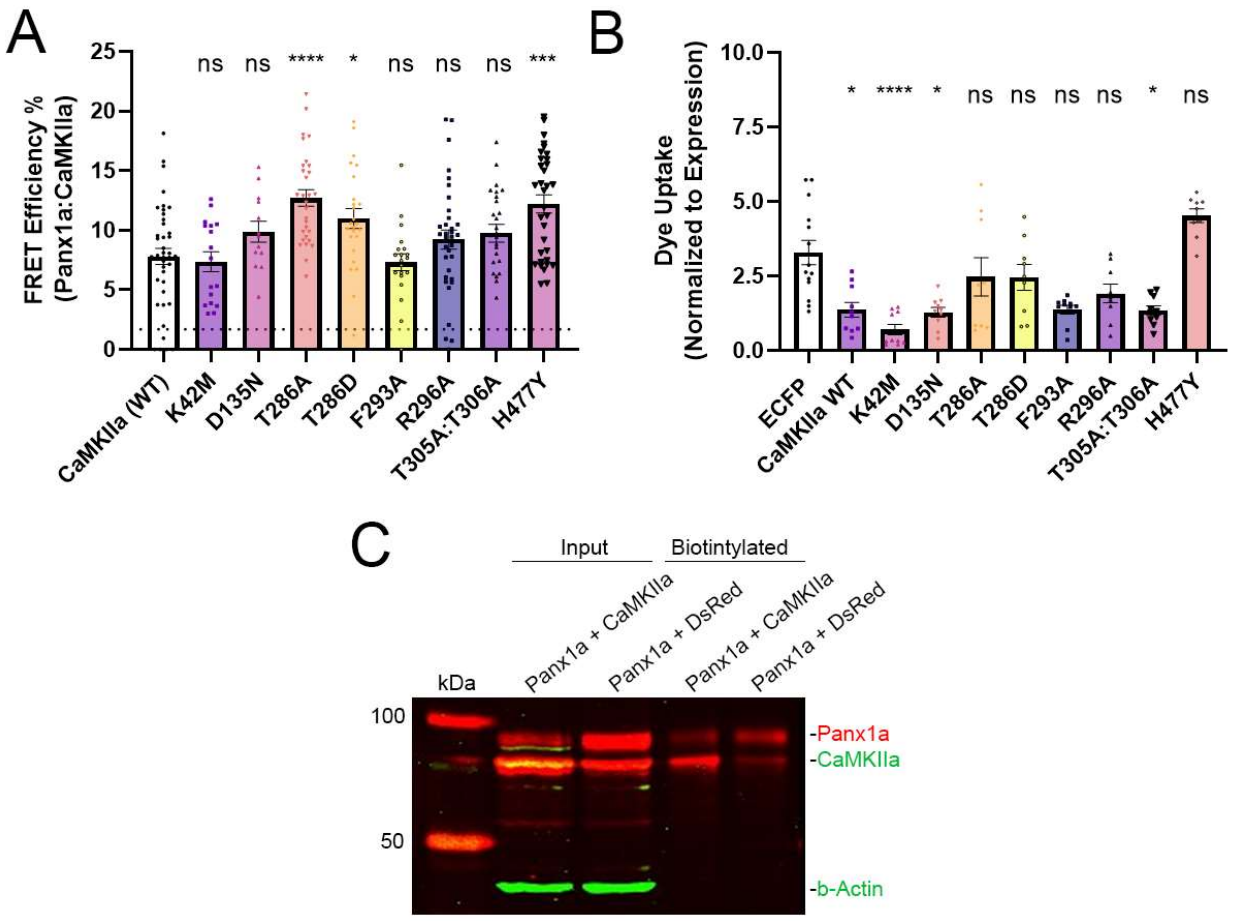
A
FRET Efficiency %
(Panx1a:CaMKIIa)
25
20
15
10
5
0
ns ns **** * ns ns ns ***
CaMKIIa (WT)
K42M
D135N
T286A
T286D
F293A
R296A
T305A:T306A
H477Y
B
Dye Uptake
(Normalized to Expression)
10.0
7.5
5.0
2.5
0.0
* **** * ns ns ns ns * ns
ECFP
CaMKIIa WT
K42M
D135N
T286A
T286D
F293A
R296A
T305A:T306A
H477Y
C
Input
Biotintylated
Panx1a + CaMKIIa
Panx1a + DsRed
Panx1a + CaMKIIa
Panx1a + DsRed
kDa
100
50
-Panx1a
-CaMKIIa
-b-Actin

*Figure 5.5. Effects of the interaction between CaMKIIa mutants and Panx1a on channel function. (A) Quantification of interaction between Panx1a-DsRed and CaMKIIa-ECFP mutants via FRET analysis. CaMKIIa was used as the control group for statistical analysis. The dotted line represents the threshold of 1.7% (equals to 10 nm distance between FRET pairs). Kruskal-Wallis multiple comparison significance test was used. Sample sizes were the following: CaMKIIa (WT): n = 41; K42M: n = 17; D135N: n=13; T286A: n=30; T286D: n=25; F293A: n=20; R286A: n=34; T305A:T306A: n=26; H477Y: n=33. (B) Dye uptake quantification of cells double transfected with Panx1a-EYFP and CaMKIIa-ECFP mutants. Values represent total dye uptake 5 minutes after EtBr (10uM) application normalized to the expression of Panx1a-EYFP. ECFP was used as the control group for statistical analysis. Kruskal-Wallis multiple comparison significance test was used. Sample sizes were the following: ECFP: n = 14; CaMKIIa (WT): n = 10; K42M: n=10; D135N: n=10; T286A: n=9; T286D: n=9; F293A: n=10; R286A: n=9; T305A:T306A: n=10; H477Y: n=9. (C) Detection of Panx1a at the cell membrane using cell surface biotinylation assay. Cells were double transfected with either Panx1a-EYFP and CaMKIIa-DsRed or Panx1a-EYFP and DsRed empty vector control and incubated with membrane impermeable biotin. Input fractions represent the total lysates prior to being subjected to streptavidin purification. Biotinylated fractions represent streptavidin-eluted biotinylated proteins. B-Actin served as the internal control. Error bars show SEM; ****p < 0.0001, **p < 0.01, *p < 0.05, ns not significant.*

5.2.3. Interaction between Panx1a and CaMKIIa occurs early in the trafficking stages of Panx1a

To test whether CaMKIIa overexpression alters Panx1a localization, as per our initial observations, we performed a co-localization analysis between Panx1a and intracellular organelle markers. We used calreticulin as the ER marker and galactosyltransferase as the Golgi apparatus marker. For the ER co-localization, cells were triple transfected with DsRed tagged ER marker, Panx1a-EYFP, and either CaMKIIa-ECFP, T286D-ECFP, or ECFP empty vector control (**Figure 5.6A**). For the Golgi co-localization, the DsRed tagged Golgi marker was used in place of ER-DsRed (**Figure 5.6B**). We quantified the co-localization between Panx1a and each organelle marker using Pearson's R-Value (**Figure 5.6C, D**). Our results show that when Panx1a

is co-expressed with the WT CaMKIIa, there is an increase in co-localization with both the ER marker (ER; Panx1a + ECFP: 0.24 ± 0.033, n = 55; Panx1a + CaMKIIa WT: 0.78 ± 0.025, n = 49, $p < 0.0001$) and the Golgi marker (Golgi; Panx1a + ECFP: 0.10 ± 0.021, n = 34; Panx1a + CaMKIIa WT: 0.42 ± 0.036, n = 43, $p < 0.0001$). Interestingly, the T286D mutant reversed this effect, showing no significant difference to ECFP empty vector control in co-localization with the ER marker (ER; Panx1a + T286D: 0.38 ± 0.035, n = 26, $p = 0.12$), and a slight difference for the Golgi marker (Golgi: Panx1a + T286D: 0.23 ± 0.031, n = 29, $p = 0.012$).

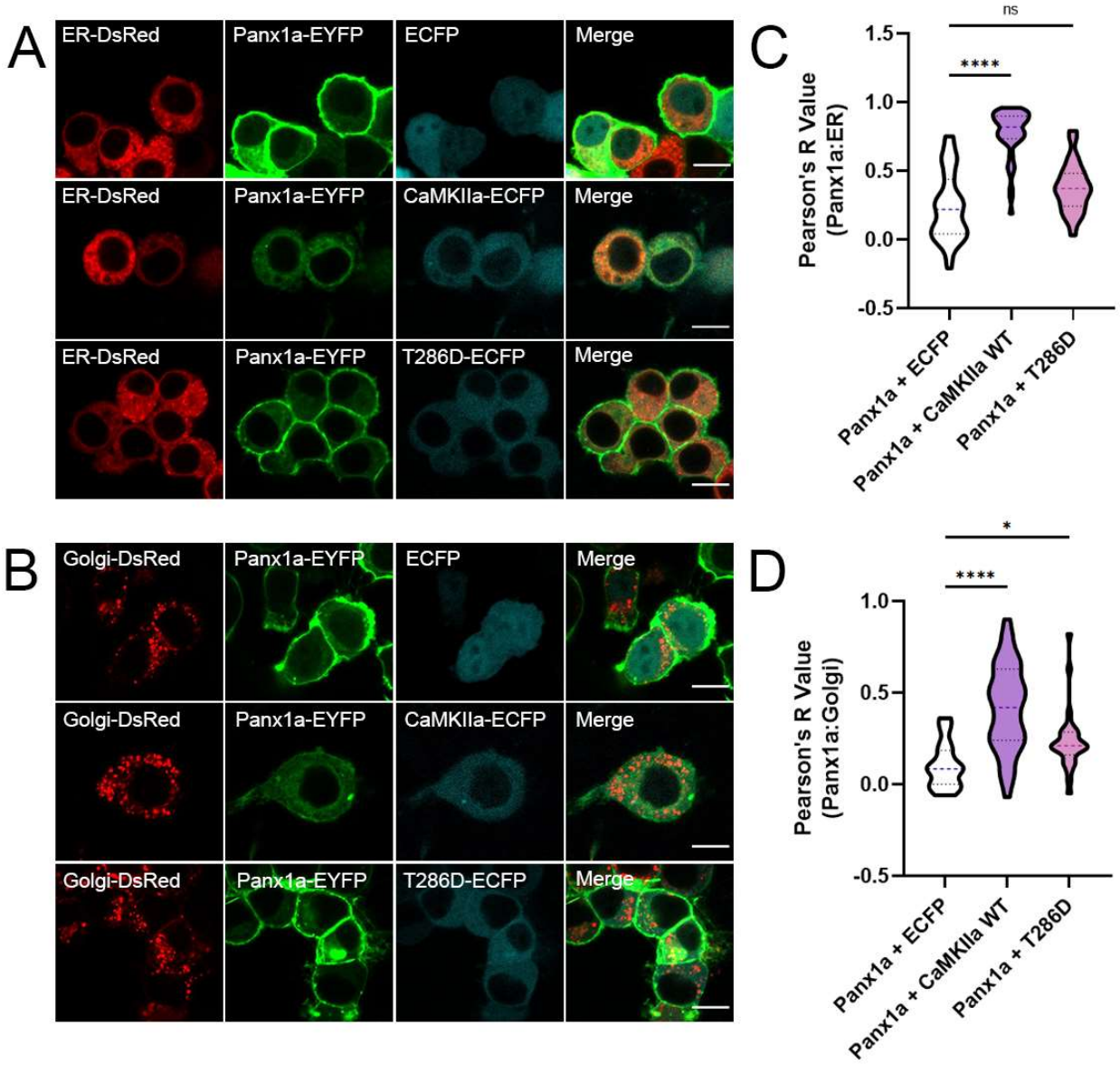
A
ER-DsRed
Panx1a-EYFP
ECFP
Merge
ER-DsRed
Panx1a-EYFP
CaMKIIa-ECFP
Merge
ER-DsRed
Panx1a-EYFP
T286D-ECFP
Merge
B
Golgi-DsRed
Panx1a-EYFP
ECFP
Merge
Golgi-DsRed
Panx1a-EYFP
CaMKIIa-ECFP
Merge
Golgi-DsRed
Panx1a-EYFP
T286D-ECFP
Merge
C
ns
****
Pearson's R Value (Panx1a:ER)
1.5
1.0
0.5
0.0
-0.5
Panx1a + ECFP
Panx1a + CaMKIIa WT
Panx1a + T286D
D
*
****
Pearson's R Value (Panx1a:Golgi)
1.0
0.5
0.0
-0.5
Panx1a + ECFP
Panx1a + CaMKIIa WT
Panx1a + T286D

*Figure 5.6. CaMKIIa T286D mutant rescues Panx1a expression at the cell surface. Co-localization images between DsRed tagged ER organelle marker (A) or Golgi marker (B) and Panx1a-EYFP when co-expressed with CaMKIIa-ECFP WT, CaMKIIa-ECFP T286D mutant, or ECFP empty vector control. Galactosyltransferase was used as the Golgi marker, and calreticulin was used as the ER marker. Scale bar: 10um. Co-localization quantification between Panx1a-EYFP and DsRed tagged ER marker (C), or DsRed tagged Golgi marker (D) as described in (A) and (B). For ER co-localization, a Kruskal-Wallis multiple comparison significance test was used. Sample sizes were the following: Panx1a + ECFP: n = 55; Panx1a + CaMKIIa WT: n = 49; Panx1a + T286D: n = 26. For Golgi co-localization, a Kruskal-Wallis multiple comparison significance test was used. Sample sizes were the following: Panx1a + ECFP: n = 34; Panx1a + CaMKIIa WT: n = 43; Panx1a + T286D: n = 29. Error bars show SEM; ****p < 0.0001, *p < 0.05, ns not significant.*

Next, we explored whether the increased intracellular localization of Panx1a in the presence of CaMKIIa means that the two proteins interact in the early trafficking stages. We performed a CoIP assay on Neuro 2a cells double transfected with Panx1a-dTomato-His and CaMKIIa-ECFP with or without BFA treatment (5ug/mL for 19h). Our western blot analysis showed that Panx1a still interacts with CaMKIIa in samples treated with BFA (**Figure 5.7A**). Although there was a decrease in the Gly2 state in the BFA treated input fraction, this decrease was not visible in the Pull-Down fractions. This is due to the concentrated Panx1a protein levels in the precipitated sample. To confirm these results, we performed FRET analysis on cells double transfected with Panx1a-DsRed and CaMKIIa-ECFP (**Figure 5.7B**). Our results show that there was no significant difference in the interaction between the two proteins when treated with BFA (Untreated: 6.72 ± 0.59, n = 18; BFA: 7.34 ± 0.49, n = 20, p = 0.59).

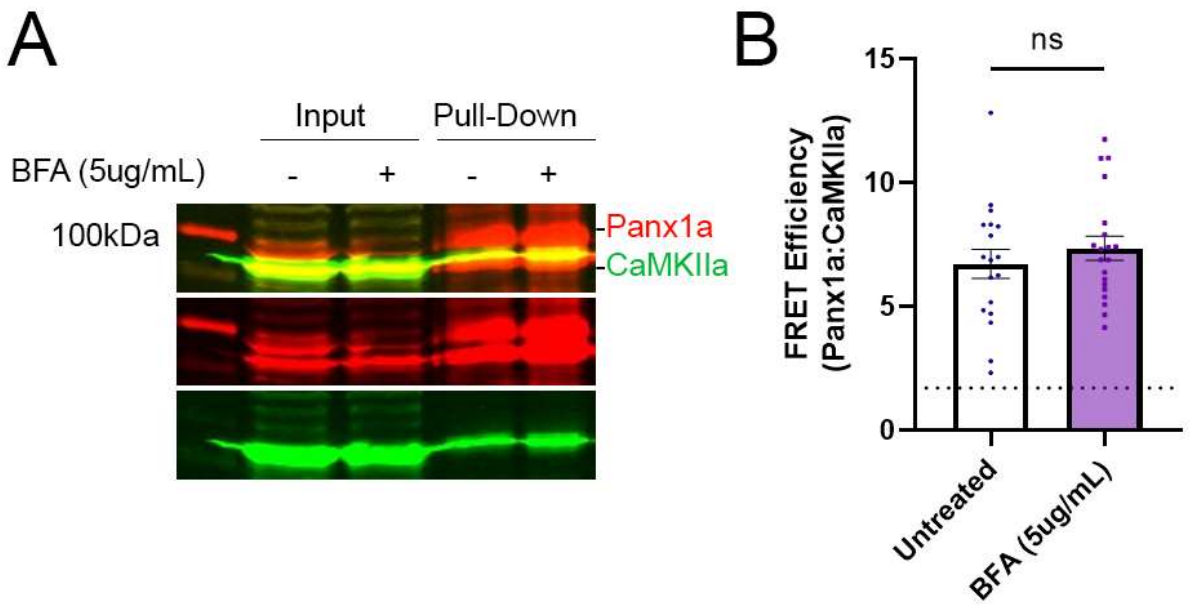

Figure 5.7. CaMKIIa and Panx1a interact in the early stages of trafficking. (A) Western blot analysis of the Co-IP interaction between Panx1a and CaMKIIa with or without BFA treatment (5ug/mL; 19h). Neuro2a cells were double transfected with Panx1a-dTomato-His and CaMKIIa-ECFP. Input fractions represent the total lysates prior to immunoprecipitation with an anti-His antibody. Pull-Down represents the immunoprecipitated fractions. Bottom: anti-GFP detection of ECFP tagged proteins, middle: anti-His detection of dTomato-His tagged proteins, top: merged channels. (B) Quantification of interaction between Panx1a-DsRed and CaMKIIa-ECFP with or without BFA treatment via FRET analysis. The dotted line represents the threshold of 1.7% (equals to 10nm distance between FRET pairs). Mann–Whitney U (two-tailed) significance test was used. Sample sizes were the following: Untreated: n = 18; BFA (5ug/mL): n = 20. Error bars show SEM; ns not significant.

Finally, we tested whether CaMKIIa affects Panx1a intracellular vesicle dynamics. We used TIRF microscopy to analyze Panx1a vesicles in cells transfected with Panx1a-EYFP and CaMKIIa-DsRed or DsRed empty vector control. We used the diameter as the measurement of size for quantification (**Figure 5.8A**). There was no significant difference in Panx1a vesicle size in cells expressing CaMKIIa or the empty vector control (Diameter; DsRed: 1.01 ± 0.043, n = 113; CaMKIIa-DsRed: 1.11 ± 0.034, n = 175, p = 0.47). However, when looking at the vesicle movement, we quantified the average displacement

per second for each Panx1a vesicle for 1 minute (**Figure 5.8B**) and found that co-expression with CaMKIIa resulted in significantly higher vesicle dynamics (Displacement; DsRed: 0.099 ± 0.017, n = 132; CaMKIIa-DsRed: 0.18 ± 0.025, n = 134, p < 0.0001).

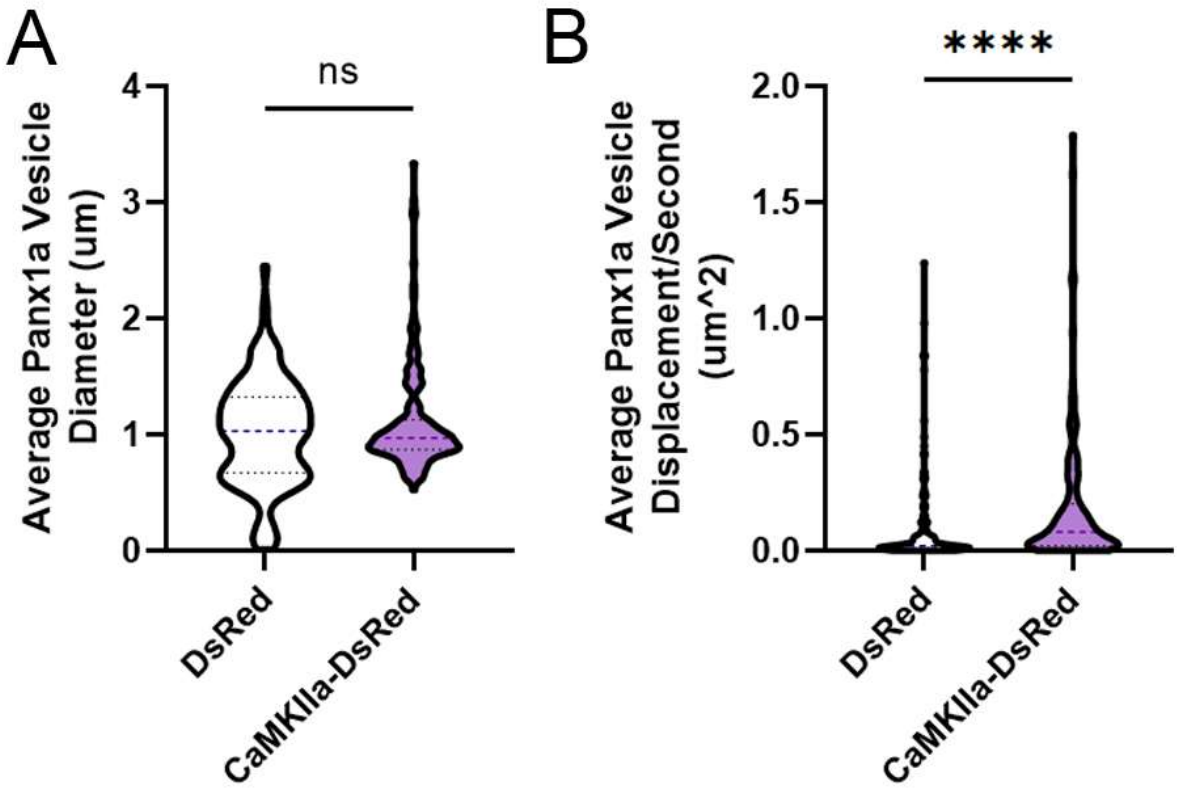

*Figure 5.8. CaMKIIa overexpression affects the movement of intracellular vesicles expressing Panx1a. TIRF quantification of average Panx1a vesicle (A) diameter and (B) displacement per second for 1 minute in cells transfected with Panx1a-EYFP and CaMKIIa-DsRed or Panx1a-EYFP and DsRed empty vector control. For vesicle diameter, a Mann–Whitney U (two-tailed) significance test was used. Sample sizes were the following: DsRed: n = 113; CaMKIIa-DsRed: n = 175. For vesicle displacement, a Mann–Whitney U (two-tailed) significance test was used. Sample sizes were the following: DsRed: n = 132; CaMKIIa-DsRed: n = 134. Error bars show SEM; ****p < 0.0001, ns not significant.*

5.3. Discussion

5.3.1. Establishing an interaction between Panx1a and CaMKIIa and its effects on Panx1a localization

With the growing evidence of Panx1s and CaMKII being found in the same pathways, we wanted to investigate a direct interaction between the two proteins. Using the zebrafish Panx1 ohnologs, Panx1a and Panx1b, we showed that both interact with CaMKIIa in transiently transfected cells. The presence of a bright band corresponding to CaMKIIa in the pulled-down fractions was surprising since establishing interaction with a kinase through a CoIP assay can be challenging, considering that the interactions between kinases and substrate proteins are innately transient. This suggests that the interaction between the Panx1a/Panx1b and CaMKIIa is strong. We confirmed this interaction using FRET analysis to show that the two interact *in vivo*.

Interestingly, overexpressing Panx1a with CaMKIIa resulted in an increased accumulation of intracellular Panx1a. This accumulation was not seen in cells overexpressing Panx1a and the ECFP empty vector control, indicating that this intracellular accumulation is not a result of overexpression in general. The regulation of Panx1a by CaMKIIa was further seen in our western blot analysis. As Panx1a exists in three states, the unmodified Gly0, the high mannose Gly1, and the complex Gly2 forms, the intensities of each band can provide insight into this expression regulation. Our results show that CaMKIIa expression leads to a decrease in the Panx1a Gly2 form. Previously, using cell surface biotinylation, it has been shown that all three glycosylation species of the mouse Panx1 can be found at the cell surface, with a preference for the Gly2 state (Penuela et al., 2009). Our results show that the same applies to Panx1a when co-

expressed with the empty vector control. However, when Panx1a is co-expressed with CaMKIIa, we see that the Gly2 is no longer the most prevalent state in the biotinylated fraction. Instead, there appears to be a preference for the Gly1 species. We also see a decrease in Panx1a mediated dye uptake when CaMKIIa is present. Taken together, these results indicate that Panx1a can still traffic to the cell surface but to a lesser extent, with apparent retention in the intracellular compartments.

5.3.2. Exploring the effects of CaMKIIa mutants on the interaction with Panx1a

As CaMKIIa is a well-studied kinase, we created mutations of residues known to impact CaMKIIa function and structure. The K42M mutant abolishes CaMKIIa activity, as the Lysine in this position is needed to interact with ATP or ADP directly and is part of the structure for the nucleotide-binding pocket (Tullis et al., 2020). Both T305 and T306 undergo phosphorylation which blocks the binding of CaMKIIa to Ca2+/calmodulin, thereby inhibiting its activity (Hanson and Schulman, 1992). The T305A:T306A mutant cannot undergo this inhibition. D135 is part of the catalytic loop and, when mutated to an asparagine (D135N), inactivates CaMKIIa (Hoffman et al., 2011). T286 undergoes autophosphorylation and is required for autonomous CaMKIIa activity (Chao et al., 2011). The T286A mutation prevents this autonomous activation, and the T286D mutant mimics the phosphorylated residue. F293 is involved in autoinhibition. Once T286 undergoes autophosphorylation, F293 can interact with Ca2+/CaM, and in the absence of T286 autophosphorylation, F293 dissociates from CaM and causes autoinhibition (Chin and Means, 2002). F293A mutation would therefore prevent autoinhibition, resulting in an active kinase. H477 is involved in CaMKIIa oligomerization and protein stability, as it is located in the association domain (Chia et al. 2018). The H477Y mutant causes problems

with self-association and oligomerization and decreases CaMKIIa stability. R296 is part of the CaM-binding region (Coultrap and Bayer, 2012) and, when mutated to R296A, may lose its ability to bind CaM, thereby preventing CaMKIIa activation. Surprisingly, our data showed that most of the mutants had restored the western blot expression of the Panx1a Gly2 species, except the R296A mutant, which further decreased the overall expression of Panx1a and the ratio of Gly2/Gly1+Gly0. Although the ratio was not as high as that of Panx1a co-expressed with the ECFP empty vector control, no significant differences were observed. Our FRET results provided inside into how CaMKIIa might interact with Panx1a. We found that all mutants were still able to interact with Panx1a. The T286 mutants and H477Y mutant showed increased FRET efficiency, indicating a more compact interaction between Panx1a and CaMKIIa. We were not surprised that T286D had increased interaction with Panx1a as this is a constitutively active mutant. However, it was interesting that the H477Y mutant had increased interaction as this mutant does not form a stable, oligomerized CaMKIIa kinase. It is possible that the individual subunits are more accessible for interaction and therefore show a more compact binding with Panx1a. Interestingly, for the T286A interaction, we have previously seen a similar pattern with Cx36 (Siu et al., 2021), where the FRET efficiency between the two was significantly higher. We believe this might be a result of the conformational changes to CaMKIIa, which resulted in a “locked” interaction state between the two proteins. The same might apply to Panx1a and CaMKIIa T286A mutant.

5.3.3. Rescue of Panx1a localization by the constitutively active CaMKIIa T286D mutant

We showed that the constitutive activity of the CaMKIIa T286D mutant restores the expression of Panx1a by using two organelle markers for co-localization studies. Although Panx1a will naturally co-localize with the ER and Golgi markers during its trafficking stages, we see that when expressed with the WT, unstimulated CaMKIIa, Panx1a co-localized more with the intracellular markers. T286D mutant was seen to rescue the expression of Panx1a at the cell surface and showed normal levels of co-localization with the intracellular markers, with a slight increase in the Golgi apparatus. We propose that the constitutively active kinase phosphorylates Panx1a causing it to travel to the cell surface. Furthermore, we show that Panx1a interacts with CaMKIIa during its trafficking stages, as seen in the CoIP assay and FRET analysis with BFA treatment. We have previously shown that BFA treatment disrupts the trafficking of the zebrafish Panx1a between the ER and Golgi compartments (Timonina et al., 2019). However, a strong interaction between Panx1a and CaMKIIa with BFA treatment can still be seen, indicating that it occurs early in the trafficking stages. With the speculation that CaMKIIa is involved in Panx1a trafficking, we explored the size and trafficking dynamics of vesicles transporting Panx1a using TIRF microscopy. Although CaMKIIa expression did not affect the size of Panx1a expressing vesicles, we noted an increase in vesicle displacement. The proposed regulation of Panx1a by CaMKIIa is summarized in **Figure 5.9**.

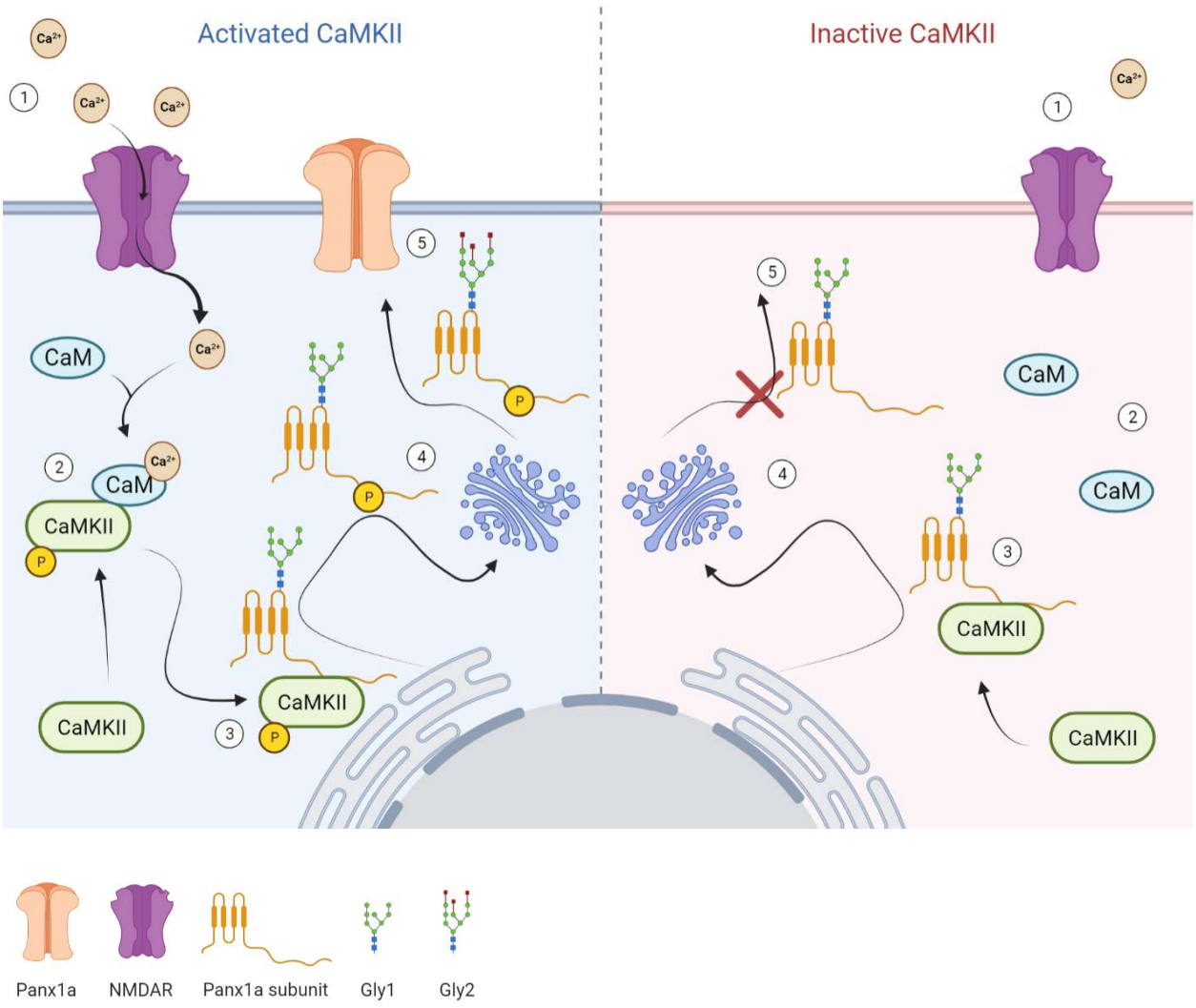

Figure 5.9. Proposed pathway of Panx1a regulation via CaMKIIa. (Left) Activated CaMKII pathway. 1) Calcium ions enter the cell when channels such as NMDA receptors are open. 2) Influx of calcium activates CaMKII kinase by binding CaM. 3) Activated CaMKII binds and phosphorylates Panx1a subunits early in its trafficking stages. 4) Phosphorylated Panx1a is trafficked through the Golgi apparatus and undergoes complex glycosylation modification. 5) Mature, complex glycosylated Panx1a is inserted into the cell membrane. (Right) Inactive CaMKII pathway. 1) Calcium ions do not enter the cell. 2) CaM molecules are not bound to calcium ions and do not activate CaMKII. 3) CaMKII binds but does not phosphorylate Panx1a. 4) Unphosphorylated Panx1a trafficks to the Golgi apparatus but does not undergo complex glycosylation post-translational modification. 5). Panx1a is not inserted into the cell membrane and accumulates in the intracellular compartments. Image was created with BioRender.com.

5.4. Supplementary materials

A

B

```
zfCamk2a          1 MATITCTRFTEEYQLFEELGKGAFSVVRRCVKVLSGQEYAAKIINTKKLS     50
                    |||||||||||||||||||||||||||||||||||:|||||||||||||||
mCamk2a           1 MATITCTRFTEEYQLFEELGKGAFSVVRRCVKVLAGQEYAAKIINTKKLS     50

zfCamk2a         51 TRDHQKLDREARICRLLKHPNIVRLHDSISEEGHHYLIFDLVTGGELFED    100
                    .|||||:|||||||||||||||||||||||||||||||||||||||||||||
mCamk2a          51 ARDHQKLEREARICRLLKHPNIVRLHDSISEEGHHYLIFDLVTGGELFED    100

zfCamk2a        101 IVAREYYSEADASHCIQQILEAVLHCHQMGVVHRDLKPENLLLASKSKGA    150
                    ||||||||||||||||||||||||||||||||||||||||||||||.|||
mCamk2a         101 IVAREYYSEADASHCIQQILEAVLHCHQMGVVHRDLKPENLLLASKLKGA    150

zfCamk2a        151 AVKLADFGLAIEVEGEQQAWFGFAGTPGYLSLEVLRKDPYGKAVDLWACG    200
                    ||||||||||||||||||||||||||||||.||||||||||.|||||||
mCamk2a         151 AVKLADFGLAIEVEGEQQAWFGFAGTPGYLSPEVLRKDPYGKPVDLWACG    200

zfCamk2a        201 VILYILLVGYPPFWDEDQHRLYQQIKAGAYDFPSPEWDTVTPEAKDLINK    250
                    ||||||||||||||||||||||||||||||||||||||||||||||||||
mCamk2a         201 VILYILLVGYPPFWDEDQHRLYQQIKAGAYDFPSPEWDTVTPEAKDLINK    250

zfCamk2a        251 MLTINPSKRITAAEALKHPWISHRSTVASCMHRQETVECLKKFNARRKLK    300
                    ||||||||||||||||||||||||||||||||||||:|||||||||||||
mCamk2a         251 MLTINPSKRITAAEALKHPWISHRSTVASCMHRQETVDCLKKFNARRKLK    300

zfCamk2a        301 GAILTTMLATRNFSGGKSGVSKKTDGVKESSESTNTTIEDEDTRVRKQEI    350
                    ||||||||||||||||||.:||:||||||||||||||||:||||||
mCamk2a         301 GAILTTMLATRNFSGGKSGGNKKSDGVKESSESTNTTIEDEDTKVRKQEI    350

zfCamk2a        351 IKVTEQLIEAISNGDFESYTKMCDPSVTAFEPEALGNLVEGLDFHRFYFE    400
                    ||||||||||||||||||||||||.:|||||||||||||||||||||||
mCamk2a         351 IKVTEQLIEAISNGDFESYTKMCDPGMTAFEPEALGNLVEGLDFHRFYFE    400

zfCamk2a        401 NLWSKNSKPVHTTILNPHIHLIGEEAACIAYIRITQYLDNNGMPCTAQSE    450
                    ||||:||||||||||||||:|:|:||||||||||||..|:|.|||||
mCamk2a         401 NLWSRNSKPVHTTILNPHIHLMGDESACIAYIRITQYLDAGGIPRTAQSE    450

zfCamk2a        451 ETRIWHRKDGKWQIVHFHRSGSPAAIAK    478
                    |||:|||:||||||||||||:|:.:...
mCamk2a         451 ETRVWHRRDGKWQIVHFHRSGAPSVLPH    478
```

Supplementary Figure 5.1. Sequence comparison of CaMKII orthologs and isoforms. (A) Sequence alignment between mouse CaMKIId and CaMKIIa shows a similarity score of 90.2%, identity score of 83.2%, and gap score of 4.6%. (B) Sequence alignment between zebrafish CaMKIIa and mouse CaMKIIa shows a similarity score of 97.5%, identity score of 93.9% and gap score of 0.0%. Alignments were performed using Pairwise Sequence Alignment with EMBOSS Needle (Madeira et al., 2022).

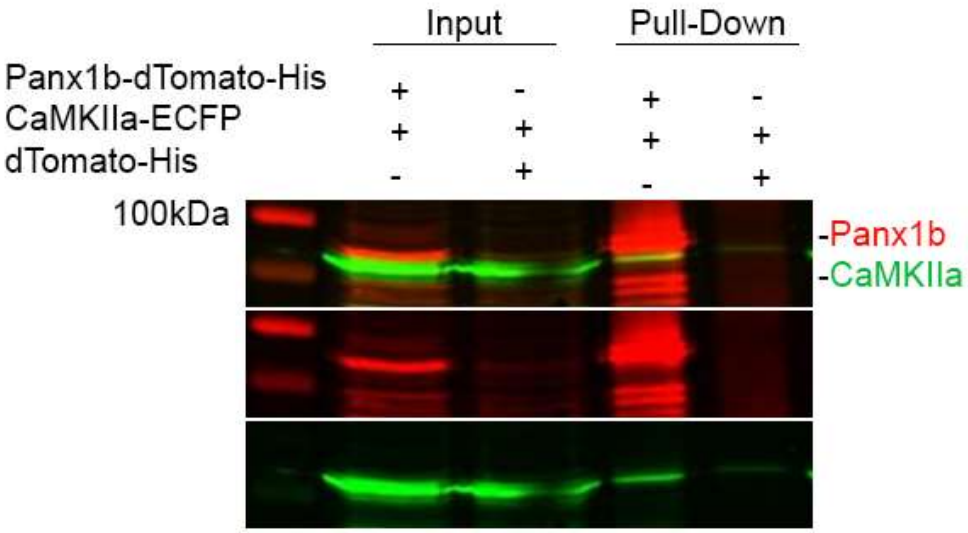

Supplementary Figure 5.2. Panx1b interacts with CaMKIIa in overexpressed Neuro 2a cells. Panx1b-dTomato-His were double transfected with CaMKIIa-ECFP and were subjected to co-immunoprecipitation. Input fractions represent the total lysates prior to immunoprecipitation with an anti-His antibody. Pull-Down represents the immunoprecipitated fractions. Cells double transfected with dTomato-His empty vector and CaMKIIa-ECFP were used as a negative control for both. Bottom: anti-GFP detection of ECFP tagged proteins, middle: anti-His detection of dTomato-His tagged proteins, top: merged channels.

Chapter 6. Concluding Remarks

6.1. General discussion

Protein phosphorylation is the most common type of post-translational modification that regulates all biological functions, including metabolism, growth, division, differentiation, motility, trafficking and transport, muscle contraction, immunity, and learning and memory (Ubersax and Ferrell, 2007). Kinases recognize preferential binding sites and target specific residues, either tyrosines or serines/threonines. When looking at an entire system *in vivo,* it can be challenging to determine which kinase targets which proteins since numerous substrates are available for single kinases, and multiple kinases can phosphorylate individual proteins. In addition, as phosphorylation modifications are reversible, phosphatases present in a biological system can also affect a protein's phosphorylation status at a given time. For these reasons, exploring the protein-kinase interactions and phosphorylation profiles of targets of interest is advantageous in a more controlled system. The research in this thesis uses the Neuro 2a cell line to overexpress Panx1a to study the protein trafficking and channel function with respect to its phosphorylation status. By overexpressing the target of interest, we effectively explore the important residues for protein trafficking/function and which kinases interact with and regulate Panx1a. In this section, I discuss my results and how they align with the current literature in the field with respect to the two aims of this thesis: the identification of novel phosphorylation residues and the exploration of the kinase interactome of Panx1a.

Previous research has suggested that the mammalian Panx1 interacts with several kinases, and its phosphorylation leads to the regulation of trafficking and activity. Lopez et al. claim that the rat Panx1 channels are phosphorylated by CaMKII at its C terminal

tail, leading to increased protein activity (Lopez et al., 2021). Although the proposed residue for this phosphorylation event is not conserved in the zebrafish Panx1a C terminal tail, our research aligns with the finding that the protein interacts with this kinase. Further, the findings in this thesis are a follow-up to a collaboration study titled "*Convergent NMDA receptor – Pannexin1 signaling pathways regulate the interaction of CaMKII with Connexin-36*" (see list of publications), which puts CaMKII in the same pathway as Panx1 (Siu et al., 2021).

The interest in CaMKII as an interacting kinase of Panx1 in the context of neurobiology is not without reason. This kinase is highly abundant in the brain and is enriched at the postsynaptic density (Lisman et al., 2002). Several factors make CaMKII an excellent kinase for neurobiological functions. Its ability to undergo autophosphorylation helps with the storage of long-term synaptic memory. Also, its interaction with the NMDA receptor allows it to control synaptic strength and affect the function and trafficking of proteins involved in synaptic pathways. Our findings demonstrate that CaMKII interacts with Panx1a and regulates its localization. The effects of CaMKII phosphorylation on protein trafficking have been previously explored in the context of the α-amino-3-hydroxy-5-methyl-4-isoxazole propionic acid (AMPA) receptors (Herring and Nicoll, 2016). An influx of calcium through NMDA receptors leads to activated CaMKII, which in turn causes an increase in AMPA receptors at the synapse. Since Panx1 is expressed in the brain tissue, and with previous evidence of its localization at the postsynaptic density (Zoidl et al., 2007), the involvement of CaMKII in regulating Panx1 expression at the postsynaptic density is a strong possibility.

We also investigated the potential interaction between Panx1a and ERK2/MAPK. The involvement of the MAPK signaling pathway has been previously detected in cells overexpressing Panx1. A study used Rhabdomyosarcoma (RMS) cells to overexpress Panx1, which led to transcriptomic changes in biological processes and pathways, which included MAPK signaling (Xiang et al., 2021). Another study puts the two proteins in the same pathway, suggesting that ATP release from Panx1 channels in T cells leads to activation of purinergic P2X receptors and propagation of the MAPK signaling pathway (Schenk et al., 2008). Although MAPK is mainly known for its role in cellular processes like proliferation and differentiation, it has also been shown to be involved in learning and memory cognitive functions and synaptic plasticity (Sweatt, 2001). The findings in this thesis suggest that MAPK may regulate Panx1a. Although we did not detect a clear interaction between Panx1a and ERK2 via co-immunoprecipitation, we believe this is due to the transient and weak interaction between some kinases and substrate proteins. However, pharmacological inhibition of the MAPK pathway using PD98059 increased Panx1a vesicular expression. Another recent study used an alternative MAPK singling pathway inhibitor, U0126, to show a decrease in the expression of Panx1 via western blotting (Wu et al., 2022). Interestingly, a study currently published in the bioRxiv Preprint Server for Biology identified MAPK as one of the interacting partners of the mammalian Panx1 via co-immunoprecipitation and mass spec in overexpressed Panx1 cells (Frederiksen et al., 2019). While the research on Panx1/MAPK interaction is limited, the results from this thesis align with the current literature and provide extra insight into the effects of MAPK on Panx1.

While phosphorylation of specific residues on the mammalian Panx1 was previously explored, no research has been conducted on the phosphorylation status of the zebrafish Panx1a. Since the zebrafish is an excellent model for studying both development and neuronal biology, it is important to study the fish Panx1 to understand its similarities and differences with the mammalian Panx1. While most of the research has been focused on tyrosine phosphorylation of mouse and human Panx1 by SFKs, the research in this thesis identifies residues that are likely phosphorylated by serine/threonine kinases. We showed that the zebrafish Panx1a is subject to phosphorylation, in line with the research on mammalian Panx1. Although we explored the potential phosphorylation of residue Y205, we found that this amino acid is not subject to phosphorylation and instead has a role in stabilizing the protein for proper trafficking to the cell membrane. Later, using purification techniques and mass spectrometry, we identified several phosphorylated residues under baseline, unstimulated conditions. One of the phosphorylated residues, T164, showed a strong localization probability of a phosphorylation event, but this residue is not conserved in the mammalian Panx1. However, we also detected a phosphorylation event around the S173/S174 residues, which are conserved in the human Panx1 at S182. Interestingly, the S173A mutant decreased Panx1 activity at baseline conditions, indicating that this post-translational modification may be necessary for channel function. From the mammalian phosphorylation residues identified in literature, the Y198 residue phosphorylated by SFKs (Lohman et al., 2015) is conserved at residue Y191 in Panx1a. Although the peptide containing this residue was detected in our mass spectrometry analysis, we did not observe any phosphorylation event. This is likely due to our analysis being conducted at

unstimulated, untreated baseline conditions. As the phosphorylation of Y198 is part of the TNF-a signaling, we believe that further stimulation would be required to induce this modification in the zebrafish Panx1a. The phosphorylation residue identified in the CT of Panx1, Y308 (Weilinger et al., 2016), is not conserved in the zebrafish Panx1a. Considering that this residue is important for the activation of the mammalian Panx1, we believe that there must be alternative phosphorylation sites in the zebrafish Panx1a which regulate its function. These findings indicate phosphorylation plays a vital role in the zebrafish Panx1a and only scratches the surface of what is occurring at the molecular level. Further research is required to continue investigating these post-translation modifications.

6.2. Future directions

The growing research of the Panx1 field is constantly expanding, and new findings are unveiled to help our understanding of neuronal biology. The research described in this thesis contributes to this fascinating field's next piece of the puzzle. However, as research is constantly evolving and new discoveries are made, several streams can be taken to build on the results presented here.

According to a study conducted in 2002, 518 protein kinase genes were identified in the human genome (Manning et al., 2002). Considering that the research in this thesis explored only a tiny portion of these kinases, a substantial investigation is required to continue identifying the kinase interactome of Panx1. Within our mass spectrometry results, several potential kinase interactors were not explored. These include serine/threonine kinases Cit and Cdk2, tyrosine kinase Ret, and the kinase anchoring protein Akap12. Further, pharmacological inhibition/activation of PKA, GSK3, and AMPK

showed promising results for modulating Panx1 expression/function, but the interaction has not yet been tested. Specifically, we believe that PKA is the ideal candidate for future investigation as it has been proposed to modulate human Panx1 (Lopez et al., 2020), has a role in synaptic plasticity (Waltereit and Weller, 2003), and when pharmacologically blocked using H-89, showed an effect on the activity of mouse Panx1 and zebrafish Panx1b, as presented in this thesis.

After investigating the relationship between ERK2/MAPK and Panx1a, we could not show a clear, direct interaction between the two. Further investigation is required to determine whether this interaction is simply too weak to be detected by the methods used in our experiments. More sensitive approaches can be applied by overexpressing both proteins and detecting interaction by co-immunoprecipitation followed by mass spectrometry. However, the downfall of using such an approach is the possible false negative results, as mass spectrometry can detect trace amounts of individual proteins. While we can also apply *in vitro* techniques to detect direct interaction, we want to try and stay as close to the natural cell environment as possible by using *in vivo* cell models. It is also important to remember that there are two Panx1 ohnologues in zebrafish: Panx1a and Panx1b. As this research only investigated the interaction with Panx1a, it is worth exploring whether Panx1b is a better candidate in the future.

Contrastingly, no issues were encountered when detecting the interaction between Panx1a (or Panx1b) and CaMKII. We identified the CaMKIId subunit in our mass spectrometry screen and showed a clear interaction between the CaMKIIa subunit and Panx1a via co-immunoprecipitation in over-expressing cells. With our results indicating that CaMKII regulates the localization of Panx1a, future research should look into

identifying the exact residue that is phosphorylated by this kinase. By doing so, the zebrafish model can then be used to create a point-mutation that abolishes (using alanine substitution) or mimics (using aspartate substitution) this phosphorylation event to study its significance in a larger biological system. Further, the existing Panx1a knockout zebrafish line, which was recently created in our lab (Safarian et al., 2020), can be used to compare to wildtype TL fish when treated with KN-93, an inhibitor of the CaMKII pathway. These fish can then be studied for differences in behavioural assays and developmental biology.

Finally, the results from this thesis and the research in literature explore the post-translational modifications, specifically phosphorylation, of Panx1. Here, we present novel residues that undergo this modification and briefly look at the effects of alanine substitution on Panx1a expression and activity at baseline activity. Further experimentation should be conducted to explore the effects of channel stimulation on Panx1a phospho-mutants compared to WT. Also, it is important to determine what proportion of the total protein is phosphorylated at the specific residues of interest to understand whether the modification produces a strong effect. Future experiments should also use the zebrafish model to purify and study the Panx1a's endogenous, natural state. However, this poses challenges, as it requires an antibody specific to Panx1a and can be used for purification purposes.

6.3. Summary

The findings in this thesis provide novel insights into the Panx1 phospho-proteomic research. Our original hypothesis was that the zebrafish Panx1a undergoes phosphorylation post-translational modifications that affect its function and trafficking. We

aimed to prove this hypothesis by exploring the specific phosphorylation events occurring on distinct residues that are either conserved or differ from the mammalian Panx1 and identifying the kinases responsible for modulating Panx1a activity and localization.

We first identified a key conserved residue, Y205, located at the border of the intracellular loop and the third transmembrane domain, which disrupted channel localization at the membrane upon mutation to an alanine. We explored the possibility of this residue being phosphorylation but found that this is an unlikely occurrence and that it instead plays a role in the stabilization of the channel and proper trafficking.

At this stage, we decided to take a different approach to address the two aims above. By purifying the overexpressed Panx1a, digesting, and analyzing via mass spectrometry, we identified novel residues undergoing phosphorylation modification and screened for potential interacting kinases. From the screen results, we identified four novel phosphorylation sites in the intracellular loop of Panx1a. T164 was determined to be phosphorylated with high localization reliability, and T158, T171, and S174 showed phosphorylation modifications with lower localization reliability. Considering that S174 neighbours a second serine residue at position 173, we considered this residue for further investigation. Functional analysis at baseline levels revealed a decrease in Panx1a activity upon mutating the S173 residue to an alanine. This residue is conserved in mouse Panx1 and should be further investigated to determine its significance.

We took two different approaches to address the second aim: 1. Identify the potential interacting kinase for residue T164 as this peptide had reliable phosphorylation localization, and 2. Select a promising kinase from the mass spectrometry screen to test the interaction further. For the former, we identified ERK2/MAPK as the potential kinase

phosphorylating T164. Based on our results, we could not detect a strong interaction between ERK2 and Panx1a but did see an increase in vesicular expression upon treatment with a MAPK inhibitor. We selected CaMKII as the kinase of interest for the second approach based on our mass spectrometry screen results. Data from this project revealed a strong interaction between Panx1a and the CaMKIIa subunit. Further, we show that overexpression of CaMKIIa results in a decrease in Panx1a expression at the cell membrane, whereas a constitutively active CaMKIIa mutant rescues this phenotype. This suggests that CaMKIIa regulates Panx1a trafficking via direct interaction and phosphorylation modification.

Together, these findings show that the zebrafish Panx1a, like the mammalian Panx1, undergoes phosphorylation modifications that regulate both function and trafficking of the protein. The results are in line with, yet are distinct, from the current literature in the Panx1 field. Combined, the research in this thesis provides new evidence and insight into the Panx1 kinase interactome and post-translational regulation that contributes to the growing field of neurobiology.

APPENDIX

A1. Mass spectrometry data

Table A. 1. Proteins identified by Accession Number via mass spectrometry in the Panx1a-dTomato-His pull-down experiments. Proteins were included only if they appeared at least once in each of the three independent experiments. Proteins were removed if they were identified as hits in the three negative control experiments with dTomato-His empty vector pull-downs.

		Total Unique Spectrum Count			Total Spectrum Count			Percent Coverage		
Accession Number	**Molecular Weight**	N=1	N=2	N=3	N=1	N=2	N=3	N=1	N=2	N=3
Panx1a-dTomato-His (bait)	75 kDa	50	66	14	77	113	19	32.40%	33.30%	14.00%
Q64737	108 kDa	1	4	3	1	4	3	2.08%	7.62%	5.54%
Q62018	133 kDa	2	2	3	2	5	3	2.90%	2.98%	3.58%
Q61941	114 kDa	1	1	3	1	1	3	1.20%	1.20%	3.22%
Q61937	33 kDa	2	2	2	2	2	2	12.30%	12.30%	7.19%
Q61749	58 kDa	6	1	1	8	1	1	12.20%	2.29%	4.20%
Q61165	91 kDa	1	3	1	1	3	1	3.54%	7.80%	3.54%
Q61001	404 kDa	6	4	2	6	4	2	2.88%	1.64%	1.24%
Q60611	86 kDa	4	5	3	4	5	3	8.25%	8.25%	9.69%
Q922P9	60 kDa	3	4	3	3	5	3	7.88%	6.96%	5.68%
Q792Z1	26 kDa	3	2	2	3	3	3	18.70%	12.60%	18.70%
Q640M1	87 kDa	7	1	3	7	1	3	11.70%	1.69%	6.00%
Q99PA7	35 kDa	2	2	4	2	2	4	9.06%	16.20%	25.00%
Q99LW0	44 kDa	2	1	1	2	1	1	7.47%	4.58%	3.86%
Q99LI5	97 kDa	2	3	1	3	5	1	4.48%	5.49%	2.02%
Q99LB0	37 kDa	2	1	6	2	1	6	9.15%	5.49%	20.10%
Q99KU0	46 kDa	1	2	2	1	2	3	7.39%	7.39%	11.30%
Q99JP7	70 kDa	3	4	1	3	4	1	9.37%	11.90%	2.87%
Q91YL2	34 kDa	1	1	2	1	1	4	10.90%	10.90%	10.20%
Q91WS0	12 kDa	1	1	3	1	1	3	13.90%	12.00%	31.50%
Q91VR2	33 kDa	1	3	3	1	3	3	4.03%	9.06%	11.70%
Q91V41	24 kDa	2	1	2	2	1	2	6.98%	5.12%	11.60%
Q80ZX0	136 kDa	1	1	10	1	1	11	2.00%	2.00%	12.00%
Q80YA8	135 kDa	2	1	1	2	1	1	2.65%	1.09%	1.09%
Q80XC3	94 kDa	2	2	2	2	2	2	5.25%	4.27%	2.56%
Q80X82	143 kDa	3	2	5	3	2	5	4.74%	2.10%	5.82%
Q80TE0	155 kDa	1	2	1	1	2	1	1.28%	2.84%	1.56%
Q80SZ6	73 kDa	4	2	1	4	2	1	9.35%	4.03%	1.45%

Q69ZB8	125 kDa	5	5	1	5	5	1	6.95%	6.35%	0.94%
P97377	39 kDa	2	2	2	2	2	2	6.36%	8.09%	6.36%
Q9Z0U1	131 kDa	2	1	6	2	1	6	1.71%	1.54%	11.20%
Q9WTQ5	181 kDa	1	1	3	1	2	3	1.13%	1.07%	3.86%
Q9R1R2	81 kDa	1	1	2	1	1	2	1.48%	1.48%	4.44%
Q9R1J0	41 kDa	1	2	8	1	2	9	2.76%	6.91%	20.40%
Q9R0E2	84 kDa	1	1	3	1	1	3	2.20%	1.37%	5.63%
Q9R0E1	85 kDa	1	1	4	1	1	4	2.16%	1.35%	7.29%
Q9R0B9	84 kDa	1	3	6	1	3	6	2.17%	5.97%	10.90%
Q9R0A0	41 kDa	3	1	2	3	1	2	20.70%	2.39%	5.85%
Q9QX47	266 kDa	2	3	1	3	4	1	0.98%	1.60%	0.57%
Q9QX11	46 kDa	2	2	2	2	2	2	6.53%	6.53%	6.28%
Q9QWT9	74 kDa	3	3	2	4	3	2	4.75%	7.86%	3.56%
Q9QWH1	90 kDa	1	2	3	1	2	3	3.18%	5.76%	8.71%
Q9JIX8	151 kDa	3	1	3	3	1	3	1.72%	1.12%	4.33%
Q9JHT5	36 kDa	1	3	2	1	3	2	3.78%	11.00%	7.27%
Q9EQH4	34 kDa	1	3	1	1	3	1	5.19%	16.20%	5.19%
Q9EQH3	92 kDa	1	1	4	1	1	4	2.89%	2.89%	8.04%
Q9EP72	26 kDa	2	2	5	2	2	5	6.64%	6.64%	34.90%
Q9DC16	33 kDa	1	1	8	1	1	8	4.83%	2.76%	34.80%
Q9D967	19 kDa	1	2	5	1	3	5	7.93%	17.70%	48.80%
Q9D7M1	27 kDa	1	1	2	1	1	2	5.70%	8.33%	12.70%
Q9D0M1	39 kDa	1	1	8	1	1	8	4.49%	4.49%	27.20%
Q9D0D5	50 kDa	1	1	3	1	1	3	2.95%	3.41%	10.00%
Q9CZP3	63 kDa	3	5	3	3	5	3	7.39%	9.24%	8.87%
Q9CZM2	24 kDa	1	2	7	1	2	9	7.84%	8.82%	25.00%
Q9CZ42	37 kDa	1	2	10	1	2	10	6.12%	12.80%	42.30%
Q9CXZ1	20 kDa	7	3	1	7	3	1	32.60%	19.40%	8.57%
Q9CRB9	26 kDa	2	3	3	2	3	3	10.10%	15.40%	13.70%
Q9CR68	29 kDa	2	1	3	2	1	4	9.49%	9.49%	14.20%
Q9CR57	24 kDa	2	1	2	2	1	3	12.90%	5.99%	10.10%
Q9CQQ7	29 kDa	2	4	2	3	4	2	5.08%	14.80%	7.81%
Q9CQC7	15 kDa	1	1	2	1	1	2	19.40%	19.40%	27.90%
Q8VI75	119 kDa	1	1	4	1	1	4	1.57%	1.39%	6.01%
Q8VEK6	47 kDa	1	3	1	1	3	1	4.99%	10.50%	3.09%
Q8VEH8	55 kDa	2	1	3	2	1	3	8.70%	4.76%	9.11%
Q8VDL4	54 kDa	1	1	3	1	1	3	3.23%	2.82%	9.07%
Q8VCM8	63 kDa	1	2	2	1	2	2	2.49%	6.22%	6.22%
Q8R5H6	62 kDa	1	2	4	1	2	4	1.97%	4.29%	10.40%
Q8R4X3	103 kDa	2	1	8	2	1	8	3.02%	1.41%	12.10%
Q8R3N1	99 kDa	2	1	2	2	1	2	2.67%	1.05%	2.67%
Q8R2N2	77 kDa	1	2	3	1	3	4	2.04%	5.25%	9.77%
Q8R1Q8	57 kDa	1	1	3	1	1	3	5.93%	2.29%	9.18%

Q8N7N5	66 kDa	3	5	6	3	5	6	7.78%	7.61%	11.80%
Q8K224	115 kDa	2	1	2	2	1	3	1.37%	1.56%	4.20%
Q8K2V1	106 kDa	4	3	2	4	4	2	7.36%	5.26%	3.05%
Q8CGP4	14 kDa	8	12	5	9	14	9	35.70%	35.70%	30.20%
Q8CFE3	53 kDa	2	1	1	2	1	1	6.04%	3.33%	3.33%
Q8CDM1	118 kDa	2	5	7	3	5	7	2.79%	7.02%	9.81%
Q8C092	87 kDa	1	3	1	1	4	1	3.62%	4.99%	3.62%
Q8C006	57 kDa	3	1	5	3	1	5	9.78%	4.59%	12.20%
Q8C3I8	43 kDa	2	2	3	2	2	3	6.36%	8.14%	15.50%
Q8C0I1	72 kDa	3	4	5	3	4	7	6.05%	12.20%	11.90%
Q8BZ21	225 kDa	2	1	1	2	1	1	1.25%	0.90%	0.90%
Q8BYM8	61 kDa	3	1	6	3	1	6	8.71%	2.72%	16.00%
Q8BYJ6	147 kDa	1	3	1	1	3	1	0.92%	3.67%	1.61%
Q8BX90	132 kDa	2	1	2	3	1	2	4.34%	2.67%	3.01%
Q8BVE3	56 kDa	2	1	3	2	1	3	4.97%	3.11%	9.73%
Q8BUI3	72 kDa	1	1	2	1	1	2	1.70%	1.70%	5.25%
Q8BT14	63 kDa	2	1	5	4	1	5	3.48%	1.39%	12.70%
Q8BR07	96 kDa	2	2	2	2	2	2	3.35%	3.35%	2.40%
Q8BP92	37 kDa	1	1	3	1	1	3	6.25%	3.75%	11.90%
Q8BJA3	47 kDa	1	1	2	1	1	2	2.63%	2.63%	4.53%
Q8BJ71	93 kDa	1	1	5	1	1	5	1.47%	1.47%	7.20%
Q8BH43	54 kDa	1	3	2	2	3	2	2.62%	8.05%	5.23%
Q8BGX2	29 kDa	2	2	1	2	2	1	14.70%	15.40%	5.26%
Q8BFY9	102 kDa	1	1	6	1	1	6	1.34%	1.34%	10.90%
Q7TMB8	145 kDa	1	2	8	1	2	8	0.96%	1.84%	6.70%
Q6ZQ08	267 kDa	5	3	8	6	3	8	2.15%	1.18%	4.46%
Q6VNS1	93 kDa	2	2	1	2	2	1	3.39%	2.55%	1.33%
Q6VN19	67 kDa	3	2	5	3	2	5	10.30%	3.87%	15.00%
Q6RHR9	162 kDa	1	2	7	1	2	7	1.29%	2.04%	8.97%
Q6PHZ2	56 kDa	1	2	3	1	2	3	2.61%	6.41%	11.40%
Q6P5F9	123 kDa	1	3	6	1	3	6	2.05%	3.17%	7.28%
Q6P5F7	58 kDa	1	1	2	1	1	2	2.10%	2.10%	4.77%
Q6NZR5	138 kDa	2	1	5	2	1	5	4.10%	0.80%	6.19%
Q6NS46	208 kDa	1	1	3	1	1	3	0.48%	0.91%	3.28%
Q6DFW4	60 kDa	1	1	3	1	1	3	2.80%	2.80%	9.33%
Q5SVQ0	71 kDa	1	3	9	1	3	10	2.45%	4.89%	14.70%
Q4FK66	37 kDa	2	3	2	2	4	2	3.85%	8.65%	6.41%
Q3UTQ7	134 kDa	1	1	2	1	1	2	1.27%	1.60%	2.96%
Q3UHB1	63 kDa	1	1	3	1	1	4	5.31%	5.31%	7.51%
Q3U1T3	38 kDa	2	2	1	2	2	1	8.05%	15.20%	5.57%
Q3TVI8	81 kDa	2	1	2	2	1	2	2.48%	7.15%	3.44%
Q3TLH4	311 kDa	12	2	2	15	2	2	6.71%	1.41%	1.09%
Q3TIX9	65 kDa	1	1	4	1	1	4	1.95%	1.95%	9.22%

Q3THW5	14 kDa	5	9	6	5	20	8	31.20%	37.50%	25.80%
P97931	34 kDa	1	1	2	1	1	2	4.25%	5.23%	7.19%
P97868	200 kDa	1	3	1	1	3	1	0.78%	2.46%	1.68%
P97310	102 kDa	1	1	13	1	1	14	1.33%	1.55%	18.50%
P81117	50 kDa	2	1	13	2	1	14	6.90%	2.14%	37.40%
P70398	291 kDa	3	1	1	3	1	1	0.86%	0.31%	0.47%
P69566	71 kDa	2	3	4	2	3	4	5.21%	6.43%	9.49%
P63163	25 kDa	2	2	1	2	2	1	6.67%	12.10%	3.33%
P63002	22 kDa	1	3	1	1	3	1	7.11%	26.40%	6.09%
P62900	14 kDa	3	2	2	3	2	2	20.00%	20.00%	18.40%
P62855	13 kDa	3	4	4	5	4	4	13.00%	13.00%	33.90%
P62835	21 kDa	2	2	2	2	2	2	7.61%	7.61%	12.50%
P62814	57 kDa	3	2	3	3	2	3	8.02%	8.81%	9.78%
P62806	11 kDa	1	2	4	1	2	4	12.60%	15.50%	32.00%
P62307	10 kDa	3	3	2	3	3	3	39.50%	39.50%	39.50%
P62192	49 kDa	3	3	3	3	3	4	9.77%	11.40%	10.70%
P62137	38 kDa	1	3	10	1	4	10	4.24%	12.70%	29.10%
P61358	16 kDa	1	1	2	1	1	2	5.88%	5.88%	14.70%
P58281	111 kDa	2	2	3	2	2	3	2.92%	1.77%	3.75%
P55012	131 kDa	3	2	2	7	6	2	2.99%	2.99%	2.90%
P54923	40 kDa	1	2	8	1	2	9	4.14%	4.14%	34.50%
P54822	55 kDa	2	1	16	2	1	22	6.82%	4.13%	33.70%
P51410	22 kDa	4	6	7	4	6	9	34.90%	33.30%	28.60%
P51150	23 kDa	1	1	2	1	1	2	6.76%	6.76%	13.00%
P50518	26 kDa	1	2	1	1	2	1	5.75%	11.90%	5.75%
P49718	82 kDa	1	1	5	2	2	5	1.50%	1.50%	10.20%
P49025	235 kDa	3	2	3	3	2	3	1.85%	1.70%	2.14%
P47962	34 kDa	1	2	2	1	2	2	4.04%	11.40%	9.43%
P46638	24 kDa	1	1	4	1	1	4	5.05%	5.05%	22.00%
P35980	22 kDa	4	2	3	4	2	3	18.10%	13.30%	19.10%
P35951	95 kDa	1	1	4	1	1	4	1.28%	3.71%	8.00%
P35546	124 kDa	1	1	2	1	1	2	0.99%	0.99%	2.87%
P25206	92 kDa	1	2	5	1	2	5	1.48%	2.71%	8.00%
P23116	162 kDa	4	1	3	4	1	3	3.65%	1.56%	2.68%
P20664	49 kDa	1	1	2	1	1	2	3.12%	3.12%	6.24%
P19096	272 kDa	2	1	19	2	1	19	1.24%	0.68%	12.00%
P18653	82 kDa	3	2	3	3	2	3	5.52%	7.32%	6.63%
P16045	15 kDa	2	1	3	2	1	3	13.30%	13.30%	19.30%
P14685	61 kDa	1	2	5	1	2	5	2.83%	5.28%	11.50%
P10853	14 kDa	5	12	8	6	13	9	27.00%	71.40%	34.90%
O19441	41 kDa	1	1	2	1	1	2	3.80%	3.80%	6.52%
P0DN34	7 kDa	2	3	1	2	3	1	19.30%	71.90%	35.10%
O88874	61 kDa	3	3	7	3	3	8	9.75%	4.15%	17.70%

O70318	110 kDa	2	6	5	2	6	5	2.33%	9.62%	6.28%
O54825	50 kDa	3	2	1	3	2	1	14.40%	5.05%	1.83%
P70333	49 kDa	7	3	11	8	3	12	14.70%	9.58%	25.20%
O35465	44 kDa	2	2	1	2	2	1	7.46%	7.46%	3.23%
O35344	58 kDa	2	1	2	2	1	2	3.65%	1.73%	8.25%
O09005	38 kDa	2	3	1	2	3	1	4.95%	10.50%	4.95%
O08810	109 kDa	2	1	16	2	1	16	2.06%	1.65%	22.20%
O08807	31 kDa	3	4	3	3	4	3	7.66%	7.66%	10.60%
O08688	73 kDa	2	2	2	2	2	2	1.88%	6.41%	5.00%
O08599	68 kDa	1	1	6	2	1	6	1.35%	1.35%	15.20%
G3X9I0	58 kDa	4	1	1	4	1	1	6.87%	4.20%	1.53%
G3UXL2	35 kDa	1	4	9	1	4	9	3.77%	14.50%	30.20%
F6YVP7	18 kDa	11	14	11	13	16	14	55.30%	56.60%	52.60%
E9Q1A5	64 kDa	3	1	1	4	1	1	3.94%	2.23%	2.05%
D3Z3H0	26 kDa	2	5	1	2	5	1	7.79%	16.80%	7.79%
B9EJ86	101 kDa	2	3	1	2	3	1	4.72%	5.62%	1.24%
B2RX14	185 kDa	2	3	1	2	3	1	1.82%	2.07%	0.73%
B2RRD7	137 kDa	6	2	2	6	2	3	6.44%	2.81%	2.72%
B2RPU8	84 kDa	1	3	2	1	3	2	3.17%	4.50%	4.50%
B1AQJ2	120 kDa	4	1	3	5	1	3	7.19%	1.09%	3.55%
A6H584	290 kDa	4	5	14	4	6	15	2.50%	2.61%	7.16%
A2AFI6	77 kDa	5	3	2	5	3	2	7.45%	7.30%	4.47%

Table A. 2. Identified proteins from the mass spectrometry Panx1a-dTomato-His pull-down experiments and the protein information for each accession number.

Accession Number	**Protein Information**
Q64737	Trifunctional purine biosynthetic protein adenosine-3 OS=Mus musculus (Mouse) OX=10090 GN=Gart PE=1 SV=3
Q62018	RNA polymerase-associated protein CTR9 homolog OS=Mus musculus (Mouse) OX=10090 GN=Ctr9 PE=1 SV=2
Q61941	NAD(P) transhydrogenase, mitochondrial OS=Mus musculus (Mouse) OX=10090 GN=Nnt PE=1 SV=2
Q61937	Nucleophosmin OS=Mus musculus (Mouse) OX=10090 GN=Npm1 PE=1 SV=1
Q61749	Translation initiation factor eIF-2B subunit delta OS=Mus musculus (Mouse) OX=10090 GN=Eif2b4 PE=1 SV=2
Q61165	Sodium/hydrogen exchanger 1 OS=Mus musculus (Mouse) OX=10090 GN=Slc9a1 PE=1 SV=1
Q61001	Laminin subunit alpha-5 OS=Mus musculus (Mouse) OX=10090 GN=Lama5 PE=1 SV=4
Q60611	DNA-binding protein SATB1 OS=Mus musculus (Mouse) OX=10090 GN=Satb1 PE=1 SV=2
Q922P9	Putative oxidoreductase GLYR1 OS=Mus musculus (Mouse) OX=10090 GN=Glyr1 PE=1 SV=1

Q792Z1	Peptidase S1 domain-containing protein OS=Mus musculus (Mouse) OX=10090 GN=Try10 PE=1 SV=1
Q640M1	U3 small nucleolar RNA-associated protein 14 homolog A OS=Mus musculus (Mouse) OX=10090 GN=Utp14a PE=1 SV=1
Q99PA7	MAGE domain-containing protein OS=Mus musculus (Mouse) OX=10090 GN=4930550L24Rik PE=1 SV=1
Q99LW0	Ankyrin repeat domain-containing protein 10 OS=Mus musculus (Mouse) OX=10090 GN=Ankrd10 PE=2 SV=2
Q99LI5	Zinc finger protein 281 OS=Mus musculus (Mouse) OX=10090 GN=Znf281 PE=1 SV=1
Q99LB0	Deoxynucleotidyltransferase terminal-interacting protein 1 OS=Mus musculus (Mouse) OX=10090 GN=Dnttip1 PE=1 SV=1
Q99KU0	Vacuole membrane protein 1 OS=Mus musculus (Mouse) OX=10090 GN=Vmp1 PE=1 SV=2
Q99JP7	Glutathione hydrolase 7 OS=Mus musculus (Mouse) OX=10090 GN=Ggt7 PE=1 SV=2
Q91YL2	E3 ubiquitin-protein ligase RNF126 OS=Mus musculus (Mouse) OX=10090 GN=Rnf126 PE=1 SV=1
Q91WS0	CDGSH iron-sulfur domain-containing protein 1 OS=Mus musculus (Mouse) OX=10090 GN=Cisd1 PE=1 SV=1
Q91VR2	ATP synthase subunit gamma, mitochondrial OS=Mus musculus (Mouse) OX=10090 GN=Atp5f1c PE=1 SV=1
Q91V41	Ras-related protein Rab-14 OS=Mus musculus (Mouse) OX=10090 GN=Rab14 PE=1 SV=3
Q80ZX0	Sec24-related gene family, member B (S. cerevisiae) OS=Mus musculus (Mouse) OX=10090 GN=Sec24b PE=1 SV=1
Q80YA8	Protein crumbs homolog 2 OS=Mus musculus (Mouse) OX=10090 GN=Crb2 PE=1 SV=3
Q80XC3	USP6 N-terminal-like protein OS=Mus musculus (Mouse) OX=10090 GN=Usp6nl PE=1 SV=2
Q80X82	Symplekin OS=Mus musculus (Mouse) OX=10090 GN=Sympk PE=1 SV=2
Q80TE0	RNA polymerase II-associated protein 1 OS=Mus musculus (Mouse) OX=10090 GN=Rpap1 PE=1 SV=2
Q80SZ6	Nuclear RNA export factor 7 OS=Mus musculus (Mouse) OX=10090 GN=Nxf7 PE=1 SV=1
Q69ZB8	Zinc finger CCHC domain-containing protein 2 OS=Mus musculus (Mouse) OX=10090 GN=Zcchc2 PE=2 SV=3
P97377	Cyclin-dependent kinase 2 OS=Mus musculus (Mouse) OX=10090 GN=Cdk2 PE=1 SV=2
Q9Z0U1	Tight junction protein ZO-2 OS=Mus musculus (Mouse) OX=10090 GN=Tjp2 PE=1 SV=2
Q9WTQ5	A-kinase anchor protein 12 OS=Mus musculus (Mouse) OX=10090 GN=Akap12 PE=1 SV=1
Q9R1R2	Tripartite motif-containing protein 3 OS=Mus musculus (Mouse) OX=10090 GN=Trim3 PE=1 SV=1
Q9R1J0	Sterol-4-alpha-carboxylate 3-dehydrogenase, decarboxylating OS=Mus musculus (Mouse) OX=10090 GN=Nsdhl PE=1 SV=1
Q9R0E2	Procollagen-lysine,2-oxoglutarate 5-dioxygenase 1 OS=Mus musculus (Mouse) OX=10090 GN=Plod1 PE=1 SV=1
Q9R0E1	Multifunctional procollagen lysine hydroxylase and glycosyltransferase LH3 OS=Mus musculus (Mouse) OX=10090 GN=Plod3 PE=1 SV=1
Q9R0B9	Procollagen-lysine,2-oxoglutarate 5-dioxygenase 2 OS=Mus musculus (Mouse) OX=10090 GN=Plod2 PE=1 SV=2
Q9R0A0	Peroxisomal membrane protein PEX14 OS=Mus musculus (Mouse) OX=10090 GN=Pex14 PE=1 SV=1
Q9QX47	Protein SON OS=Mus musculus (Mouse) OX=10090 GN=Son PE=1 SV=2
Q9QX11	Cytohesin-1 OS=Mus musculus (Mouse) OX=10090 GN=Cyth1 PE=1 SV=2
Q9QWT9	Kinesin-like protein KIFC1 OS=Mus musculus (Mouse) OX=10090 GN=Kifc1 PE=1 SV=2

Q9QWH1	Polyhomeotic-like protein 2 OS=Mus musculus (Mouse) OX=10090 GN=Phc2 PE=1 SV=1
Q9JIX8	Apoptotic chromatin condensation inducer in the nucleus OS=Mus musculus (Mouse) OX=10090 GN=Acin1 PE=1 SV=3
Q9JHT5	AMME syndrome candidate gene 1 protein homolog OS=Mus musculus (Mouse) OX=10090 GN=Ammecr1 PE=2 SV=1
Q9EQH4	Transcription initiation factor TFIID subunit 8 OS=Mus musculus (Mouse) OX=10090 GN=Taf8 PE=2 SV=1
Q9EQH3	Vacuolar protein sorting-associated protein 35 OS=Mus musculus (Mouse) OX=10090 GN=Vps35 PE=1 SV=1
Q9EP72	ER membrane protein complex subunit 7 OS=Mus musculus (Mouse) OX=10090 GN=Emc7 PE=1 SV=1
Q9DC16	Endoplasmic reticulum-Golgi intermediate compartment protein 1 OS=Mus musculus (Mouse) OX=10090 GN=Ergic1 PE=1 SV=1
Q9D967	Magnesium-dependent phosphatase 1 OS=Mus musculus (Mouse) OX=10090 GN=Mdp1 PE=1 SV=1
Q9D7M1	Glucose-induced degradation protein 8 homolog OS=Mus musculus (Mouse) OX=10090 GN=Gid8 PE=1 SV=1
Q9D0M1	Phosphoribosyl pyrophosphate synthase-associated protein 1 OS=Mus musculus (Mouse) OX=10090 GN=Prpsap1 PE=1 SV=1
Q9D0D5	General transcription factor IIE subunit 1 OS=Mus musculus (Mouse) OX=10090 GN=Gtf2e1 PE=1 SV=1
Q9CZP3	Zinc finger protein 655 OS=Mus musculus (Mouse) OX=10090 GN=Zfp655 PE=1 SV=1
Q9CZM2	60S ribosomal protein L15 OS=Mus musculus (Mouse) OX=10090 GN=Rpl15 PE=1 SV=4
Q9CZ42	ATP-dependent (S)-NAD(P)H-hydrate dehydratase OS=Mus musculus (Mouse) OX=10090 GN=Naxd PE=1 SV=1
Q9CXZ1	NADH dehydrogenase [ubiquinone] iron-sulfur protein 4, mitochondrial OS=Mus musculus (Mouse) OX=10090 GN=Ndufs4 PE=1 SV=3
Q9CRB9	MICOS complex subunit Mic19 OS=Mus musculus (Mouse) OX=10090 GN=Chchd3 PE=1 SV=1
Q9CR68	Cytochrome b-c1 complex subunit Rieske, mitochondrial OS=Mus musculus (Mouse) OX=10090 GN=Uqcrfs1 PE=1 SV=1
Q9CR57	60S ribosomal protein L14 OS=Mus musculus (Mouse) OX=10090 GN=Rpl14 PE=1 SV=3
Q9CQQ7	ATP synthase F(0) complex subunit B1, mitochondrial OS=Mus musculus (Mouse) OX=10090 GN=Atp5pb PE=1 SV=1
Q9CQC7	NADH dehydrogenase [ubiquinone] 1 beta subcomplex subunit 4 OS=Mus musculus (Mouse) OX=10090 GN=Ndufb4 PE=1 SV=3
Q8VI75	Importin-4 OS=Mus musculus (Mouse) OX=10090 GN=Ipo4 PE=1 SV=1
Q8VEK6	Inhibitor of growth protein 3 OS=Mus musculus (Mouse) OX=10090 GN=Ing3 PE=1 SV=2
Q8VEH8	Endoplasmic reticulum lectin 1 OS=Mus musculus (Mouse) OX=10090 GN=Erlec1 PE=1 SV=1
Q8VDL4	ADP-dependent glucokinase OS=Mus musculus (Mouse) OX=10090 GN=Adpgk PE=1 SV=2
Q8VCM8	Nicalin OS=Mus musculus (Mouse) OX=10090 GN=Ncln PE=1 SV=2
Q8R5H6	Wiskott-Aldrich syndrome protein family member 1 OS=Mus musculus (Mouse) OX=10090 GN=Wasf1 PE=1 SV=2
Q8R4X3	RNA-binding protein 12 OS=Mus musculus (Mouse) OX=10090 GN=Rbm12 PE=1 SV=3
Q8R3N1	Nucleolar protein 14 OS=Mus musculus (Mouse) OX=10090 GN=Nop14 PE=1 SV=2
Q8R2N2	U3 small nucleolar RNA-associated protein 4 homolog OS=Mus musculus (Mouse) OX=10090 GN=Utp4 PE=2 SV=3
Q8R1Q8	Cytoplasmic dynein 1 light intermediate chain 1 OS=Mus musculus (Mouse) OX=10090 GN=Dync1li1 PE=1 SV=1

Q8N7N5	DDB1- and CUL4-associated factor 8 OS=Mus musculus (Mouse) OX=10090 GN=Dcaf8 PE=1 SV=1
Q8K224	RNA cytidine acetyltransferase OS=Mus musculus (Mouse) OX=10090 GN=Nat10 PE=1 SV=1
Q8K2V1	Serine/threonine-protein phosphatase 4 regulatory subunit 1 OS=Mus musculus (Mouse) OX=10090 GN=Ppp4r1 PE=1 SV=2
Q8CGP4	Histone H2A OS=Mus musculus (Mouse) OX=10090 GN=H2ac1 PE=1 SV=1
Q8CFE3	REST corepressor 1 OS=Mus musculus (Mouse) OX=10090 GN=Rcor1 PE=1 SV=3
Q8CDM1	ATPase family AAA domain-containing protein 2 OS=Mus musculus (Mouse) OX=10090 GN=Atad2 PE=1 SV=1
Q8C092	Transcription initiation factor TFIID subunit 5 OS=Mus musculus (Mouse) OX=10090 GN=Taf5 PE=1 SV=1
Q8C006	Tripartite motif-containing protein 35 OS=Mus musculus (Mouse) OX=10090 GN=Trim35 PE=1 SV=2
Q8C3I8	Protein HGH1 homolog OS=Mus musculus (Mouse) OX=10090 GN=Hgh1 PE=1 SV=1
Q8C0I1	Alkyldihydroxyacetonephosphate synthase, peroxisomal OS=Mus musculus (Mouse) OX=10090 GN=Agps PE=1 SV=1
Q8BZ21	Histone acetyltransferase KAT6A OS=Mus musculus (Mouse) OX=10090 GN=Kat6a PE=1 SV=2
Q8BYM8	Probable cysteine--tRNA ligase, mitochondrial OS=Mus musculus (Mouse) OX=10090 GN=Cars2 PE=1 SV=2
Q8BYJ6	TBC1 domain family member 4 OS=Mus musculus (Mouse) OX=10090 GN=Tbc1d4 PE=1 SV=2
Q8BX90	Fibronectin type-III domain-containing protein 3A OS=Mus musculus (Mouse) OX=10090 GN=Fndc3a PE=1 SV=3
Q8BVE3	V-type proton ATPase subunit H OS=Mus musculus (Mouse) OX=10090 GN=Atp6v1h PE=1 SV=1
Q8BUI3	Leucine-rich repeat and WD repeat-containing protein 1 OS=Mus musculus (Mouse) OX=10090 GN=LRWD1 PE=2 SV=1
Q8BT14	CCR4-NOT transcription complex subunit 4 OS=Mus musculus (Mouse) OX=10090 GN=Cnot4 PE=1 SV=2
Q8BR07	Protein bicaudal D homolog 1 OS=Mus musculus (Mouse) OX=10090 GN=Bicd1 PE=1 SV=2
Q8BP92	Reticulocalbin-2 OS=Mus musculus (Mouse) OX=10090 GN=Rcn2 PE=1 SV=1
Q8BJA3	Homeobox-containing protein 1 OS=Mus musculus (Mouse) OX=10090 GN=Hmbox1 PE=1 SV=1
Q8BJ71	Nuclear pore complex protein Nup93 OS=Mus musculus (Mouse) OX=10090 GN=Nup93 PE=1 SV=1
Q8BH43	Wiskott-Aldrich syndrome protein family member 2 OS=Mus musculus (Mouse) OX=10090 GN=Wasf2 PE=1 SV=1
Q8BGX2	Mitochondrial import inner membrane translocase subunit Tim29 OS=Mus musculus (Mouse) OX=10090 GN=Timm29 PE=1 SV=1
Q8BFY9	Transportin-1 OS=Mus musculus (Mouse) OX=10090 GN=Tnpo1 PE=1 SV=2
Q7TMB8	Cytoplasmic FMR1-interacting protein 1 OS=Mus musculus (Mouse) OX=10090 GN=Cyfip1 PE=1 SV=1
Q6ZQ08	CCR4-NOT transcription complex subunit 1 OS=Mus musculus (Mouse) OX=10090 GN=Cnot1 PE=1 SV=2
Q6VNS1	NT-3 growth factor receptor OS=Mus musculus (Mouse) OX=10090 GN=Ntrk3 PE=1 SV=1
Q6VN19	Ran-binding protein 10 OS=Mus musculus (Mouse) OX=10090 GN=Ranbp10 PE=1 SV=2
Q6RHR9	Membrane-associated guanylate kinase, WW and PDZ domain-containing protein 1 OS=Mus musculus (Mouse) OX=10090 GN=Magi1 PE=1 SV=1
Q6PHZ2	Calcium/calmodulin-dependent protein kinase type II subunit delta OS=Mus musculus (Mouse) OX=10090 GN=CaMKIId PE=1 SV=1

Q6P5F9	Exportin-1 OS=Mus musculus (Mouse) OX=10090 GN=Xpo1 PE=1 SV=1
Q6P5F7	Protein tweety homolog 3 OS=Mus musculus (Mouse) OX=10090 GN=Ttyh3 PE=1 SV=1
Q6NZR5	Superkiller viralicidic activity 2-like (S. cerevisiae) OS=Mus musculus (Mouse) OX=10090 GN=Skiv2l PE=1 SV=1
Q6NS46	Protein RRP5 homolog OS=Mus musculus (Mouse) OX=10090 GN=Pdcd11 PE=1 SV=2
Q6DFW4	Nucleolar protein 58 OS=Mus musculus (Mouse) OX=10090 GN=Nop58 PE=1 SV=1
Q5SVQ0	Histone acetyltransferase KAT7 OS=Mus musculus (Mouse) OX=10090 GN=Kat7 PE=1 SV=1
Q4FK66	Pre-mRNA-splicing factor 38A OS=Mus musculus (Mouse) OX=10090 GN=Prpf38a PE=1 SV=1
Q3UTQ7	PR domain zinc finger protein 10 OS=Mus musculus (Mouse) OX=10090 GN=Prdm10 PE=1 SV=2
Q3UHB1	5'-nucleotidase domain-containing protein 3 OS=Mus musculus (Mouse) OX=10090 GN=Nt5dc3 PE=1 SV=1
Q3U1T3	Breast cancer metastasis-suppressor 1-like protein OS=Mus musculus (Mouse) OX=10090 GN=Brms1l PE=2 SV=1
Q3TVI8	Pre-B-cell leukemia transcription factor-interacting protein 1 OS=Mus musculus (Mouse) OX=10090 GN=Pbxip1 PE=1 SV=2
Q3TLH4	Protein PRRC2C OS=Mus musculus (Mouse) OX=10090 GN=Prrc2c PE=1 SV=3
Q3TIX9	U4/U6.U5 tri-snRNP-associated protein 2 OS=Mus musculus (Mouse) OX=10090 GN=Usp39 PE=1 SV=2
Q3THW5	Histone H2A.V OS=Mus musculus (Mouse) OX=10090 GN=H2az2 PE=1 SV=3
P97931	Uracil-DNA glycosylase OS=Mus musculus (Mouse) OX=10090 GN=Ung PE=1 SV=3
P97868	E3 ubiquitin-protein ligase RBBP6 OS=Mus musculus (Mouse) OX=10090 GN=Rbbp6 PE=1 SV=5
P97310	DNA replication licensing factor MCM2 OS=Mus musculus (Mouse) OX=10090 GN=Mcm2 PE=1 SV=3
P81117	Nucleobindin-2 OS=Mus musculus (Mouse) OX=10090 GN=Nucb2 PE=1 SV=2
P70398	Probable ubiquitin carboxyl-terminal hydrolase FAF-X OS=Mus musculus (Mouse) OX=10090 GN=Usp9x PE=1 SV=2
P69566	Ran-binding protein 9 OS=Mus musculus (Mouse) OX=10090 GN=Ranbp9 PE=1 SV=1
P63163	Small nuclear ribonucleoprotein-associated protein N OS=Mus musculus (Mouse) OX=10090 GN=Snrpn PE=1 SV=1
P63002	TLE family member 5 OS=Mus musculus (Mouse) OX=10090 GN=Tle5 PE=1 SV=1
P62900	60S ribosomal protein L31 OS=Mus musculus (Mouse) OX=10090 GN=Rpl31 PE=1 SV=1
P62855	40S ribosomal protein S26 OS=Mus musculus (Mouse) OX=10090 GN=Rps26 PE=1 SV=3
P62835	Ras-related protein Rap-1A OS=Mus musculus (Mouse) OX=10090 GN=Rap1a PE=1 SV=1
P62814	V-type proton ATPase subunit B, brain isoform OS=Mus musculus (Mouse) OX=10090 GN=Atp6v1b2 PE=1 SV=1
P62806	Histone H4 OS=Mus musculus (Mouse) OX=10090 GN=H4f16 PE=1 SV=2
P62307	Small nuclear ribonucleoprotein F OS=Mus musculus (Mouse) OX=10090 GN=Snrpf PE=1 SV=1
P62192	26S proteasome regulatory subunit 4 OS=Mus musculus (Mouse) OX=10090 GN=Psmc1 PE=1 SV=1
P62137	Serine/threonine-protein phosphatase PP1-alpha catalytic subunit OS=Mus musculus (Mouse) OX=10090 GN=Ppp1ca PE=1 SV=1
P61358	60S ribosomal protein L27 OS=Mus musculus (Mouse) OX=10090 GN=Rpl27 PE=1 SV=2
P58281	Dynamin-like 120 kDa protein, mitochondrial OS=Mus musculus (Mouse) OX=10090 GN=Opa1 PE=1 SV=1

P55012	Solute carrier family 12 member 2 OS=Mus musculus (Mouse) OX=10090 GN=Slc12a2 PE=1 SV=2
P54923	[Protein ADP-ribosylarginine] hydrolase OS=Mus musculus (Mouse) OX=10090 GN=Adprh PE=1 SV=1
P54822	Adenylosuccinate lyase OS=Mus musculus (Mouse) OX=10090 GN=Adsl PE=1 SV=2
P51410	60S ribosomal protein L9 OS=Mus musculus (Mouse) OX=10090 GN=Rpl9 PE=2 SV=2
P51150	Ras-related protein Rab-7a OS=Mus musculus (Mouse) OX=10090 GN=Rab7a PE=1 SV=2
P50518	V-type proton ATPase subunit E 1 OS=Mus musculus (Mouse) OX=10090 GN=Atp6v1e1 PE=1 SV=2
P49718	DNA replication licensing factor MCM5 OS=Mus musculus (Mouse) OX=10090 GN=Mcm5 PE=1 SV=2
P49025	Citron Rho-interacting kinase OS=Mus musculus (Mouse) OX=10090 GN=Cit PE=1 SV=3
P47962	60S ribosomal protein L5 OS=Mus musculus (Mouse) OX=10090 GN=Rpl5 PE=1 SV=3
P46638	Ras-related protein Rab-11B OS=Mus musculus (Mouse) OX=10090 GN=Rab11b PE=1 SV=3
P35980	60S ribosomal protein L18 OS=Mus musculus (Mouse) OX=10090 GN=Rpl18 PE=1 SV=3
P35951	Low-density lipoprotein receptor OS=Mus musculus (Mouse) OX=10090 GN=Ldlr PE=1 SV=2
P35546	Proto-oncogene tyrosine-protein kinase receptor Ret OS=Mus musculus (Mouse) OX=10090 GN=Ret PE=1 SV=2
P25206	DNA replication licensing factor MCM3 OS=Mus musculus (Mouse) OX=10090 GN=Mcm3 PE=1 SV=2
P23116	Eukaryotic translation initiation factor 3 subunit A OS=Mus musculus (Mouse) OX=10090 GN=Eif3a PE=1 SV=5
P20664	DNA primase small subunit OS=Mus musculus (Mouse) OX=10090 GN=Prim1 PE=1 SV=1
P19096	Fatty acid synthase OS=Mus musculus (Mouse) OX=10090 GN=Fasn PE=1 SV=2
P18653	Ribosomal protein S6 kinase alpha-1 OS=Mus musculus (Mouse) OX=10090 GN=Rps6ka1 PE=1 SV=1
P16045	Galectin-1 OS=Mus musculus (Mouse) OX=10090 GN=Lgals1 PE=1 SV=3
P14685	26S proteasome non-ATPase regulatory subunit 3 OS=Mus musculus (Mouse) OX=10090 GN=Psmd3 PE=1 SV=3
P10853	Histone H2B type 1-F/J/L OS=Mus musculus (Mouse) OX=10090 GN=H2bc7 PE=1 SV=2
O19441	Ig-like domain-containing protein OS=Mus musculus (Mouse) OX=10090 GN=H2-Q1 PE=2 SV=1
P0DN34	NADH dehydrogenase [ubiquinone] 1 beta subcomplex subunit 1 OS=Mus musculus (Mouse) OX=10090 GN=Ndufb1 PE=1 SV=1
O88874	Cyclin-K OS=Mus musculus (Mouse) OX=10090 GN=Ccnk PE=1 SV=3
O70318	Band 4.1-like protein 2 OS=Mus musculus (Mouse) OX=10090 GN=Epb41l2 PE=1 SV=2
O54825	Bystin OS=Mus musculus (Mouse) OX=10090 GN=Bysl PE=1 SV=3
P70333	Heterogeneous nuclear ribonucleoprotein H2 OS=Mus musculus (Mouse) OX=10090 GN=Hnrnph2 PE=1 SV=1
O35465	Peptidyl-prolyl cis-trans isomerase FKBP8 OS=Mus musculus (Mouse) OX=10090 GN=Fkbp8 PE=1 SV=2
O35344	Importin subunit alpha-4 OS=Mus musculus (Mouse) OX=10090 GN=Kpna3 PE=1 SV=1
O09005	Sphingolipid delta(4)-desaturase DES1 OS=Mus musculus (Mouse) OX=10090 GN=Degs1 PE=1 SV=1
O08810	116 kDa U5 small nuclear ribonucleoprotein component OS=Mus musculus (Mouse) OX=10090 GN=Eftud2 PE=1 SV=1
O08807	Peroxiredoxin-4 OS=Mus musculus (Mouse) OX=10090 GN=Prdx4 PE=1 SV=1

O08688	Calpain-5 OS=Mus musculus (Mouse) OX=10090 GN=Capn5 PE=1 SV=1
O08599	Syntaxin-binding protein 1 OS=Mus musculus (Mouse) OX=10090 GN=Stxbp1 PE=1 SV=2
G3X9I0	Zinc finger protein 105 OS=Mus musculus (Mouse) OX=10090 GN=Zfp105 PE=4 SV=1
G3UXL2	Ribose-phosphate diphosphokinase OS=Mus musculus (Mouse) OX=10090 GN=Prps1l3 PE=3 SV=1
F6YVP7	40S ribosomal protein S18 OS=Mus musculus (Mouse) OX=10090 GN=Rps18-ps6 PE=3 SV=2
E9Q1A5	Zinc finger protein 384 OS=Mus musculus (Mouse) OX=10090 GN=Zfp384 PE=1 SV=1
D3Z3H0	INO80 complex subunit E OS=Mus musculus (Mouse) OX=10090 GN=Ino80e PE=1 SV=1
B9EJ86	Oxysterol-binding protein-related protein 8 OS=Mus musculus (Mouse) OX=10090 GN=Osbpl8 PE=1 SV=1
B2RX14	Terminal uridylyltransferase 4 OS=Mus musculus (Mouse) OX=10090 GN=Tut4 PE=1 SV=2
B2RRD7	Peregrin OS=Mus musculus (Mouse) OX=10090 GN=Brpf1 PE=1 SV=1
B2RPU8	SCAN domain containing 3 OS=Mus musculus (Mouse) OX=10090 GN=Zbed5 PE=1 SV=1
B1AQJ2	Ubiquitin carboxyl-terminal hydrolase 36 OS=Mus musculus (Mouse) OX=10090 GN=Usp36 PE=1 SV=1
A6H584	Collagen alpha-5(VI) chain OS=Mus musculus (Mouse) OX=10090 GN=Col6a5 PE=1 SV=4
A2AFI6	Transmembrane 9 superfamily member OS=Mus musculus (Mouse) OX=10090 GN=Gm364 PE=1 SV=1

A2. Plasmid maps

This section contains the plasmid maps of the DNA constructs used in this thesis. Maps were generated using SnapGene Viewer. To avoid repetition, only the pEYFP-N1 and pdTomato-His-N1 plasmid maps are shown for Panx1a. Other vectors used in this thesis include pECFP, pDsRed2-monomer, and pEGFP.

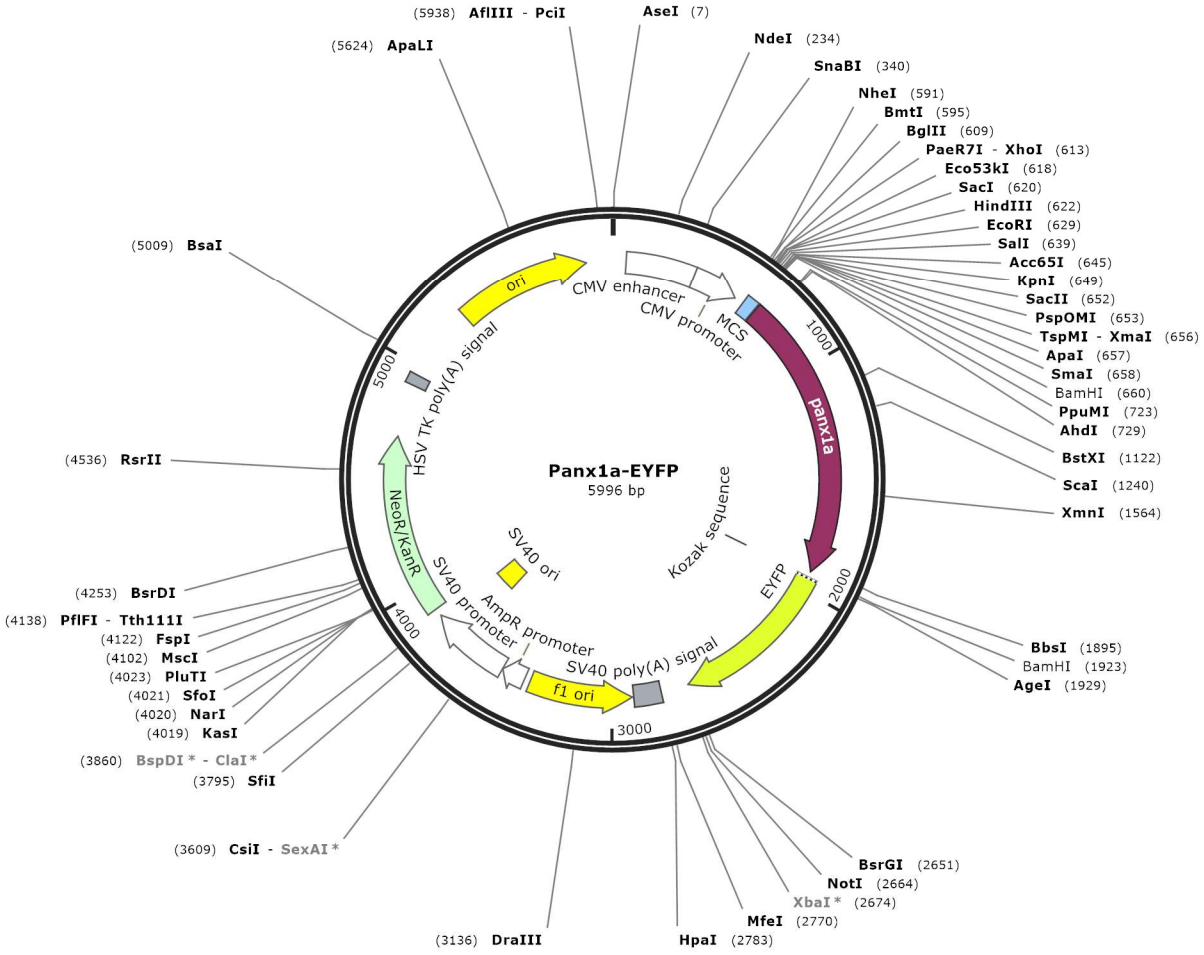

Figure A. 1. Plasmid map of Panx1a-EYFP. Danio rerio Panx1a was cloned into the pEYFP-N1 vector using BamHI restriction enzymes, and an orientation check was performed. EYFP tag is C terminal of Panx1a.

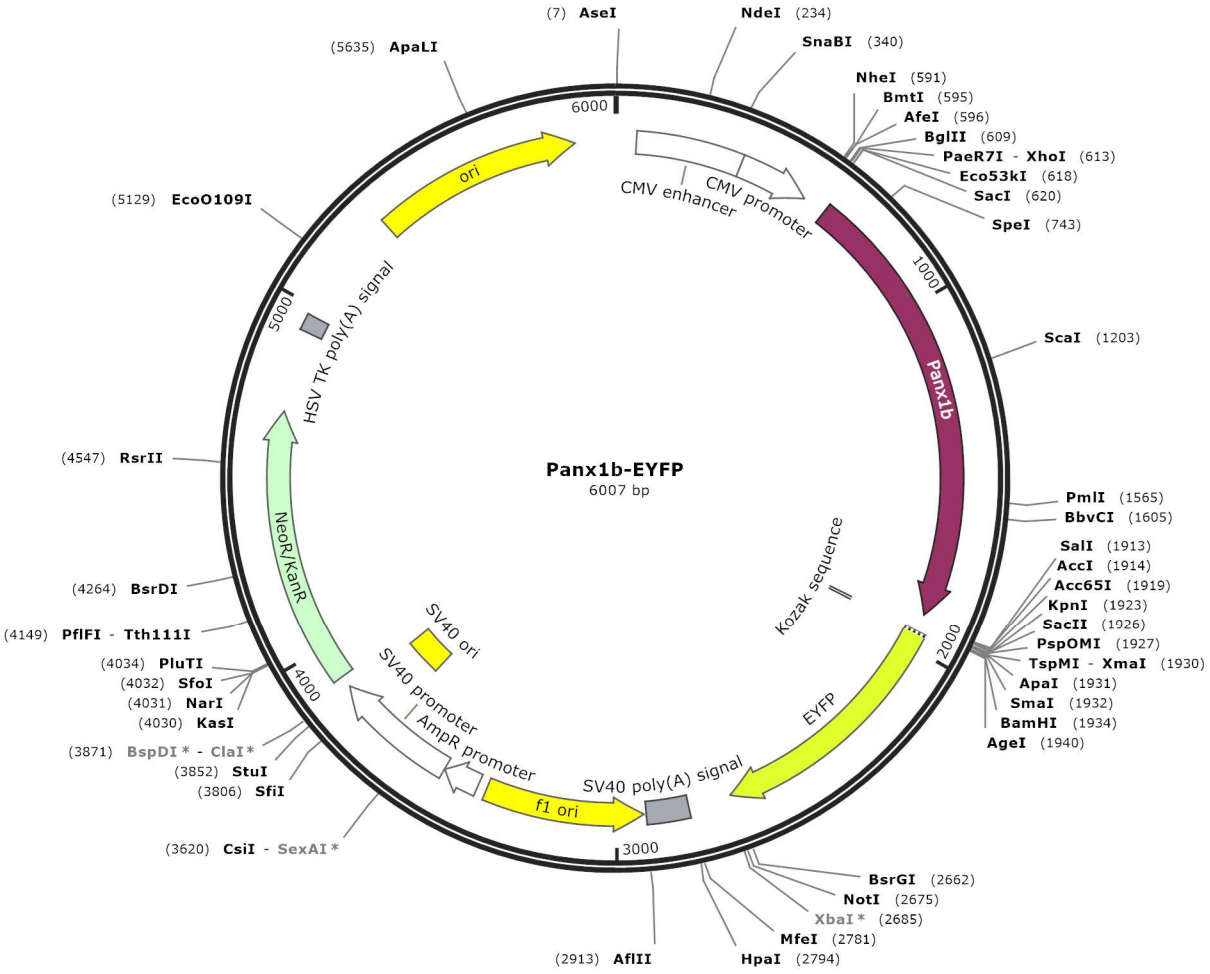

Figure A. 2. Plasmid map of Panx1b-EYFP. Danio rerio Panx1b was cloned into the pEYFP-N1 vector using EcoRI restriction enzymes, and an orientation check was performed. EYFP tag is C terminal of Panx1b.

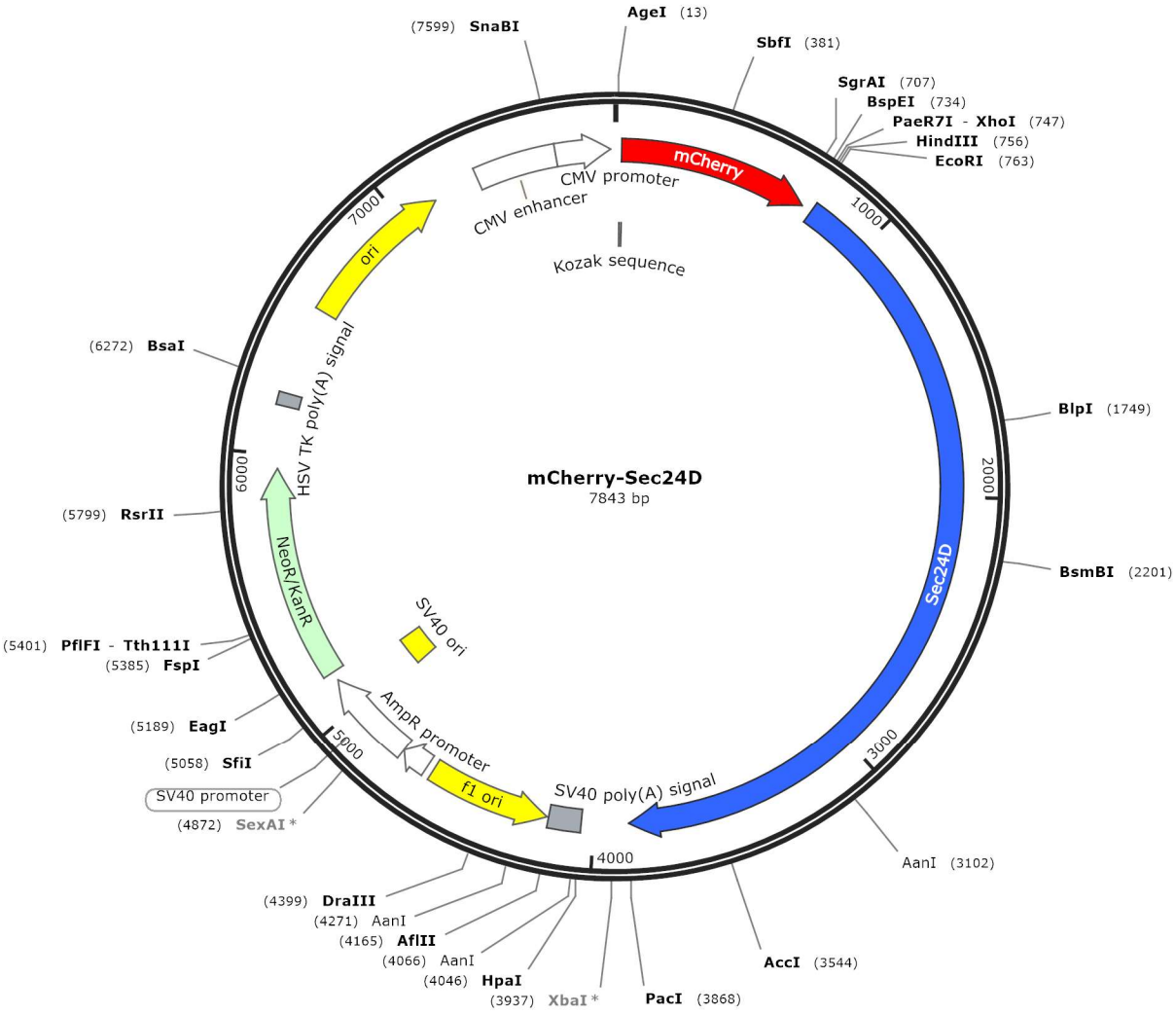

Figure A. 3. Plasmid map of mCherry-Sec24D. The plasmid was purchased and, the sequence was obtained from Addgene. Homo sapiens Sec24D was cloned into the pEYFP-C1 vector using EcoRI and XbaI, and EYFP was replaced with mCherry. mCherry tag is N terminal of Sec24D. pmCherry-Sec24D was a gift from Henry Lester (Addgene plasmid # 32677 ; http://n2t.net/addgene:32677 ; RRID:Addgene_32677).

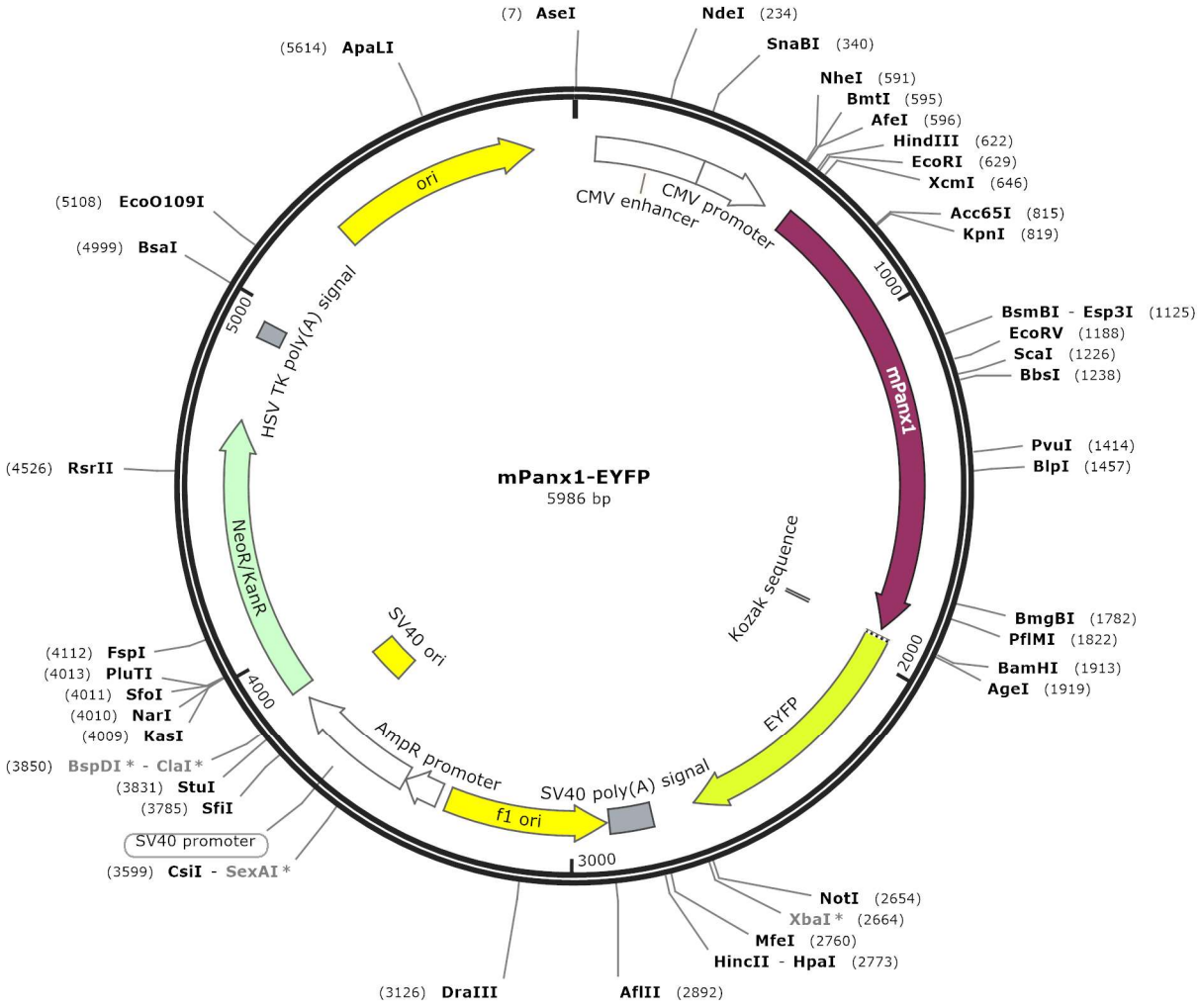

Figure A. 4. Plasmid map of mPanx1-EYFP. Mus musculus Panx1 was cloned into the pEYFP-N1 vector using BamHI and EcoRI restriction enzymes. EYFP tag is C terminal of Panx1.

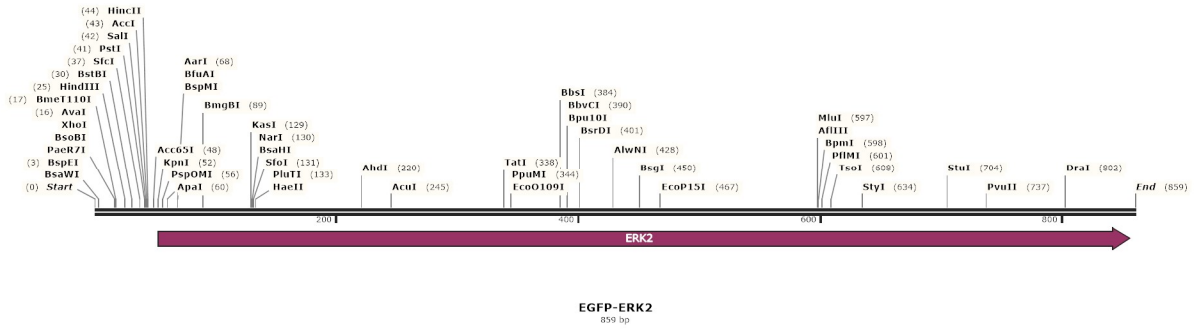

Figure A. 5. Plasmid map of EGFP-ERK2. The plasmid was purchased, and the sequence was obtained from Addgene. Only a partial sequence is available. Rattus norvegicus ERK2 was cloned into the pEGFP-C1 vector using ApaI and XbaI restriction sites. EGFP tag is N terminal of ERK2. GFP-ERK2 was a gift from Rony Seger (Addgene plasmid # 37145 ; http://n2t.net/addgene:37145 ; RRID:Addgene_37145).

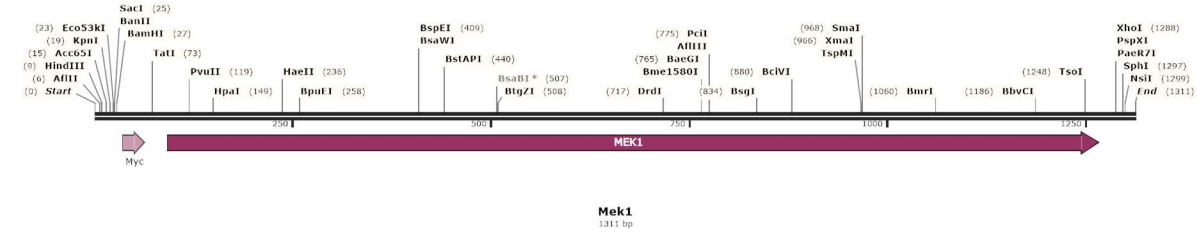

Figure A. 6. Plasmid map of MEK1. The plasmid was purchased, and the sequence was obtained from Addgene. Only partial sequence is available. Homo sapiens MEK1 was cloned into the pcDNA3.1-Hygro vector. Myc tag is N terminal of MEK1. Mek1 was a gift from Dustin Maly (Addgene plasmid # 40774 ; http://n2t.net/addgene:40774 ; RRID:Addgene_40774).

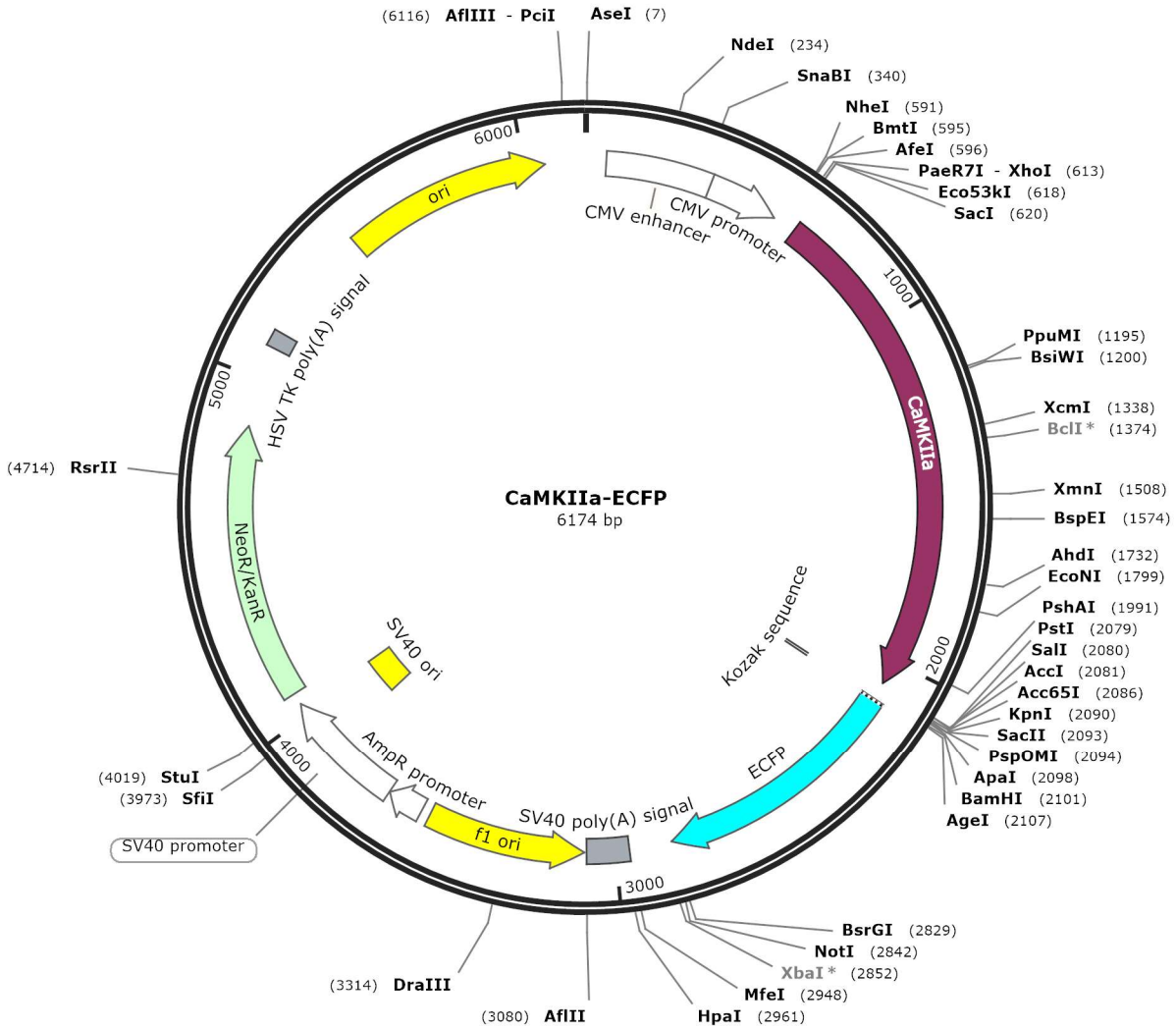

Figure A. 7. Plasmid map of CaMKIIa-ECFP. Mus musculus CaMKIIa was cloned into the pECFP-N1 vector using EcoRI restriction enzymes. ECFP tag is C terminal of CaMKIIA.

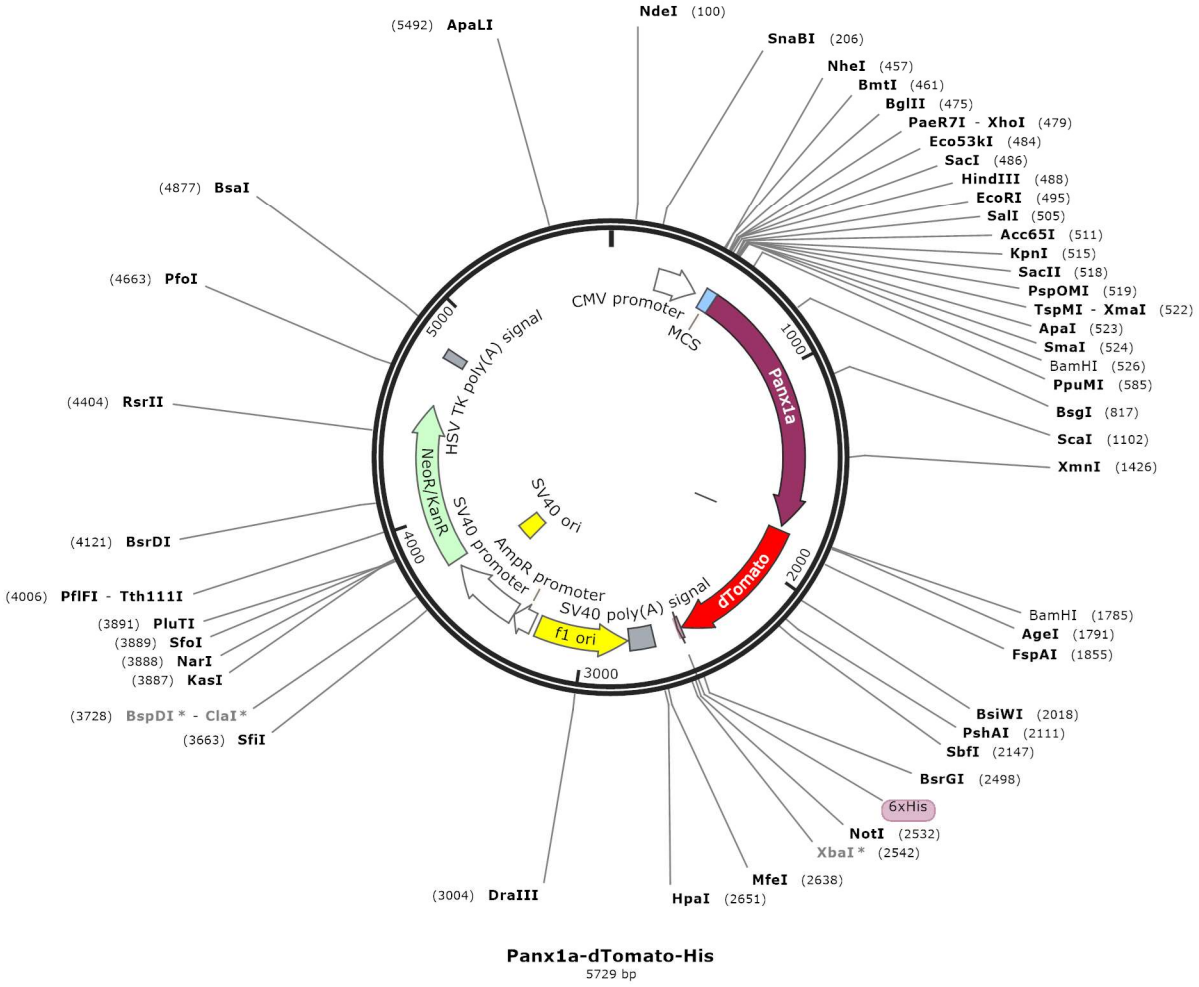

Figure A. 8. Plasmid map of Panx1a-dTomato-His. The pdTomato-His plasmid was created in-house by replacing EGFP with dTomato from the pEGFP-His-N1 plasmid. Danio rerio Panx1a was cloned into the pdTomato-His vector using EcoRI and AgeI restriction enzymes. dTomato-His tag is C terminal of Panx1a.

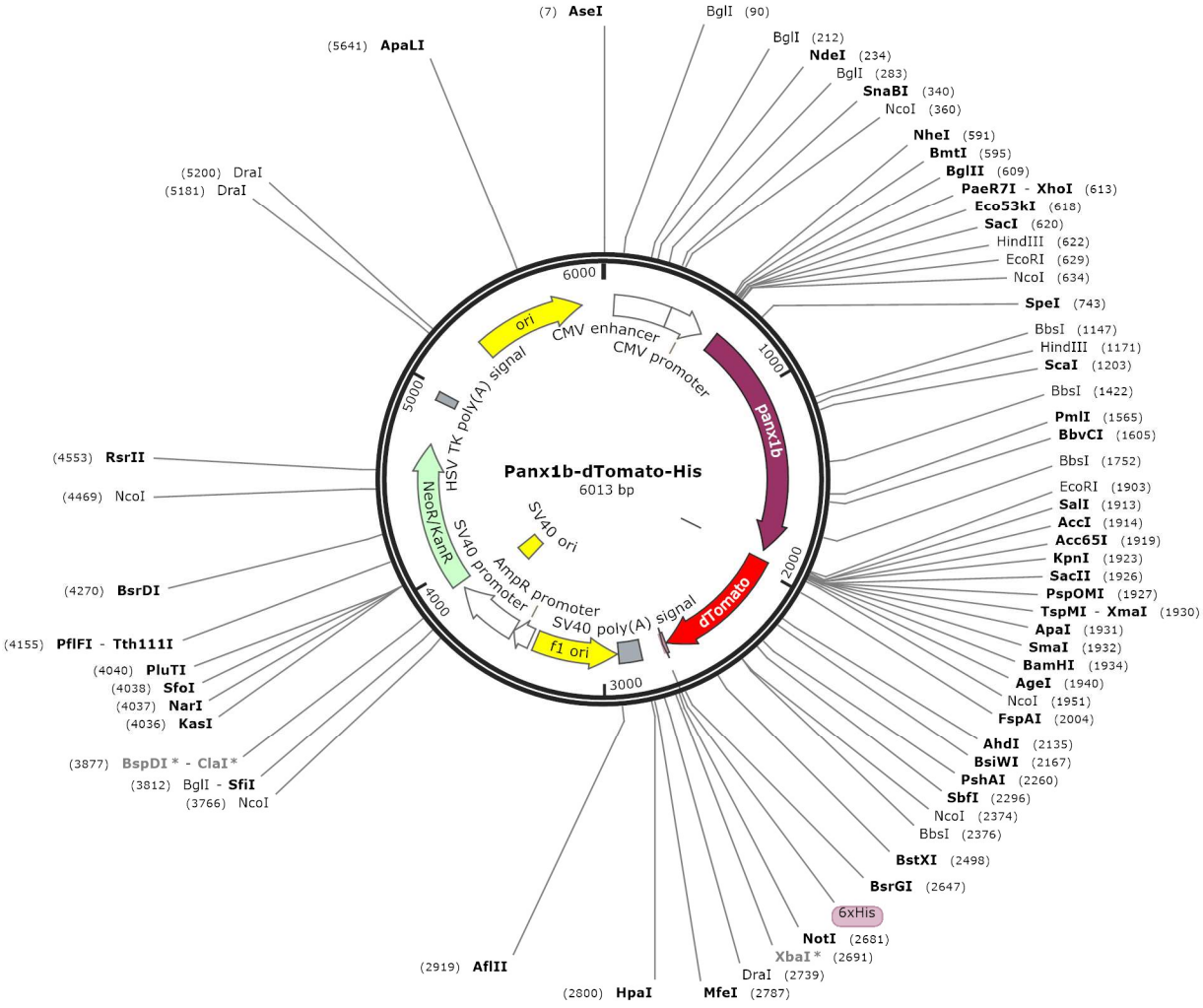

Figure A. 9. Plasmid map of Panx1b-dTomato-His. The pdTomato-His plasmid was created in-house by replacing EGFP with dTomato from the pEGFP-His-N1 plasmid. Danio rerio Panx1b was cloned into the pdTomato-His vector using EcoRI restriction enzymes, and an orientation check was performed. dTomato-His tag is C terminal of Panx1b.

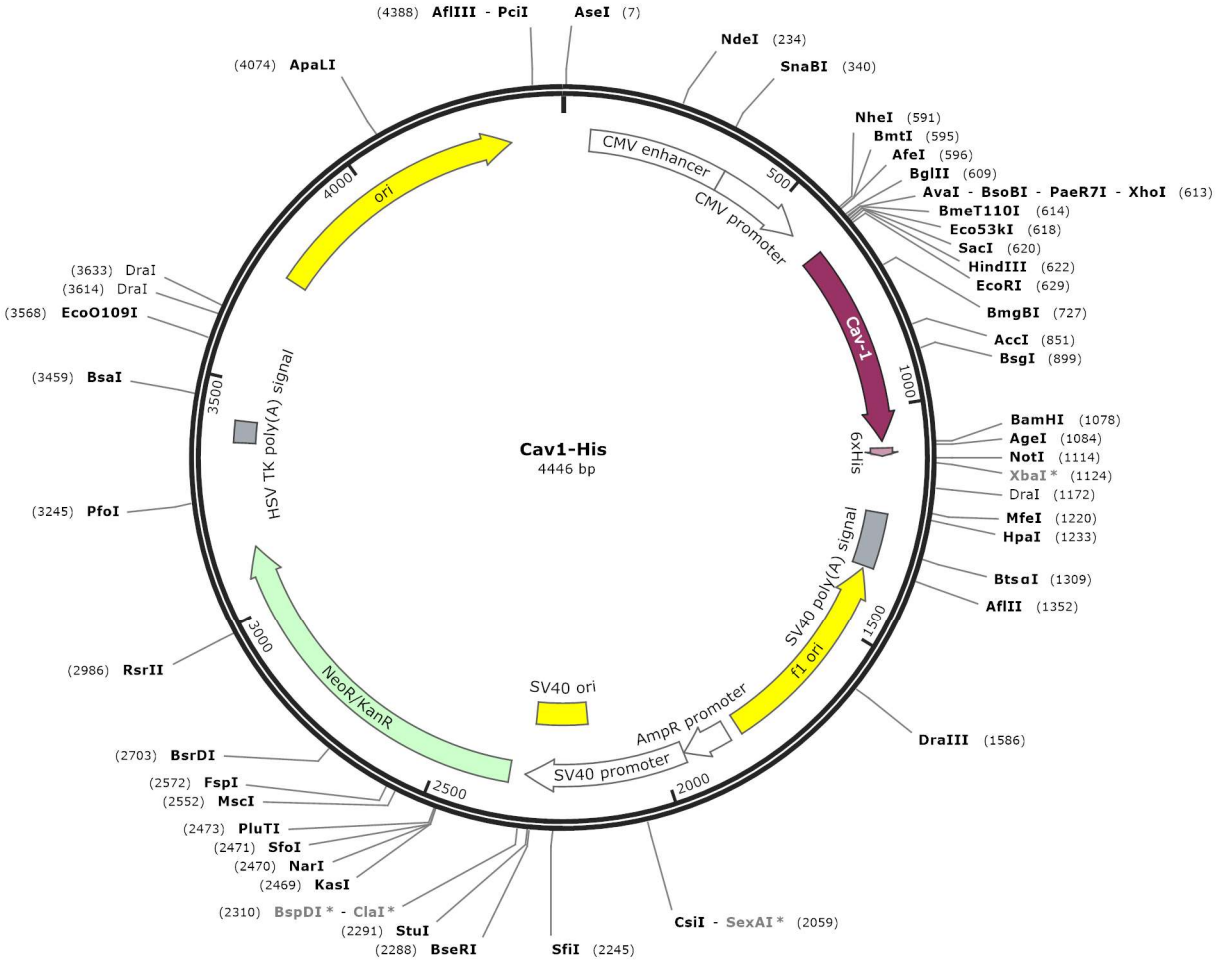

Figure A. 10. Plasmid map of Cav1-His. Mus musculus Caveolin-1 was cloned into the His-N1 vector using EcoRI and BamHI. His tag is C terminal of Caveolin-1.

BIBLIOGRAPHY

Abeele, F. V., Bidaux, G., Gordienko, D., Beck, B., Panchin, Y. V., Baranova, A. V., ... & Prevarskaya, N. (2006). Functional implications of calcium permeability of the channel formed by pannexin 1. The Journal of cell biology, 174(4), 535-546.

Adamson, S. E., Meher, A. K., Chiu, Y. H., Sandilos, J. K., Oberholtzer, N. P., Walker, N. N., ... & Leitinger, N. (2015). Pannexin 1 is required for full activation of insulin-stimulated glucose uptake in adipocytes. Molecular metabolism, 4(9), 610-618.

Ambrosi, C., Gassmann, O., Pranskevich, J. N., Boassa, D., Smock, A., Wang, J., ... & Sosinsky, G. E. (2010). Pannexin1 and Pannexin2 channels show quaternary similarities to connexons and different oligomerization numbers from each other. Journal of Biological Chemistry, 285(32), 24420-24431.

Bao, L., Locovei, S., & Dahl, G. (2004). Pannexin membrane channels are mechanosensitive conduits for ATP. FEBS letters, 572(1-3), 65-68.

Baranova, A., Ivanov, D., Petrash, N., Pestova, A., Skoblov, M., Kelmanson, I., ... & Panchin, Y. (2004). The mammalian pannexin family is homologous to the invertebrate innexin gap junction proteins. Genomics, 83(4), 706-716.

Barcomb, K., Buard, I., Coultrap, S. J., Kulbe, J. R., O'Leary, H., Benke, T. A., & Bayer, K. U. (2014). Autonomous CaMKII requires further stimulation by Ca2+/calmodulin for enhancing synaptic strength. The FASEB Journal, 28(8), 3810-3819.

Bargiotas, P., Krenz, A., Hormuzdi, S. G., Ridder, D. A., Herb, A., Barakat, W., ... & Schwaninger, M. (2011). Pannexins in ischemia-induced neurodegeneration. Proceedings of the National Academy of Sciences, 108(51), 20772-20777.

Beckel, J. M., Argall, A. J., Lim, J. C., Xia, J., Lu, W., Coffey, E. E., ... & Mitchell, C. H. (2014). Mechanosensitive release of adenosine 5′-triphosphate through pannexin channels and mechanosensitive upregulation of pannexin channels in optic nerve head astrocytes: A mechanism for purinergic involvement in chronic strain. Glia, 62(9), 1486-1501.

Berman, H. M., Westbrook, J., Feng, Z., Gilliland, G., Bhat, T. N., Weissig, H., ... & Bourne, P. E. (2000). The protein data bank. *Nucleic acids research*, *28*(1), 235-242.

Bhalla-Gehi, R., Penuela, S., Churko, J. M., Shao, Q., & Laird, D. W. (2010). Pannexin1 and pannexin3 delivery, cell surface dynamics, and cytoskeletal interactions. Journal of Biological Chemistry, 285(12), 9147-9160.

Billaud, M., Lohman, A. W., Straub, A. C., Looft-Wilson, R., Johnstone, S. R., Araj, C. A., ... & Isakson, B. E. (2011). Pannexin1 regulates α1-adrenergic receptor–mediated vasoconstriction. Circulation research, 109(1), 80-85.

Blaser, R. E., & Vira, D. G. (2014). Experiments on learning in zebrafish (Danio rerio): A promising model of neurocognitive function. Neuroscience & Biobehavioral Reviews, 42, 224-231.

Boassa, D., Ambrosi, C., Qiu, F., Dahl, G., Gaietta, G., & Sosinsky, G. (2007). Pannexin1 channels contain a glycosylation site that targets the hexamer to the plasma membrane. Journal of Biological Chemistry, 282(43), 31733-31743.

Boassa, D., Nguyen, P., Hu, J., Ellisman, M. H., & Sosinsky, G. E. (2015). Pannexin2 oligomers localize in the membranes of endosomal vesicles in mammalian cells while Pannexin1 channels traffic to the plasma membrane. Frontiers in cellular neuroscience, 8, 468.

Boassa, D., Qiu, F., Dahl, G., & Sosinsky, G. (2008). Trafficking dynamics of glycosylated pannexin1 proteins. Cell communication & adhesion, 15(1-2), 119-132.

Bond, S. R., & Naus, C. C. (2014). The pannexins: past and present. Frontiers in physiology, 5, 58.

Bond, S. R., Wang, N., Leybaert, L., & Naus, C. C. (2012). Pannexin 1 ohnologs in the teleost lineage. The Journal of membrane biology, 245(8), 483-493.

Boyce, A. K., Kim, M. S., Wicki-Stordeur, L. E., & Swayne, L. A. (2015). ATP stimulates pannexin 1 internalization to endosomal compartments. Biochemical Journal, 470(3), 319-330.

Bruzzone, R., Barbe, M. T., Jakob, N. J., & Monyer, H. (2005). Pharmacological properties of homomeric and heteromeric pannexin hemichannels expressed in Xenopus oocytes. Journal of neurochemistry, 92(5), 1033-1043.

Bruzzone, R., Hormuzdi, S. G., Barbe, M. T., Herb, A., & Monyer, H. (2003). Pannexins, a family of gap junction proteins expressed in brain. Proceedings of the national academy of sciences, 100(23), 13644-13649.

Bunse, S., Schmidt, M., Prochnow, N., Zoidl, G., & Dermietzel, R. (2010). Intracellular cysteine 346 is essentially involved in regulating Panx1 channel activity. Journal of Biological Chemistry, 285(49), 38444-38452.

Cargnello, M., & Roux, P. P. (2011). Activation and function of the MAPKs and their substrates, the MAPK-activated protein kinases. Microbiology and molecular biology reviews, 75(1), 50-83.

Celetti, S. J., Cowan, K. N., Penuela, S., Shao, Q., Churko, J., & Laird, D. W. (2010). Implications of pannexin 1 and pannexin 3 for keratinocyte differentiation. Journal of cell science, 123(8), 1363-1372.

Chao, L. H., Stratton, M. M., Lee, I. H., Rosenberg, O. S., Levitz, J., Mandell, D. J., ... & Kuriyan, J. (2011). A mechanism for tunable autoinhibition in the structure of a human Ca2+/calmodulin-dependent kinase II holoenzyme. Cell, 146(5), 732-745.

Chekeni, F. B., Elliott, M. R., Sandilos, J. K., Walk, S. F., Kinchen, J. M., Lazarowski, E. R., ... & Ravichandran, K. S. (2010). Pannexin 1 channels mediate 'find-me'signal release and membrane permeability during apoptosis. Nature, 467(7317), 863-867.

Cheung, J. C., & Reithmeier, R. A. (2007). Scanning N-glycosylation mutagenesis of membrane proteins. *Methods*, *41*(4), 451-459.

Chia, P. H., Zhong, F. L., Niwa, S., Bonnard, C., Utami, K. H., Zeng, R., ... & Reversade, B. (2018). A homozygous loss-of-function CAMKIIA mutation causes growth delay, frequent seizures and severe intellectual disability. Elife, 7, e32451.

Chin, D., & Means, A. R. (2002). Mechanisms for regulation of calmodulin kinase IIα by Ca2+/calmodulin and autophosphorylation of threonine 286. Biochemistry, 41(47), 14001-14009.

Chiu, Y. H., Medina, C. B., Doyle, C. A., Zhou, M., Narahari, A. K., Sandilos, J. K., ... & Bayliss, D. A. (2021). Deacetylation as a receptor-regulated direct activation switch for pannexin channels. Nature communications, 12(1), 1-14.

Choi, A. Y., Choi, J. H., Yoon, H., Hwang, K. Y., Noh, M. H., Choe, W., ... & Kang, I. (2011). Luteolin induces apoptosis through endoplasmic reticulum stress and mitochondrial dysfunction in Neuro-2a mouse neuroblastoma cells. European journal of pharmacology, 668(1-2), 115-126.

Cohen, P. (2002). The origins of protein phosphorylation. Nature cell biology, 4(5), E127-E130.

Cook, S. G., Buonarati, O. R., Coultrap, S. J., & Bayer, K. U. (2021). CaMKII holoenzyme mechanisms that govern the LTP versus LTD decision. Science Advances, 7(16), eabe2300.

Coultrap, S. J., & Bayer, K. U. (2012). CaMKII regulation in information processing and storage. Trends in neurosciences, 35(10), 607-618.

Cowan, S. W., Schirmer, T., Rummel, G., Steiert, M., Ghosh, R., Pauptit, R. A., ... & Rosenbusch, J. P. (1992). Crystal structures explain functional properties of two E. coli porins. Nature, 358(6389), 727-733.

Dahl, G. (2015). ATP release through pannexon channels. Philosophical Transactions of the Royal Society B: Biological Sciences, 370(1672), 20140191.

Dahl, G., & Muller, K. J. (2014). Innexin and pannexin channels and their signaling. FEBS letters, 588(8), 1396-1402.

Dahl, G., Qiu, F., & Wang, J. (2013). The bizarre pharmacology of the ATP release channel pannexin1. Neuropharmacology, 75, 583-593.

Dahl, G., Werner, R., Levine, E., & Rabadan-Diehl, C. (1992). Mutational analysis of gap junction formation. Biophysical journal, 62(1), 172-182.

Dando, R., & Roper, S. D. (2009). Cell-to-cell communication in intact taste buds through ATP signalling from pannexin 1 gap junction hemichannels. The Journal of physiology, 587(24), 5899-5906.

De Gassart, A., & Martinon, F. (2015). Pyroptosis: caspase-11 unlocks the gates of death. Immunity, 43(5), 835-837.

DeLalio, L. J., Keller, A. S., Chen, J., Boyce, A. K., Artamonov, M. V., Askew-Page, H. R., ... & Isakson, B. E. (2018). Interaction between pannexin 1 and caveolin-1 in smooth muscle can regulate blood pressure. Arteriosclerosis, thrombosis, and vascular biology, 38(9), 2065-2078.

Deng, Z., He, Z., Maksaev, G., Bitter, R. M., Rau, M., Fitzpatrick, J. A., & Yuan, P. (2020). Cryo-EM structures of the ATP release channel pannexin 1. Nature Structural & Molecular Biology, 27(4), 373-381.

Dickey, A., Schleicher, S., Leahy, K., Hu, R., Hallahan, D., & Thotala, D. K. (2011). GSK-3β inhibition promotes cell death, apoptosis, and in vivo tumor growth delay in neuroblastoma Neuro-2A cell line. Journal of neuro-oncology, 104(1), 145-153.

DiNuzzo, M., Mangia, S., Maraviglia, B., & Giove, F. (2014). Physiological bases of the K+ and the glutamate/GABA hypotheses of epilepsy. Epilepsy research, 108(6), 995-1012.

Dvoriantchikova, G., Ivanov, D., Panchin, Y., & Shestopalov, V. I. (2006). Expression of pannexin family of proteins in the retina. FEBS letters, 580(9), 2178-2182.

Epp, A. L., Ebert, S. N., Sanchez-Arias, J. C., Wicki-Stordeur, L. E., Boyce, A. K., & Swayne, L. A. (2019). A novel motif in the proximal C-terminus of Pannexin 1 regulates cell surface localization. Scientific reports, 9(1), 1-12.

Force, A., Lynch, M., Pickett, F. B., Amores, A., Yan, Y. L., & Postlethwait, J. (1999). Preservation of duplicate genes by complementary, degenerative mutations. Genetics, 151(4), 1531-1545.

Frederiksen, S. D., Wicki-Stordeur, L. E., Sanchez-Arias, J. C., & Swayne, L. A. (2019). Exploring the Pannexin 1 interactome: In silico cross-analyses with postsynaptic proteins and neuropsychiatric disorder susceptibility genes. BioRxiv, 801563.

Gajardo, I., Salazar, C. S., Lopez-Espíndola, D., Estay, C., Flores-Muñoz, C., Elgueta, C., ... & Ardiles, Á. O. (2018). Lack of pannexin 1 alters synaptic GluN2 subunit composition and spatial reversal learning in mice. Frontiers in Molecular Neuroscience, 11, 114.

Gebhardt, M., Hoffgaard, F., Hamacher, K., Kast, S. M., Moroni, A., & Thiel, G. (2011). Membrane anchoring and interaction between transmembrane domains are crucial for K+ channel function. Journal of Biological Chemistry, 286(13), 11299-11306.

Gehi, R., Shao, Q., & Laird, D. W. (2011). Pathways regulating the trafficking and turnover of pannexin1 protein and the role of the C-terminal domain. Journal of Biological Chemistry, 286(31), 27639-27653.

Gerlai, R. (2016). Learning and memory in zebrafish (Danio rerio). In Methods in Cell Biology (Vol. 134, pp. 551-586). Academic Press.

Gulbransen, B. D., Bashashati, M., Hirota, S. A., Gui, X., Roberts, J. A., MacDonald, J. A., ... & Sharkey, K. A. (2012). Activation of neuronal P2X7 receptor–pannexin-1 mediates death of enteric neurons during colitis. Nature medicine, 18(4), 600-604.

Guo, H. J., & Tadi, P. (2021). Biochemistry, Ubiquitination. In StatPearls [Internet]. StatPearls Publishing.

Gupta, A., Bisht, B., & Dey, C. S. (2011). Peripheral insulin-sensitizer drug metformin ameliorates neuronal insulin resistance and Alzheimer's-like changes. Neuropharmacology, 60(6), 910-920.

Hanson, P. I., & Schulman, H. (1992). Inhibitory autophosphorylation of multifunctional Ca2+/calmodulin-dependent protein kinase analyzed by site-directed mutagenesis. Journal of Biological Chemistry, 267(24), 17216-17224.

Herring, B. E., & Nicoll, R. A. (2016). Long-term potentiation: from CaMKII to AMPA receptor trafficking. Annu Rev Physiol, 78(1), 351-365.

Hoffman, L., Stein, R. A., Colbran, R. J., & Mchaourab, H. S. (2011). Conformational changes underlying calcium/calmodulin-dependent protein kinase II activation. The EMBO journal, 30(7), 1251-1262.

Huang, Y. J., Maruyama, Y., Dvoryanchikov, G., Pereira, E., Chaudhari, N., & Roper, S. D. (2007). The role of pannexin 1 hemichannels in ATP release and cell–cell communication in mouse taste buds. Proceedings of the National Academy of Sciences, 104(15), 6436-6441.

Iglesias, R., Locovei, S., Roque, A., Alberto, A. P., Dahl, G., Spray, D. C., & Scemes, E. (2008). P2X7 receptor-Pannexin1 complex: pharmacology and signaling. American Journal of Physiology-Cell Physiology, 295(3), C752-C760.

Jackson, D. G., Wang, J., Keane, R. W., Scemes, E., & Dahl, G. (2014). ATP and potassium ions: a deadly combination for astrocytes. Scientific reports, 4(1), 1-9.

Jensen, L. J., Kuhn, M., Stark, M., Chaffron, S., Creevey, C., Muller, J., ... & von Mering, C. (2009). STRING 8—a global view on proteins and their functional interactions in 630 organisms. *Nucleic acids research*, *37*(suppl_1), D412-D416.

Jiang, T., Long, H., Ma, Y., Long, L., Li, Y., Li, F., ... & Xiao, B. (2013). Altered expression of pannexin proteins in patients with temporal lobe epilepsy. Molecular medicine reports, 8(6), 1801-1806.

Jin, Q., Zhang, B., Zheng, X., Li, N., Xu, L., Xie, Y., ... & Ye, S. (2020). Cryo-EM structures of human pannexin 1 channel. Cell research, 30(5), 449-451.

Johnson, R. M., Hecht, K., & Deber, C. M. (2007). Aromatic and cation− π interactions enhance helix− helix association in a membrane environment. Biochemistry, 46(32), 9208-9214.

Kienitz, M. C., Bender, K., Dermietzel, R., Pott, L., & Zoidl, G. (2011). Pannexin 1 constitutes the large conductance cation channel of cardiac myocytes. Journal of Biological Chemistry, 286(1), 290-298.

Killian, J. A., & von Heijne, G. (2000). How proteins adapt to a membrane–water interface. Trends in biochemical sciences, 25(9), 429-434.

Kim, H. Y., Kim, S. J., & Lee, S. M. (2015). Activation of NLRP 3 and AIM2 inflammasomes in Kupffer cells in hepatic ischemia/reperfusion. The FEBS journal, 282(2), 259-270.

Kim, J. E., & Kang, T. C. (2011). The P2X7 receptor–pannexin-1 complex decreases muscarinic acetylcholine receptor–mediated seizure susceptibility in mice. The Journal of clinical investigation, 121(5), 2037-2047.

Kim, W., Bennett, E. J., Huttlin, E. L., Guo, A., Li, J., Possemato, A., ... & Gygi, S. P. (2011). Systematic and quantitative assessment of the ubiquitin-modified proteome. Molecular cell, 44(2), 325-340.

Krick, S., Wang, J., St-Pierre, M., Gonzalez, C., Dahl, G., & Salathe, M. (2016). Dual oxidase 2 (Duox2) regulates pannexin 1-mediated ATP release in primary human airway epithelial cells via changes in intracellular pH and not H2O2 production. Journal of Biological Chemistry, 291(12), 6423-6432.

Kurtenbach, S., Prochnow, N., Kurtenbach, S., Klooster, J., Zoidl, C., Dermietzel, R., ... & Zoidl, G. (2013). Pannexin1 channel proteins in the zebrafish retina have shared and unique properties. PLoS One, 8(10), e77722.

Kurtenbach, S., Whyte-Fagundes, P., Gelis, L., Kurtenbach, S., Brazil, É., Zoidl, C., ... & Zoidl, G. (2014). Investigation of olfactory function in a Panx1 knock out mouse model. Frontiers in cellular neuroscience, 8, 266.

Lampert, A., O'Reilly, A. O., Dib-Hajj, S. D., Tyrrell, L., Wallace, B. A., & Waxman, S. G. (2008). A pore-blocking hydrophobic motif at the cytoplasmic aperture of the closed-state Nav1. 7 channel is disrupted by the erythromelalgia-associated F1449V mutation. Journal of Biological Chemistry, 283(35), 24118-24127.

Le Vasseur, M., Lelowski, J., Bechberger, J. F., Sin, W. C., & Naus, C. C. (2014). Pannexin 2 protein expression is not restricted to the CNS. Frontiers in cellular neuroscience, 8, 392.

Li, S., Bjelobaba, I., & Stojilkovic, S. S. (2018). Interactions of Pannexin1 channels with purinergic and NMDA receptor channels. Biochimica et Biophysica Acta (BBA)-Biomembranes, 1860(1), 166-173.

Li, S., Tomić, M., & Stojilkovic, S. S. (2011). Characterization of novel Pannexin 1 isoforms from rat pituitary cells and their association with ATP-gated P2X channels. General and comparative endocrinology, 174(2), 202-210.

Li, S., Zang, Z., He, J., Chen, X., Yu, S., Pei, Y., ... & Liu, S. (2017). Expression of pannexin 1 and 2 in cortical lesions from intractable epilepsy patients with focal cortical dysplasia. Oncotarget, 8(4), 6883.

Lisman, J., Schulman, H., & Cline, H. (2002). The molecular basis of CaMKII function in synaptic and behavioural memory. Nature Reviews Neuroscience, 3(3), 175-190.

Locovei, S., Bao, L., & Dahl, G. (2006). Pannexin 1 in erythrocytes: function without a gap. Proceedings of the National Academy of Sciences, 103(20), 7655-7659.

Locovei, S., Scemes, E., Qiu, F., Spray, D. C., & Dahl, G. (2007). Pannexin1 is part of the pore forming unit of the P2X7 receptor death complex. FEBS letters, 581(3), 483-488.

Locovei, S., Wang, J., & Dahl, G. (2006). Activation of pannexin 1 channels by ATP through P2Y receptors and by cytoplasmic calcium. FEBS letters, 580(1), 239-244.

Lohman, A. W., Leskov, I. L., Butcher, J. T., Johnstone, S. R., Stokes, T. A., Begandt, D., ... & Isakson, B. E. (2015). Pannexin 1 channels regulate leukocyte emigration through the venous endothelium during acute inflammation. Nature communications, 6(1), 1-12.

Lohman, A. W., Weaver, J. L., Billaud, M., Sandilos, J. K., Griffiths, R., Straub, A. C., ... & Isakson, B. E. (2012). S-nitrosylation inhibits pannexin 1 channel function. Journal of Biological Chemistry, 287(47), 39602-39612.

López, X., Escamilla, R., Fernández, P., Duarte, Y., González-Nilo, F., Palacios-Prado, N., ... & Sáez, J. C. (2020). Stretch-induced activation of Pannexin 1 channels can be prevented by PKA-dependent phosphorylation. International journal of molecular sciences, 21(23), 9180.

López, X., Palacios-Prado, N., Güiza, J., Escamilla, R., Fernández, P., Vega, J. L., ... & Sáez, J. C. (2021). A physiologic rise in cytoplasmic calcium ion signal increases pannexin1 channel activity via a C-terminus phosphorylation by CaMKII. Proceedings of the National Academy of Sciences, 118(32).

Macdonald, S. G., Crews, C. M., Wu, L. E. L. I. A., Driller, J., Clark, R., Erikson, R. L., & McCormick, F. (1993). Reconstitution of the Raf-1-MEK-ERK signal transduction pathway in vitro. Molecular and cellular biology, 13(11), 6615-6620.

Madeira, F., Pearce, M., Tivey, A. R., Basutkar, P., Lee, J., Edbali, O., ... & Lopez, R. (2022). Search and sequence analysis tools services from EMBL-EBI in 2022. *Nucleic acids research*, *50*(W1), W276-W279.

Manning, G., Whyte, D. B., Martinez, R., Hunter, T., & Sudarsanam, S. (2002). The protein kinase complement of the human genome. Science, 298(5600), 1912-1934.

Michalski, K., Henze, E., Nguyen, P., Lynch, P., & Kawate, T. (2018). The weak voltage dependence of pannexin 1 channels can be tuned by N-terminal modifications. Journal of General Physiology, 150(12), 1758-1768.

Michalski, K., Syrjanen, J. L., Henze, E., Kumpf, J., Furukawa, H., & Kawate, T. (2020). The Cryo-EM structure of pannexin 1 reveals unique motifs for ion selection and inhibition. Elife, 9, e54670.

Mim, C., Perkins, G., & Dahl, G. (2021). Structure versus function: Are new conformations of pannexin 1 yet to be resolved?. Journal of General Physiology, 153(5), e202012754.

Mou, L., Ke, M., Song, M., Shan, Y., Xiao, Q., Liu, Q., ... & Deng, D. (2020). Structural basis for gating mechanism of Pannexin 1 channel. Cell research, 30(5), 452-454.

Müller, S. M., Galliardt, H., Schneider, J., Barisas, B. G., & Seidel, T. (2013). Quantification of Förster resonance energy transfer by monitoring sensitized emission in living plant cells. Frontiers in plant science, 4, 413.

Myers, J. B., Zaegel, V., Coultrap, S. J., Miller, A. P., Bayer, K. U., & Reichow, S. L. (2017). The CaMKII holoenzyme structure in activation-competent conformations. Nature communications, 8(1), 1-15.

Mylvaganam, S., Zhang, L., Wu, C., Zhang, Z. J., Samoilova, M., Eubanks, J., ... & Poulter, M. O. (2010). Hippocampal seizures alter the expression of the pannexin and connexin transcriptome. Journal of neurochemistry, 112(1), 92-102.

Namsi, A., Nury, T., Hamdouni, H., Yammine, A., Vejux, A., Vervandier-Fasseur, D., ... & Lizard, G. (2018). Induction of neuronal differentiation of murine N2a cells by two polyphenols present in the mediterranean diet mimicking neurotrophins activities: resveratrol and apigenin. Diseases, 6(3), 67.

Nouri-Nejad, D., O'Donnell, B. L., Patil, C. S., Sanchez-Pupo, R. E., Johnston, D., Sayedyahossein, S., ... & Penuela, S. (2021). Pannexin 1 mutation found in melanoma tumor reduces phosphorylation, glycosylation, and trafficking of the channel-forming protein. Molecular biology of the cell, 32(5), 376-390.

Omasits, U., Ahrens, C. H., Müller, S., & Wollscheid, B. (2014). Protter: interactive protein feature visualization and integration with experimental proteomic data. Bioinformatics, 30(6), 884-886.

Oshima, A. (2017). Structure of an innexin gap junction channel and cryo-EM sample preparation. Microscopy, 66(6), 371-379.

Oshima, A., Tani, K., & Fujiyoshi, Y. (2016). Atomic structure of the innexin-6 gap junction channel determined by cryo-EM. Nature communications, 7(1), 1-8.

Oslowski, C. M., & Urano, F. (2011). Measuring ER stress and the unfolded protein response using mammalian tissue culture system. In Methods in enzymology (Vol. 490, pp. 71-92). Academic Press.

Panchin, Y., Kelmanson, I., Matz, M., Lukyanov, K., Usman, N., & Lukyanov, S. (2000). A ubiquitous family of putative gap junction molecules. Current biology, 10(13), R473-R474.

Pelegrin, P., & Surprenant, A. (2006). Pannexin-1 mediates large pore formation and interleukin-1β release by the ATP-gated P2X7 receptor. The EMBO journal, 25(21), 5071-5082.

Penuela, S., Bhalla, R., Gong, X. Q., Cowan, K. N., Celetti, S. J., Cowan, B. J., ... & Laird, D. W. (2007). Pannexin 1 and pannexin 3 are glycoproteins that exhibit many distinct characteristics from the connexin family of gap junction proteins. Journal of cell science, 120(21), 3772-3783.

Penuela, S., Bhalla, R., Nag, K., & Laird, D. W. (2009). Glycosylation regulates pannexin intermixing and cellular localization. Molecular biology of the cell, 20(20), 4313-4323.

Penuela, S., Gehi, R., & Laird, D. W. (2013). The biochemistry and function of pannexin channels. Biochimica et Biophysica Acta (BBA)-Biomembranes, 1828(1), 15-22.

Pfaffl, M. W., Horgan, G. W., & Dempfle, L. (2002). Relative expression software tool (REST©) for group-wise comparison and statistical analysis of relative expression results in real-time PCR. Nucleic acids research, 30(9), e36-e36.

Pi, H. J., Otmakhov, N., El Gaamouch, F., Lemelin, D., De Koninck, P., & Lisman, J. (2010). CaMKII control of spine size and synaptic strength: role of phosphorylation states and nonenzymatic action. Proceedings of the National Academy of Sciences, 107(32), 14437-14442.

Poornima, V., Vallabhaneni, S., Mukhopadhyay, M., & Bera, A. K. (2015). Nitric oxide inhibits the pannexin 1 channel through a cGMP–PKG dependent pathway. Nitric oxide, 47, 77-84.

Prochnow, N., Abdulazim, A., Kurtenbach, S., Wildförster, V., Dvoriantchikova, G., Hanske, J., ... & Zoidl, G. (2012). Pannexin1 stabilizes synaptic plasticity and is needed for learning. PloS one, 7(12), e51767.

Prochnow, N., Hoffmann, S., Dermietzel, R., & Zoidl, G. (2009). Replacement of a single cysteine in the fourth transmembrane region of zebrafish pannexin1 alters hemichannel gating behavior. Experimental brain research, 199(3), 255-264.

Prochnow, N., Hoffmann, S., Vroman, R., Klooster, J., Bunse, S., Kamermans, M., ... & Zoidl, G. (2009). Pannexin1 in the outer retina of the zebrafish, Danio rerio. Neuroscience, 162(4), 1039-1054.

Qiu, F., & Dahl, G. (2009). A permeant regulating its permeation pore: inhibition of pannexin 1 channels by ATP. American Journal of Physiology-Cell Physiology.

Qu, R., Dong, L., Zhang, J., Yu, X., Wang, L., & Zhu, S. (2020). Cryo-EM structure of human heptameric Pannexin 1 channel. Cell Research, 30(5), 446-448.

Ransford, G. A., Fregien, N., Qiu, F., Dahl, G., Conner, G. E., & Salathe, M. (2009). Pannexin 1 contributes to ATP release in airway epithelia. American journal of respiratory cell and molecular biology, 41(5), 525-534.

Ray, A., Zoidl, G., Wahle, P., & Dermietzel, R. (2006). Pannexin expression in the cerebellum. The cerebellum, 5(3), 189-192.

Ray, A., Zoidl, G., Weickert, S., Wahle, P., & Dermietzel, R. (2005). Site-specific and developmental expression of pannexin1 in the mouse nervous system. The European journal of neuroscience, 21(12), 3277-3290.

Richards, C. I., Srinivasan, R., Xiao, C., Mackey, E. D., Miwa, J. M., Lester, H. A. (2011). Trafficking of {alpha}4* Nicotinic Receptors Revealed by Superecliptic Phluorin: EFFECTS OF A {beta}4 AMYOTROPHIC LATERAL SCLEROSIS-ASSOCIATED MUTATION AND CHRONIC EXPOSURE TO NICOTINE. J Biol Chem., 286(36), 31241-9.

Riquelme, M. A., Cea, L. A., Vega, J. L., Boric, M. P., Monyer, H., Bennett, M. V., ... & Sáez, J. C. (2013). The ATP required for potentiation of skeletal muscle contraction is released via pannexin hemichannels. Neuropharmacology, 75, 594-603.

Roskoski Jr, R. (2005). Src kinase regulation by phosphorylation and dephosphorylation. Biochemical and biophysical research communications, 331(1), 1-14.

Ruan, Z., Orozco, I. J., Du, J., & Lü, W. (2020). Structures of human pannexin 1 reveal ion pathways and mechanism of gating. Nature, 584(7822), 646-651.

Rubinfeld, H., Hanoch, T., & Seger, R. (1999). Identification of a cytoplasmic-retention sequence in ERK2. Journal of Biological Chemistry, 274(43), 30349-30352.

Safarian, N., Houshangi-Tabrizi, S., Zoidl, C., & Zoidl, G. R. (2021). Panx1b Modulates the Luminance Response and Direction of Locomotion in the Zebrafish. International Journal of Molecular Sciences, 22(21), 11750.

Safarian, N., Whyte-Fagundes, P., Zoidl, C., Grigull, J., & Zoidl, G. (2020). Visuomotor deficiency in panx1a knockout zebrafish is linked to dopaminergic signaling. Scientific reports, 10(1), 1-14.

Sandilos, J. K., Chiu, Y. H., Chekeni, F. B., Armstrong, A. J., Walk, S. F., Ravichandran, K. S., & Bayliss, D. A. (2012). Pannexin 1, an ATP Release Channel, Is Activated by Caspase Cleavage of Its Pore-associated C-terminal Autoinhibitory Region*♦. Journal of Biological Chemistry, 287(14), 11303-11311.

Scemes, E., Suadicani, S. O., Dahl, G., & Spray, D. C. (2007). Connexin and pannexin mediated cell–cell communication. Neuron glia biology, 3(3), 199-208.

Schenk, U., Westendorf, A. M., Radaelli, E., Casati, A., Ferro, M., Fumagalli, M., ... & Grassi, F. (2008). Purinergic control of T cell activation by ATP released through pannexin-1 hemichannels. Science signaling, 1(39), ra6-ra6.

Sehnal, D., Bittrich, S., Deshpande, M., Svobodová, R., Berka, K., Bazgier, V., ... & Rose, A. S. (2021). Mol* Viewer: modern web app for 3D visualization and analysis of large biomolecular structures. *Nucleic Acids Research*, *49*(W1), W431-W437.

Seminario-Vidal, L., Kreda, S., Jones, L., O'Neal, W., Trejo, J., Boucher, R. C., & Lazarowski, E. R. (2009). Thrombin promotes release of ATP from lung epithelial cells through coordinated activation of rho-and Ca2+-dependent signaling pathways. Journal of Biological Chemistry, 284(31), 20638-20648.

Sertori, R., Trengove, M., Basheer, F., Ward, A. C., & Liongue, C. (2016). Genome editing in zebrafish: a practical overview. Briefings in functional genomics, 15(4), 322-330.

Shestopalov, V. I., & Panchin, Y. (2008). Pannexins and gap junction protein diversity. Cellular and Molecular Life Sciences, 65(3), 376-394.

Silverman, W. R., de Rivero Vaccari, J. P., Locovei, S., Qiu, F., Carlsson, S. K., Scemes, E., ... & Dahl, G. (2009). The pannexin 1 channel activates the inflammasome in neurons and astrocytes. Journal of Biological Chemistry, 284(27), 18143-18151.

Siu, R. C., Kotova, A., Timonina, K., Zoidl, C., & Zoidl, G. R. (2021). Convergent NMDA receptor—Pannexin1 signaling pathways regulate the interaction of CaMKII with Connexin-36. Communications biology, 4(1), 1-14.

Siu, R. C., Smirnova, E., Brown, C. A., Zoidl, C., Spray, D. C., Donaldson, L. W., & Zoidl, G. (2016). Structural and functional consequences of connexin 36 (Cx36) interaction with calmodulin. Frontiers in Molecular Neuroscience, 9, 120.

Sosinsky, G. E., Boassa, D., Dermietzel, R., Duffy, H. S., Laird, D. W., MacVicar, B., ... & Dahl, G. (2011). Pannexin channels are not gap junction hemichannels. Channels, 5(3), 193-197.

Spagnol, G., Sorgen, P. L., & Spray, D. C. (2014). Structural order in Pannexin 1 cytoplasmic domains. Channels, 8(2), 157-166.

Sweatt, J. D. (2001). The neuronal MAP kinase cascade: a biochemical signal integration system subserving synaptic plasticity and memory. Journal of neurochemistry, 76(1), 1-10.

Szklarczyk, D., Gable, A. L., Lyon, D., Junge, A., Wyder, S., Huerta-Cepas, J., ... & Mering, C. V. (2019). STRING v11: protein–protein association networks with increased coverage, supporting functional discovery in genome-wide experimental datasets. Nucleic acids research, 47(D1), D607-D613.

Tullis, J. E., Rumian, N. L., Brown, C. N., & Bayer, K. U. (2020). The CaMKII K42M and K42R mutations are equivalent in suppressing kinase activity and targeting. Plos one, 15(7), e0236478.

Ubersax, J. A., & Ferrell Jr, J. E. (2007). Mechanisms of specificity in protein phosphorylation. Nature reviews Molecular cell biology, 8(7), 530-541.

Ulmschneider, M. B., & Sansom, M. S. (2001). Amino acid distributions in integral membrane protein structures. Biochimica et Biophysica Acta (BBA)-Biomembranes, 1512(1), 1-14.

Vogt, A., Hormuzdi, S. G., & Monyer, H. (2005). Pannexin1 and Pannexin2 expression in the developing and mature rat brain. Molecular brain research, 141(1), 113-120.

Walsh, C. T., Garneau-Tsodikova, S., & Gatto Jr, G. J. (2005). Protein posttranslational modifications: the chemistry of proteome diversifications. Angewandte Chemie International Edition, 44(45), 7342-7372.

Waltereit, R., & Weller, M. (2003). Signaling from cAMP/PKA to MAPK and synaptic plasticity. Molecular neurobiology, 27(1), 99-106.

Wang, J., & Dahl, G. (2018). Pannexin1: a multifunction and multiconductance and/or permeability membrane channel. American Journal of Physiology-Cell Physiology, 315(3), C290-C299.

Wang, J., & Dahl, G. (2010). SCAM analysis of Panx1 suggests a peculiar pore structure. Journal of General Physiology, 136(5), 515-527.

Wang, X. H., Streeter, M., Liu, Y. P., & Zhao, H. B. (2009). Identification and characterization of pannexin expression in the mammalian cochlea. Journal of Comparative Neurology, 512(3), 336-346.

Weaver, J. L., Arandjelovic, S., Brown, G., K Mendu, S., S Schappe, M., Buckley, M. W., ... & Bayliss, D. A. (2017). Hematopoietic pannexin 1 function is critical for neuropathic pain. Scientific reports, 7(1), 1-15.

Wei, L., Sheng, H., Chen, L., Hao, B., Shi, X., & Chen, Y. (2016). Effect of pannexin-1 on the release of glutamate and cytokines in astrocytes. Journal of Clinical Neuroscience, 23, 135-141.

Weilinger, N. L., Lohman, A. W., Rakai, B. D., Ma, E. M., Bialecki, J., Maslieieva, V., ... & Thompson, R. J. (2016). Metabotropic NMDA receptor signaling couples Src family kinases to pannexin-1 during excitotoxicity. Nature neuroscience, 19(3), 432-442.

Weilinger, N. L., Tang, P. L., & Thompson, R. J. (2012). Anoxia-induced NMDA receptor activation opens pannexin channels via Src family kinases. Journal of Neuroscience, 32(36), 12579-12588.

Whyte-Fagundes, P., Kurtenbach, S., Zoidl, C., Shestopalov, V. I., Carlen, P. L., & Zoidl, G. (2018). A potential compensatory role of Panx3 in the VNO of a Panx1 knock out mouse model. Frontiers in molecular neuroscience, 11, 135.

Whyte-Fagundes, P., & Zoidl, G. (2018). Mechanisms of pannexin1 channel gating and regulation. Biochimica et Biophysica Acta (BBA)-Biomembranes, 1860(1), 65-71.

Wicki-Stordeur, L. E., Boyce, A. K., & Swayne, L. A. (2013). Analysis of a pannexin 2-pannexin 1 chimeric protein supports divergent roles for pannexin C-termini in cellular localization. Cell communication & adhesion, 20(3-4), 73-79.

Woehrle, T., Yip, L., Elkhal, A., Sumi, Y., Chen, Y., Yao, Y., ... & Junger, W. G. (2010). Pannexin-1 hemichannel–mediated ATP release together with P2X1 and P2X4 receptors regulate T-cell activation at the immune synapse. Blood, The Journal of the American Society of Hematology, 116(18), 3475-3484.

Wu, Z., Chen, S., He, Y., Zhang, D., Zou, S., Xie, J., & Zhou, C. (2022). Connective tissue growth factor promotes cell-to-cell communication in human periodontal ligament stem cells via MAPK and PI3K pathway. Journal of Periodontology, 93(3), e60-e72.

Xia, J., Lim, J. C., Lu, W., Beckel, J. M., Macarak, E. J., Laties, A. M., & Mitchell, C. H. (2012). Neurons respond directly to mechanical deformation with pannexin-mediated ATP release and autostimulation of P2X7 receptors. The Journal of physiology, 590(10), 2285-2304.

Xiang, X., Langlois, S., St-Pierre, M. E., Blinder, A., Charron, P., Graber, T. E., ... & Cowan, K. N. (2021). Identification of pannexin 1-regulated genes, interactome, and pathways in rhabdomyosarcoma and its tumor inhibitory interaction with AHNAK. Oncogene, 40(10), 1868-1883.

Yang, D., He, Y., Muñoz-Planillo, R., Liu, Q., & Núñez, G. (2015). Caspase-11 requires the pannexin-1 channel and the purinergic P2X7 pore to mediate pyroptosis and endotoxic shock. Immunity, 43(5), 923-932.

Ye, J., Das, S., Roy, A., Wei, W., Huang, H., Lorenz-Guertin, J. M., ... & Wang, Q. J. (2019). Ischemic injury-induced CaMKIIδ and CaMKIIγ confer neuroprotection through the NF-κB signaling pathway. Molecular neurobiology, 56(3), 2123-2136.

Yen, M. R., & Saier Jr, M. H. (2007). Gap junctional proteins of animals: the innexin/pannexin superfamily. Progress in biophysics and molecular biology, 94(1-2), 5-14.

Zalcman, G., Federman, N., & Romano, A. (2018). CaMKII isoforms in learning and memory: localization and function. Frontiers in molecular neuroscience, 445.

Zhang, L., Deng, T., Sun, Y., Liu, K., Yang, Y., & Zheng, X. (2008). Role for nitric oxide in permeability of hippocampal neuronal hemichannels during oxygen glucose deprivation. Journal of neuroscience research, 86(10), 2281-2291.

Zoidl, G., Kremer, M., Zoidl, C., Bunse, S., & Dermietzel, R. (2008). Molecular diversity of connexin and pannexin genes in the retina of the zebrafish Danio rerio. Cell communication & adhesion, 15(1-2), 169-183.

Zoidl, G., Petrasch-Parwez, E., Ray, A., Meier, C., Bunse, S., Habbes, H. W., ... & Dermietzel, R. (2007). Localization of the pannexin1 protein at postsynaptic sites in the cerebral cortex and hippocampus. Neuroscience, 146(1), 9-16.

PUBLICATIONS

Timonina, K., Kotova, A., & Zoidl, G. (2020). Role of an aromatic–aromatic interaction in the assembly and trafficking of the zebrafish panx1a membrane channel. Biomolecules, 10(2), 272. https://doi.org/10.3390/biom10020272

- Peer reviewed, open access

Kotova, A., **Timonina, K**., & Zoidl, G. R. (2020). Endocytosis of connexin 36 is mediated by interaction with caveolin-1. International Journal of Molecular Sciences, 21(15), 5401. https://doi.org/10.3390/ijms21155401

- Peer reviewed, open access

Siu, R. C., Kotova, A., **Timonina, K.,** Zoidl, C., & Zoidl, G. R. (2021). Convergent NMDA receptor—Pannexin1 signaling pathways regulate the interaction of CaMKII with Connexin-36. Communications biology, 4(1), 1-14. https://doi.org/10.1038/s42003-021-02230-x

- Peer reviewed, open access

Yousefi, T., **Timonina, K.**, Zoidl, G., & Kassiri, H. (2021, October). A Temperature-Aware Fully-Wireless mm-Scale Optically-Enhanced Optogenetic Neuro-Stimulator. In 2021 IEEE Biomedical Circuits and Systems Conference (BioCAS) (pp. 01-05). IEEE. https://doi.org/ 10.1109/BioCAS49922.2021.9644947

- Peer reviewed

Yousefi, T., **Timonina, K**., Zoidl, G., & Kassiri, H. (2022). An Implantable Optogenetic Neuro-Stimulator SoC with Extended Optical Pulse-Width Enabled by Supply-Variation-Immune Cycled Light-Toggling Stimulation. IEEE Transactions on Biomedical Circuits and Systems. https://doi.org/ 10.1109/TBCAS.2022.3198911.

- Peer reviewed

Tetenborg, S., Liss, V., Breitsprecher, L., **Timonina, K**., Kotova, A., Hecker, A. J. A., ... & John, O. (2022). Intralumenal docking of Cx36 channels in the ER isolates mis-trafficked protein. bioRxiv. https://doi.org/10.1101/2022.07.15.500247

- Preprint, open access